Bulletin of the Geological Survey of Japan, vol. 70 (1/2), p. 43–89, 2019

Article

Conodont-based age calibration of the Middle Triassic Anisian radiolarian biozones in pelagic deep-sea bedded chert

Shun Muto[1,*], Satoshi Takahashi[1], Satoshi Yamakita[2], Katsuhito Soda[3] and Tetsuji Onoue[3]

Shun Muto, Satoshi Takahashi, Satoshi Yamakita, Katsuhito Soda and Tetsuji Onoue (2019) Conodont-based age calibration of the Middle Triassic Anisian radiolarian biozones in pelagic deep-sea bedded chert. *Bull. Geol. Surv. Japan*, vol. 70 (1/2), p. 43–89, 14 figs, 2 tables, 10 plates.

Abstract: The age of pelagic Panthalassic deep-sea bedded chert has been assigned based on radiolarian biostratigraphy. However, Triassic radiolarian biostratigraphy is in many cases not precisely correlated to the conodont zones and the standard geological timescale. In this study, we investigated the conodont biostratigraphy of two radiolarian-controlled bedded chert sections of Anisian age: the Ajiro Island section in Oita Prefecture and the Kurusu section in Aichi Prefecture. We recognised six conodont biozones in the studied sections: the upper Olenekian *Novispathodus brevissimus-Icriospathodus collinsoni* and *Triassospathodus homeri* Zones, the lower Anisian *Chiosella timorensis* Zone, the middle Anisian *Paragondolella bulgarica* Zone, the upper Anisian *Paragondolella excelsa* Zone and the uppermost Anisian to lowermost Ladinian *Paragondolella trammeri* Zone. These conodont zones were successfully correlated to the standard Triassic radiolarian zonation proposed by Sugiyama (1997, *Bull. Mizunami Foss. Mus*., vol. 24, p. 79–193). Sugiyama's radiolarian TR 1 Zone, previously considered to be of Olenekian age, extends to the middle Anisian. The TR 2A Zone, the TR 2B Zone and the lower part of the TR 2C Zone are correlated to the middle Anisian, while the upper part of the TR 2C Zone and the lower part of the TR 3A Zone are correlated to the upper Anisian. The upper part of the TR 3A Zone and the lower part of the TR 3B Zone are probably correlative to the uppermost Anisian, but the possibility that they are correlative to the lowermost Ladinian cannot be ruled out.

Keywords: biostratigraphy, conodont, radiolarian biozone, Panthalassa, Middle Triassic

1. Introduction

Carboniferous to Jurassic pelagic deep-sea bedded chert preserved in the accretionary complex of Japan provides precious sedimentary records of the Panthalassa sea floor (Kojima *et al.*, 2016; Matsuda and Isozaki, 1991; Wakita and Metcalfe, 2005) (Fig. 1A). For instance, evidence of oceanic anoxia (Fujisaki *et al.*, 2016; Takahashi *et al.*, 2009), bolide impact (Sato *et al.*, 2013, 2016) and climate change (Nakada *et al.*, 2014) have been documented from Triassic bedded chert in Japan. The prerequisite for such studies is the recognition of reliable geochronological controls for the bedded chert sequence, which was attempted by biostratigraphic correlations. The age assignment of bedded chert is commonly based on radiolarian biostratigraphy, which has been successfully established in many regions due to the abundant occurrence of radiolarians from bedded chert (e.g. Matsuoka and Yao, 1986; Sugiyama, 1997). Currently, the radiolarian biozones of Sugiyama (1997) established in the Inuyama area in central Japan are regarded as the most complete radiolarian zonation of Triassic deep-sea bedded chert deposited in the pelagic Panthalassa (e.g., O'Dogherty *et al.*, 2010). However, the Triassic radiolarian biozones of Sugiyama (1997) is not precisely correlated to the global standard geological timescale (Ogg, 2012). Hence, it is necessary to calibrate the radiolarian biozones based on geochronological controls that can be robustly correlated to the global standard geological timescale. Calibration by conodont biostratigraphy as in Sato *et al.* (2013, 2016) and Nakada *et al.* (2014) is a useful method, because although much rarer than radiolarians, conodont fossils occur reasonably frequently from deep-sea bedded chert (Hayashi, 1968; Isozaki and Matsuda, 1982, 1983;

[1] Graduate School of Science, The University of Tokyo, 7-3-1 Bunkyo-ku, Tokyo, 113-0033, Japan

[2] Faculty of Education, University of Miyazaki, 1-1, Gakuen Kibanadainishi, Miyazaki, 889-2192, Japan

[3] Graduate School of Science and Technology, Kumamoto University, 2-39-1, Kurokami, Chuo-ku, Kumamoto, 860-8555, Japan

[*] Corresponding author: S. Muto, Email: smuto@eps.s.u-tokyo.ac.jp

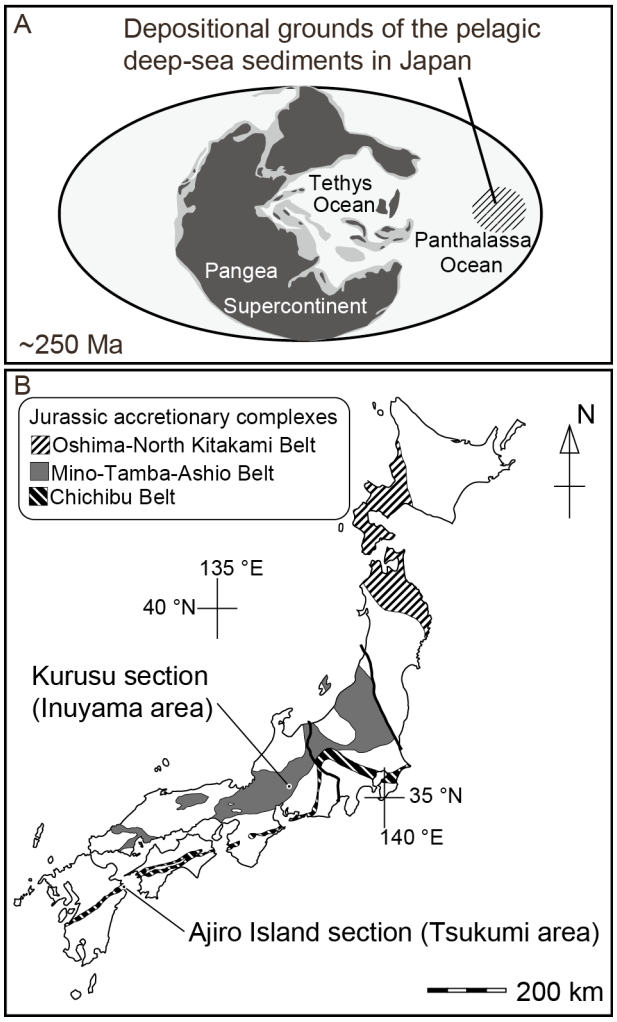

Fig. 1 (A) Palaeogeographic map of the Anisian (Ziegler *et al.*, 1998) showing the location of the depositional site of the pelagic deep-sea sediments in the Jurassic accretionary complex of Japan. (B) Location of the studied sections. The distribution of Jurassic accretionary complexes is after Isozaki *et al.* (2010).

Nishikane *et al.*, 2011). In this article, we focused on the radiolarian biozones previously assigned to the Anisian Age (the TR 2A to TR 3A Zones of Sugiyama, 1997), and calibrated their ages based on conodont biostratigraphy.

Previous reports of Anisian conodonts from bedded chert have been sporadic (Ando *et al.*, 2001; Matsuda and Isozaki, 1982; Mizutani and Koike, 1982; Sugiyama, 1997; Tanaka, 1980). The conodont *Chiosella timorensis*, which has been proposed as a marker for the base of the Anisian (Ogg, 2012; Orchard, 2010) has been found from pelagic deep-sea sediments including bedded chert in the Kuzuu area in east Japan (Muto *et al.*, 2018), the Nichihara area in southwest Japan (Tanaka, 1980) and the Kamiaso area in central Japan (Matsuda and Isozaki, 1982). In particular, Muto *et al.* (2018) indicated that the radiolarian based Olenekian-Anisian boundary, which is placed at the base of the TR 2A Zone of Sugiyama (1997) is within the middle Anisian. Therefore, the age of the "lower Anisian" radiolarian biozones of Sugiyama (1997) needs to be reinvestigated. On the other hand, the finding of middle Anisian conodonts *Paragondolella bulgarica* and *Nicoraella kockeli* from the TR 2B and TR 2C Zones in the Inuyama area (Ando *et al.*, 2001; Mizutani and Koike, 1982; Sugiyama, 1997) ensures that a part of these zones is correlative to the Anisian. However, the full range of these conodonts with regard to the radiolarian biozones remains unknown. The occurrence of the late Anisian conodont *Paragondolella excelsa* followed by that of the Ladinian conodont *Budurovignathus hungaricus* from a continuous bedded chert section in the Nichihara area (Tanaka, 1980) likely indicates the presence of the Anisian-Ladinian boundary. Unfortunately, radiolarians were not reported from this section, and the boundary cannot be correlated with radiolarian biozones. A more intensive investigation on conodont biostratigraphy and its correlation with radiolarian biozones based on high-resolution sampling are required to calibrate the age of the radiolarian biozones.

Two sections were selected for investigation of conodont biostratigraphy in this study. The first is the Ajiro Island section in the Tsukumi area, southwest Japan (Onoue *et al.*, 2011; Soda *et al.*, 2015; Uno *et al.*, 2012) (Figs. 1B, 2). This section was chosen because the TR 2A to TR 3A Zones can be collectively observed in one continuous section (Onoue *et al.*, 2011). Although the stratotype of the radiolarian biozones of Sugiyama (1997) was defined in the Inuyama area, the stratotype sections of the TR 2A to TR 3A Zones were defined in separate outcrops, which is a large disadvantage to the Ajiro Island section. In addition, the Ajiro Island section was logged bed-by-bed in Onoue *et al.* (2011) and Soda *et al.* (2015). Radiolarian biostratigraphy was based on their logs, which meant that we could compare conodont and radiolarian biostratigraphy at bed-by-bed resolutions.

The second section is the Kurusu section in the Inuyama area in central Japan (Yao and Kuwahara, 1997) (Figs. 1B, 3). Although this is not one of the stratotype sections of Sugiyama (1997), it provides crucial evidence on the age of the TR 2A Zone, as detailed below. The stratotype section of the TR 2A Zone is Section M in the Inuyama area, but the base of this zone is not observed there (Sugiyama, 1997). In the Ajiro Island section, the base of the TR 2A section was determined, but the underlying TR 1 Zone did not yield the radiolarian *Parentactinia nakatsugawaensis*, which is the species that most characterises the TR 1 Zone. Therefore, the TR 1 Zone in the Ajiro Island section may not be directly correlative to its type section in the Inuyama area. In contrast, in the Kurusu section, the *Pa. nakatsugawaensis* Assemblage Zone is overlain by the *Hozmadia gifuensis* Assemblage Zone (Yao and Kuwahara, 1997) and the boundary of the two zones can be approximated as the base of the TR 2A Zone. The boundary of the *Pa. nakatsugawaensis* Assemblage Zone

and the *H. gifuensis* Assemblage Zone was also reported from the Momotaro-jinja section in the Inuyama area (Fig. 3; Yao and Kuwahara, 1997). However, the *H. gifuensis* Assemblage Zone in this section did not yield the nominal species *H. gifuensis*. Furthermore, according to Sugiyama (1997) who investigated the lateral extension of the Momotaro-jinja section (Section T of Sugiyama (1997)), the interval assigned to the *H. gifuensis* Assemblage Zone by Yao and Kuwahara (1997) is within the TR 1 Zone. In sum, the Kurusu section is the only well-studied section that includes the base of the TR 2A Zone.

In this article, we present the lithostratigraphy and conodont biostratigraphy of the Ajiro Island and Kurusu sections. The conodont biostratigraphy is illustrated parallel to previous results on radiolarian biostratigraphy. Based on correlation with conodont biostratigraphy established in the Tethys region and North America, including the global boundary stratotype section and point (GSSP) candidate for the base of the Anisian and the GSSP of the base of the Ladinian, the radiolarian biozones were calibrated to the global standard geological timescale.

2. Geologic setting of the study sections

The studied sections belong to the Jurassic accretionary complex in southwest Japan. The Jurassic accretionary complex is mainly composed of Carboniferous to Middle Jurassic oceanic rocks (ocean floor basalt, deep-sea chert, hemipelagic siliceous mudstone, seamount basalt and seamount-capping carbonate), and Middle Jurassic to lowermost Cretaceous trench-fill terrigenous clastic rocks (mudstone and sandstone) (Isozaki *et al.*, 2010; Wakita and Metcalfe, 2005). Of the Carboniferous to Middle Jurassic oceanic rocks, the deep-sea sedimentary rocks were deposited in the pelagic Panthalassa superocean several thousand kilometres away from the nearest continent (Fig. 1A), after which they traveled to a subduction zone along the paleo-continent and formed a part of accretionary complexes by the tectonic movement of the oceanic plates (Isozaki *et al.*, 2010; Matsuda and Isozaki, 1991; Wakita and Metcalfe, 2005).

2. 1 Ajiro Island section

The Ajiro Island section is located in Ajiro Island (Ajiro Jima in Japanese) on the northern coast of the Youra Peninsula, Tsukumi City, Oita Prefecture, Kyushu District (33°4'10" N 131°55'10"E). The studied section belongs to the Southern Chichibu Belt (Fujii, 1954; Hoshizumi *et al.*, 2015; Kambe and Teraoka, 1968: Matsuoka *et al.*, 1998), which is mostly composed of a Jurassic accretionary complex (Isozaki *et al.* 2010; Matsuoka and Yao, 1990; Matsuoka *et al.*, 1998). The studied section is a part of the Shakumasan Group, which preserves the upper part of the original sequence on the oceanic plate (Nishi, 1994). The Shakumasan Group is further subdivided into the lower Enoura Formation and the upper Youra Formation (Nishi, 1994). The Enoura Formation is composed of Lower Triassic to Middle Jurassic pelagic deep-sea sedimentary rocks (mostly chert) (Matsuoka, 1986; Nishi, 1994), and is overlain conformably by trench-fill clastic rocks of the Youra Formation (Fig. 2; Nishi, 1994). The succession of these two formations occurs repeatedly due to the imbricate structure formed by thrusts (Fig. 2; Nishi, 1994).

The section investigated in this study belongs to the lowermost part of the Enoura Formation (Fig. 2B). The Ajiro Island section is located in the southernmost part of the Ajiro Island on the northern coast of the Tsukumi area. The studied outcrop corresponds to the "alternation beds of siliceous claystone and chert" and "red chert" in Fig. 2 of Uno *et al.* (2012). According to the age assignment based on radiolarian biostratigraphy, the bedded chert of the Ajiro Island has been dated as latest Spathian to early Ladinian, and has a northward younging trend (Onoue *et al.*, 2011; Takahashi *et al.*, 1998). The palaeolatitude of the depositional grounds have been estimated to be 2.1 ± 5.2°S based on rock magnetic records (Uno *et al.*, 2012).

2. 2 Kurusu section

The Kurusu section (Kr-2 section of Yao and Kuwahara, 1997) is located on the eastern bank of the Kiso River in Inuyama City, Aichi Prefecture, Chubu District (35°25'8"N 136°57'50"E). The Kurusu section belongs to the Mino-Tamba-Ashio Belt, which is mostly composed of a Jurassic accretionary complex (Isozaki *et al.*, 2010; Yamakita and Otoh, 2000; Kojima *et al.*, 2016). The Kurusu section is a part of the Kamiaso Unit (Wakita, 1988), which is a coherent tectonostratigraphic unit composed of Lower Triassic siliceous claystone, Middle Triassic to Lower Jurassic pelagic deep-sea bedded chert, Middle Jurassic hemipelagic siliceous shale and Upper Jurassic turbidite and massive sandstone in ascending order (Yao *et al.*, 1980). Thus, the upper part of the original sequence on the oceanic plate is preserved in the Kamiaso Unit. The Kamiaso Unit in the Inuyama area has been studied in detail by Kimura and Hori (1993). They clarified that the coherent sequence from pelagic siliceous claystone and chert to trench-fill clastic rocks ("Inuyama Sequence" in their paper) repeated six times as thrust sheets, which together form a synclinal structure with a W-plunging, WNW-ESE trending axis (the Sakahogi syncline; Mizutani, 1964). The Kurusu section corresponds to the lowermost strata of "sheet 4" in Kimura and Hori (1993), and is located on the northern wing of the Sakahogi syncline, close to the axis (Fig. 3).

Yao and Kuwahara (1997) studied the radiolarian biostratigraphy of the Kurusu section and indicated that the section is correlated to the *Parentactinia nakatsugawaensis* Zone and the *Hozmadia gifuensis* Zone. The radiolarian biostratigraphy indicates a southward younging trend for this section. This younging trend is consistent with the fact that the south of the section faces the axis of the Sakahogi syncline. The palaeolatitude of the depositional site of the Anisian bedded chert in the Inuyama area has been estimated to be 12.3 ± 15.6°N

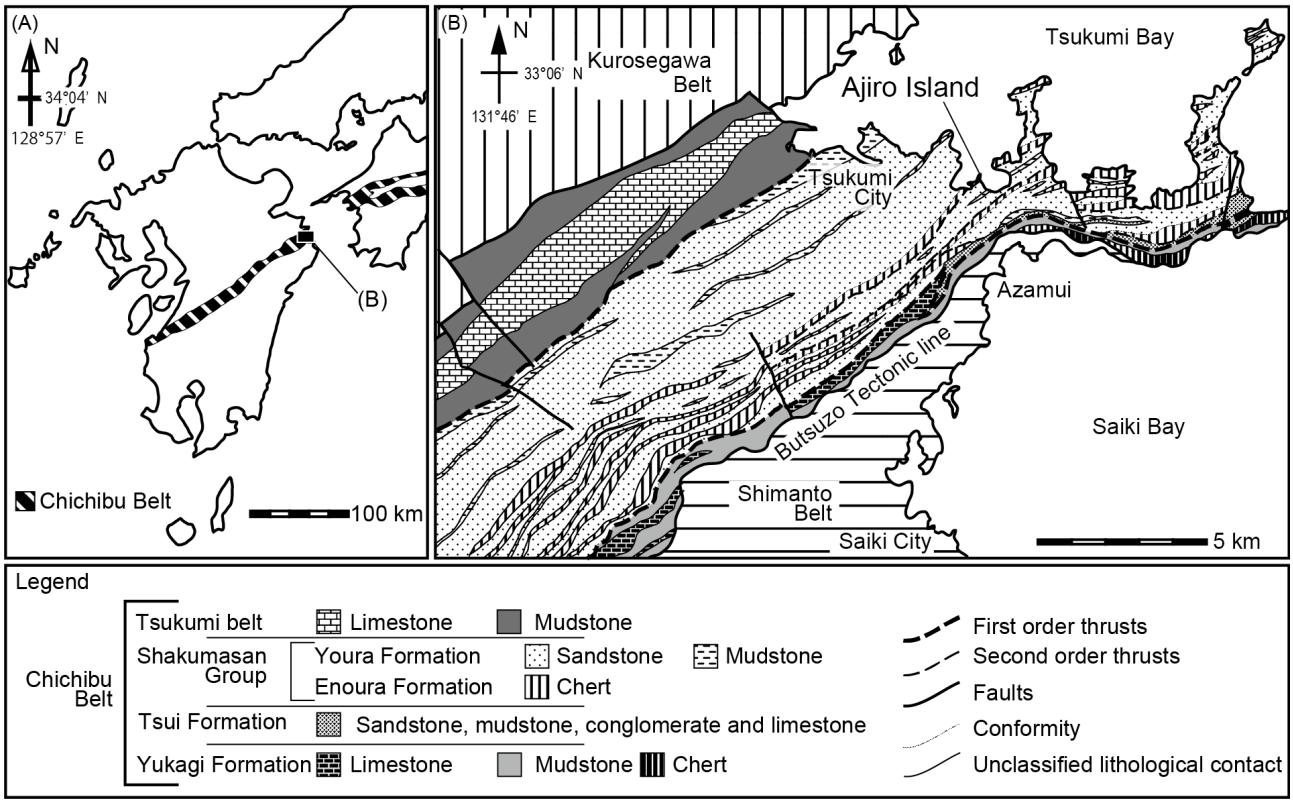

Fig. 2 (A) Distribution of the Chichibu Belt in Kyushu District (after Isozaki *et al.*, 2010). (B) Geological map of the Tsukumi area (Nishi, 1994).

or S (Oda and Suzuki, 2000) or 5.6 ± 2.2°S by (Ando *et al.*, 2001) based on palaeomagnetic records. Ikeda *et al.* (2010) investigated the "Kr-2 section of Yao and Kuwahara (1997)" for cyclostratigraphy, but their section was observed in a different part of the outcrop (compare Fig. 4 of Yao and Kuwahara (1997) and Fig. 1S in the supplementary materials of Ikeda *et al.* (2010)). In this study, we investigated the studied section of Ikeda *et al.* (2010) in addition to the section of Yao and Kuwahara (1997).

3. Methods

3. 1 Field mapping

For both the Ajiro Island and Kurusu sections, geological maps of the outcrop were made based on examination of the geological structure and lithology at the sub-metre scale. For the major part of the Ajiro Island section, detailed lithostratigraphy has been reported by Onoue *et al.* (2011), Soda *et al.* (2015) and Uno *et al.* (2012). We conducted a biostratigraphic investigation building on the lithostratigraphic section constructed by these studies. For the lower part of the Ajiro Island section, lithostratigraphy has not been investigated thoroughly by previous studies. Therefore, we reconstructed the lithostratigraphy of this part of the outcrop based on detailed mapping with careful attention to deformation and continuity. Lithostratigraphy of the Kurusu section has been reported by Yao and Kuwahara (1997) and Ikeda *et al.* (2010). However, both studies did not investigate the entire outcrop. In this study, we present an original outcrop sketch map and lithostratigraphic columns that include, but are not restricted to, stratigraphic intervals that were investigated by these studies.

3. 2 Conodont biostratigraphy

Conodonts were found by observing the surfaces of sample rocks cleaved parallel to the bedding into small "chips" (the "chip method"; Muto *et al.*, 2018; Takemura *et al.*, 2001). This method allows us to find conodonts that are cracked or preserved as moulds and impossible to extract by dissolving the host rock. A preliminary search for conodonts by the "chip method" was conducted at the outcrop using a hand lens (20 magnifications), and horizons that yielded conodonts were selected for further investigation. Following Muto *et al.* (2018), 2–5 kg blocks of the selected horizons were brought back to the laboratory, and then cleaved into thin planar chips. These chips were moistened with tap water and then examined under a stereoscopic microscope of 20 to 60 magnifications. Early attempts of the "chip method" resulted in larger numbers of specimens from greenish grey parts of the bedded chert compared to red or purple parts. This is probably because conodont fossils have more chances of being found in the more transparent greenish

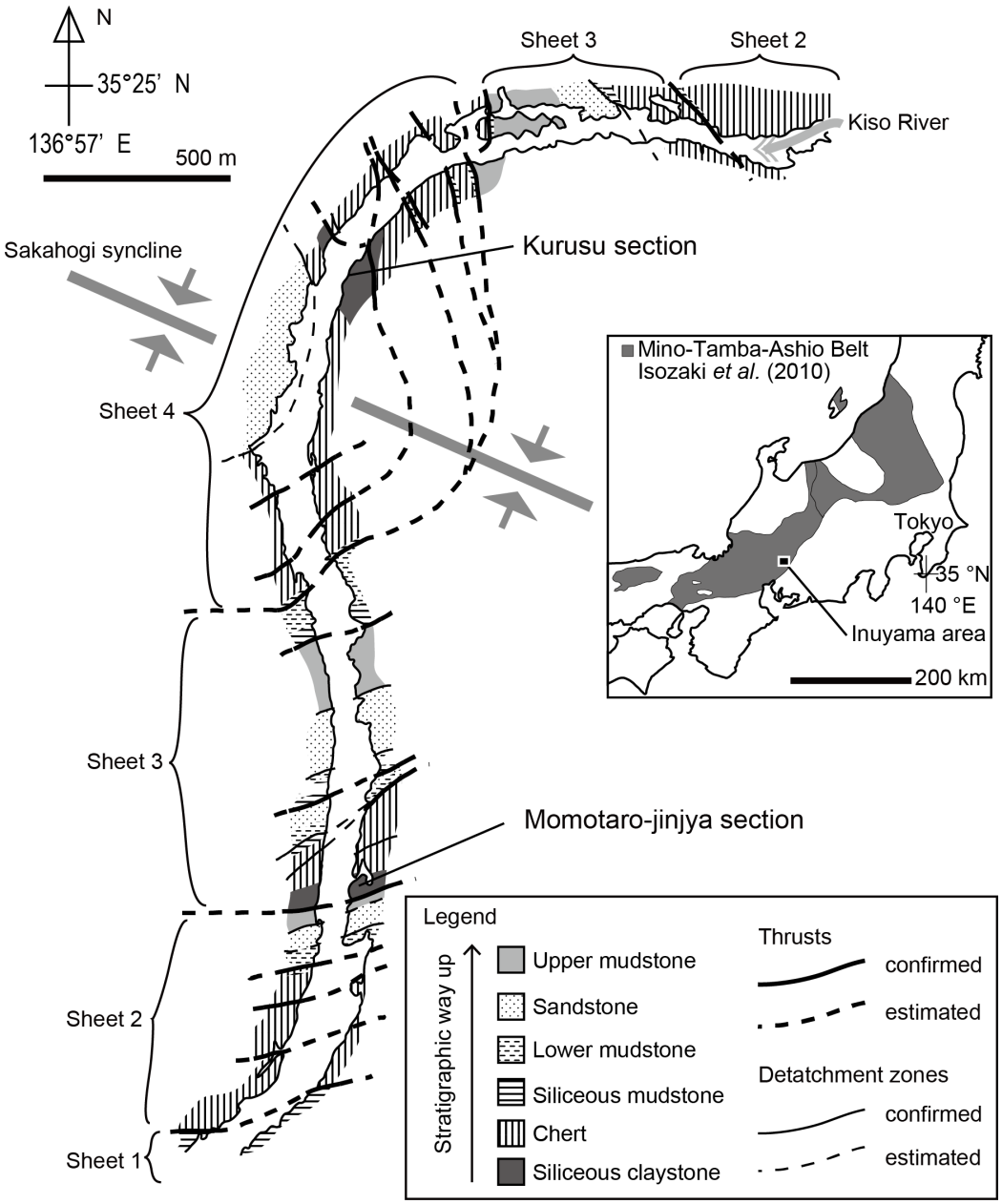

Fig. 3 Geological map of the Inuyama area (Kimura and Hori, 1993).

grey chert compared to purple or red chert. Therefore, the parts of strata that have been altered to greenish grey were targeted in the later attempts to find conodonts from dominantly purple or red intervals.

For specific identification, the chips were observed under a stereoscopic microscope of 100 magnifications. The surface of the chips were dried, soaked with water or coated with oil depending on the type of host rock and the state of preservation of the specimens. Moulds in siliceous claystone without grey fillings were best observed on dry surfaces, while moulds in siliceous claystone with grey fillings were better observed when soaked with water. Specimens in chert were best observed when the surface of the chert was coated with oil.

4. Results

4. 1 Ajiro Island section

4. 1. 1 Field mapping

The Ajiro Island section is exposed on the southern coast of Ajiro Island, Tsukumi City, Oita Prefecture (Fig. 2). The outcrop of the Ajiro Island section consists of two parts that have different geological structure and lithology. The main part of the section (the AJR section), which is exposed along the south to southeast coast of Ajiro Island, comprises bedded chert (Fig. 4). The AJR section

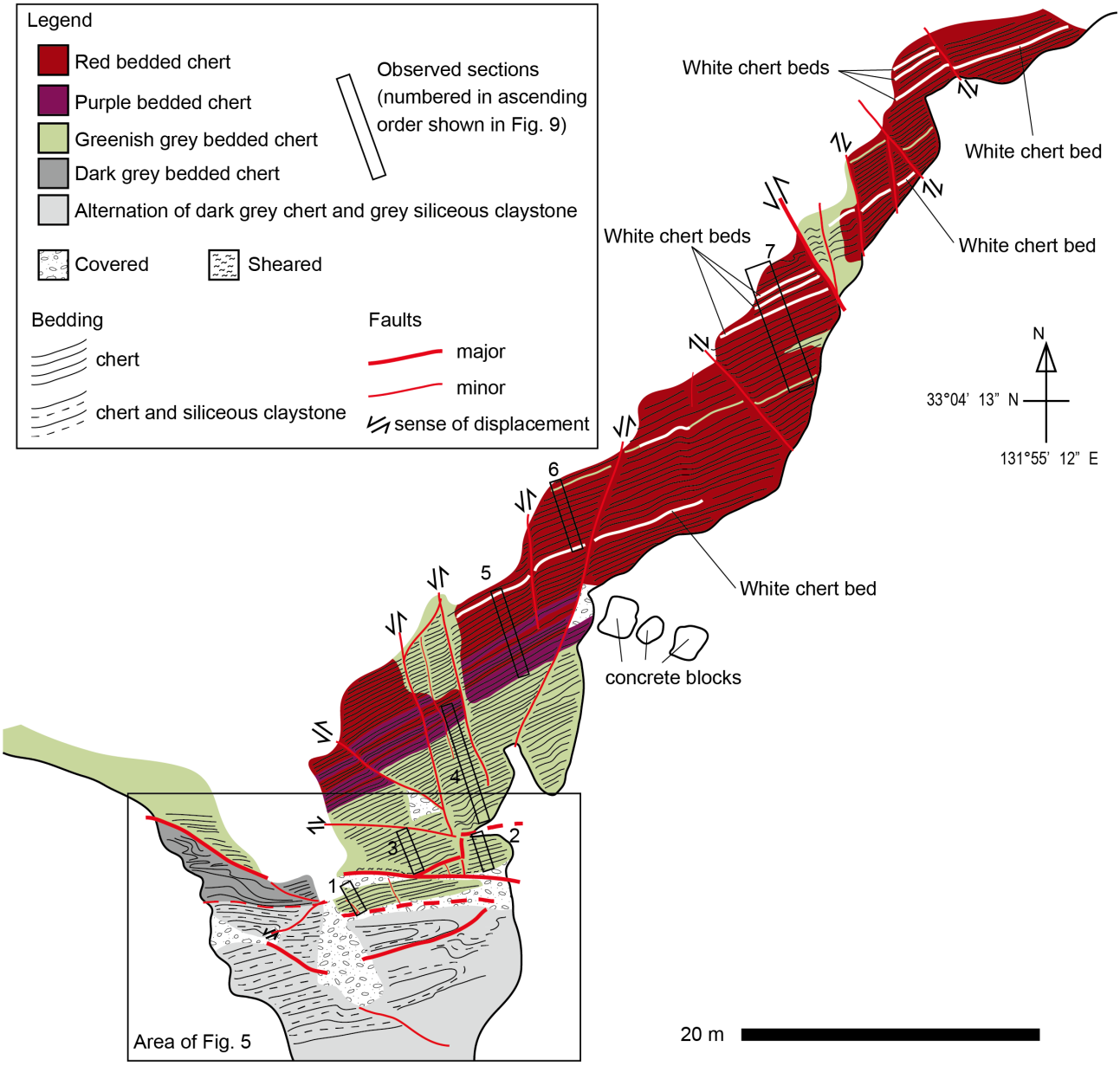

Fig. 4 Geological map of the southeast coast of Ajiro Island. The stratigraphic way up of the bedded chert is to the north (Onoue *et al.*, 2011; Takahashi *et al.*, 1998; Uno *et al.*, 2012).

has already been studied in detail by previous studies (Onoue *et al.*, 2011; Soda *et al.*, 2015; Uno *et al.*, 2012), and therefore we will only give a brief description of the outcrop. The other part is exposed at the southern tip of Ajiro Island, and comprises alternating beds of siliceous claystone and chert that are more intensely folded and faulted compared to strata of the AJR section (Figs. 4, 5). This part has been mapped by Onoue *et al.* (2011) and Uno *et al.* (2012), but lithostratigraphy was not examined in detail. Here, we provide a more detailed geological map and lithostratigraphic columns for this part of the section (the AJ-1, AJ-2, AJ-3-1 and AJ-3-2 sections). In the following text, we will explain the geological structures and lithofacies of the Ajiro Island section in stratigraphically ascending order (stratigraphic order is explained in Section 4.1.2.).

The lower part of the Ajiro Island section corresponds to the AJ-1, AJ-2, AJ-3-1 and AJ-3-2 sections exposed at the southern tip of Ajiro Island (Fig. 5). The strata here generally strike ENE-WSW and dip steeply to the north, apart from the northwestern part where the strata strike E-W to WNW-ESE. Isoclinal folds with wavelengths up to 2 m are present throughout the outcrop, and the strata are locally overturned. The axial planes of these folds are almost parallel to the bedding. The faults in this part of the outcrop can be distinguished into the following

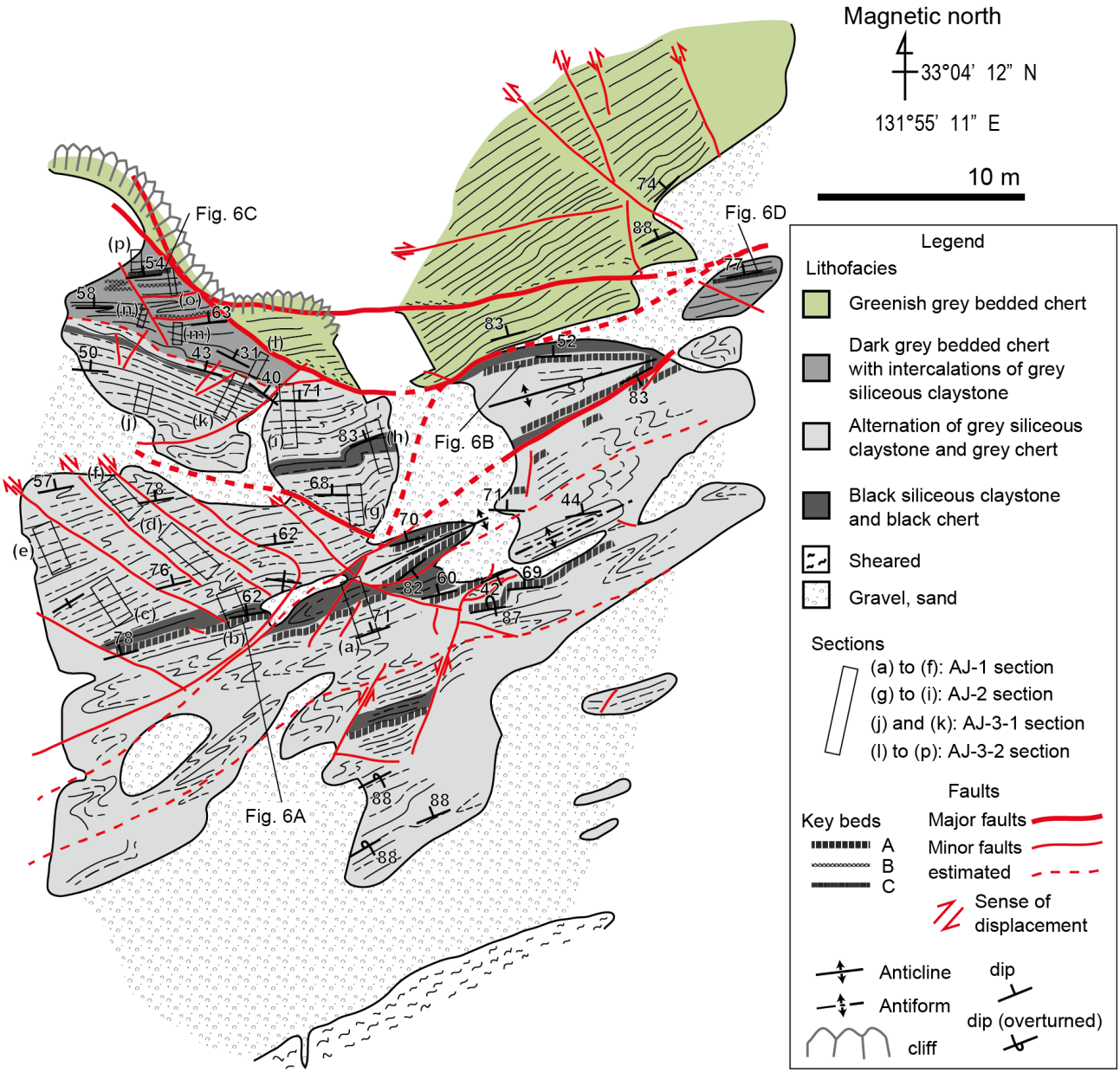

Fig. 5 Geological map of the southern tip of Ajiro Island. The lower part of the Ajiro Island section is exposed in this area. Sections (a) to (p) are labelled in stratigraphically ascending order.

two types. Major faults with displacements of at least several metres were identified in the northern part. These faults are characterised by sheared zones about 50 cm wide on either side of the fault plane. Minor faults with displacements of up to 2 m are present throughout the outcrop. These faults are not accompanied by wide sheared zones. Recognition of three key beds (Figs. 5, 6) revealed that strata in the western half of the outcrop are relatively weakly deformed. Therefore, we observed the lithostratigraphy in the western half of the outcrop, avoiding areas where strata are deformed by faults and folds. The reconstructed lithostratigraphic column comprises four continuous sequences: AJ-1 section, AJ-2 section, AJ-3-1 section and AJ-3-2 section in ascending order (Figs. 5, 9). On the other hand, in the eastern part of the outcrop, strata in the lower part of the AJ-1 section are repeated by faults and folds, while the upper part of the AJ-1 section, the AJ-2 section, the AJ-3-1 section and most of the AJ-3-2 section are missing.

The AJ-1 section is approximately 8.4 m thick, and is composed mainly of alternating beds of grey siliceous claystone and dark grey chert (Fig. 7A). An interval composed of black siliceous claystone and black chert occurs in the lower part of this sequence. The AJ-2 section is approximately 4.8 m thick, and is composed mainly of alternating beds of grey siliceous claystone and dark grey

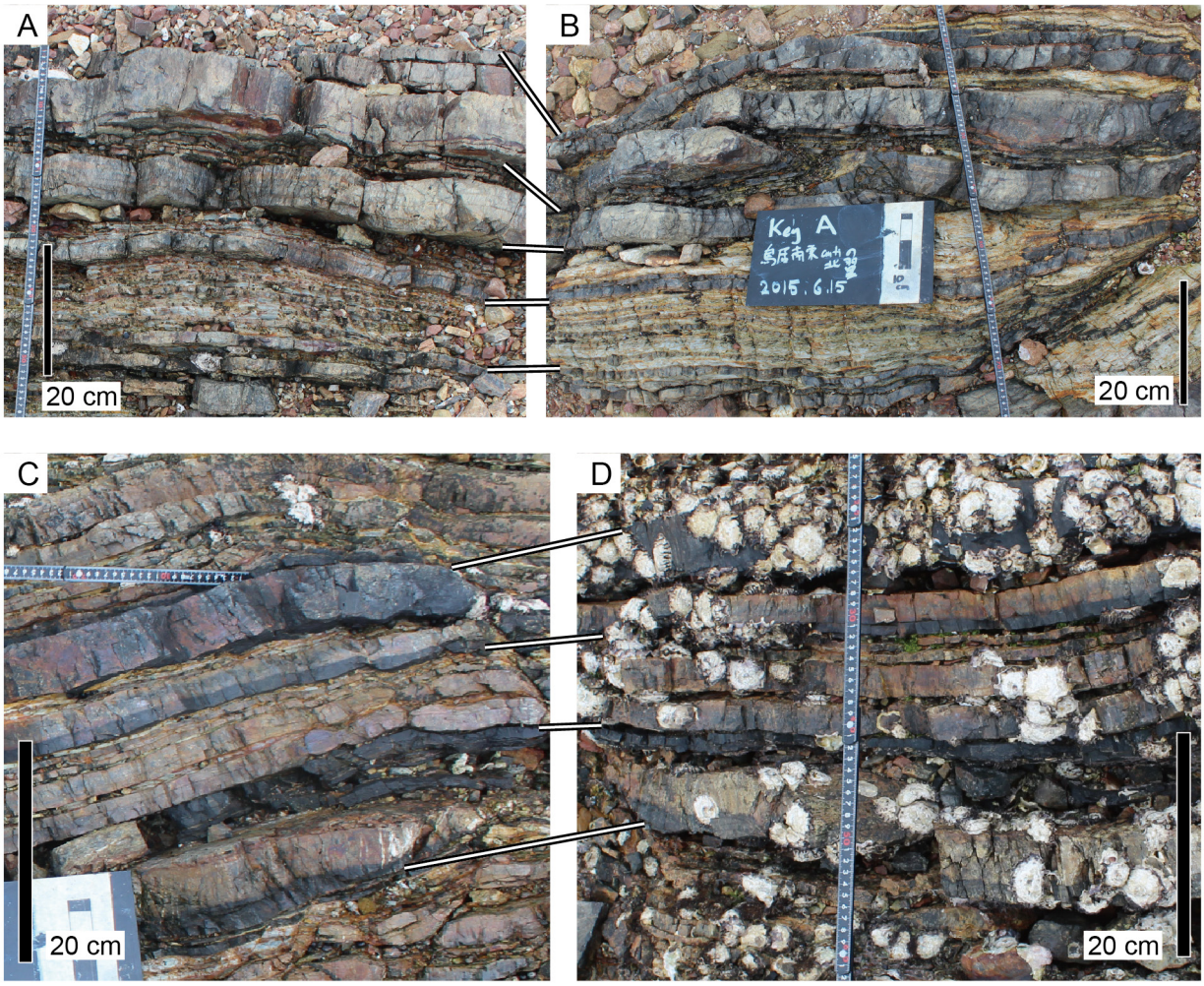

Fig. 6 Photographs of key beds in the lower part of the Ajiro Island section. White lines indicate the correlation between the same key bed in different places (see Fig. 5 for location). (A, B) Key bed A. (C, D) Key bed C.

or black chert (Fig. 7B). Thin (~10 mm thick) red siliceous claystone beds occur characteristically in this section. The AJ-3-1 section is approximately 2.0 m thick, and is composed mainly of alternating beds of grey siliceous claystone and grey or dark grey chert (Fig. 7C). The AJ-3-2 section lies directly above the AJ-3-1 section, but a slip plane exists between the two sections, and therefore they are not confirmed to be continuous (Fig. 7C, D). The AJ-3-2 section is approximately 3 m thick, and is composed of dark grey bedded chert with intercalations of grey siliceous claystone (Fig. 7D). This section is in fault contact with greenish grey bedded chert to the north.

In the outcrop of the AJR section, the strata strike ENE-WSW and dip steeply to the north (Fig. 4). A major fault with an apparent displacement of ~10 m occurs in the northern part. Minor faults with apparent displacements of up to 2 m occur throughout the outcrop. Deformation of the strata is negligible, apart from drags and shears near faults. The colour of bedded chert changes from greenish grey to purple, then to red in ascending order (Figs. 8A–D, Fig. 9). Some white highly recrystallised chert beds occur in the red bedded chert. Some parts of the purple and red bedded chert are altered to greenish grey (Fig. 8D). Our study section mostly corresponds to the section illustrated in previous studies (Onoue *et al.*, 2011; Soda *et al.*, 2015; Uno *et al.*, 2012). However, we observed an additional ~2 m of red bedded chert above the top of their section. In addition, we identified a stratigraphic discontinuity at the basal part of the lithologic column by Onoue *et al.* (2011) (the two faults within the AJR section in Fig. 9). Our reinvestigation of the geological structure showed that the stratigraphic intervals corresponding to the TR 1 and TR 2A Zones in their section are separated by a fault. Furthermore, a block of greenish grey bedded chert occurs structurally between these two intervals. The lithostratigraphic column illustrated in this study incorporates this new finding.

4. 1. 2 Conodont biostratigraphy

Conodont fossils were found from all of the investigated

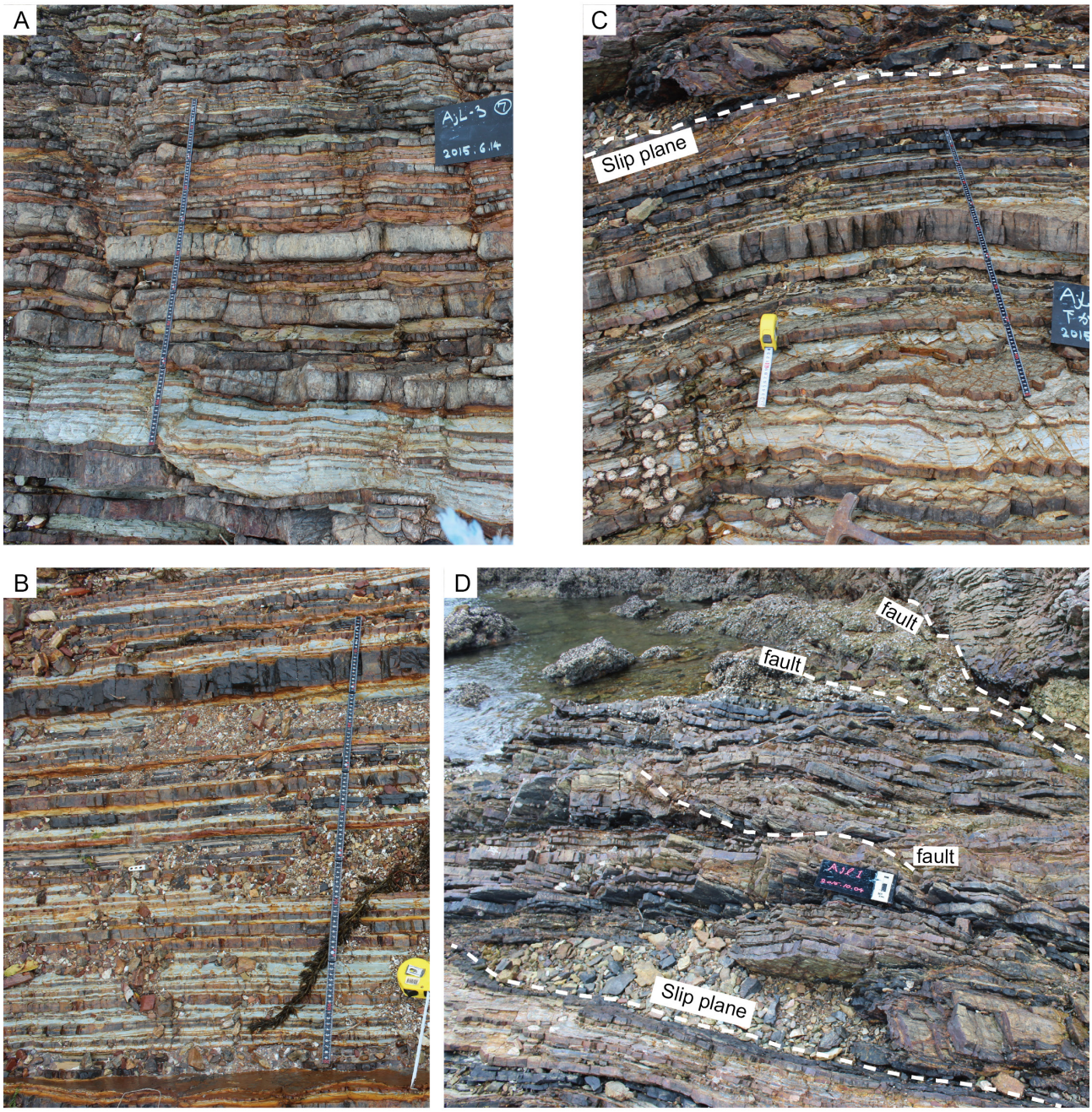

Fig. 7 Outcrop photographs of the lower part of the Ajiro Island section. (A) Alternating beds of grey siliceous claystone and dark grey chert in the AJ-1 section. (B) Alternating beds of grey siliceous claystone and dark grey or black chert in the AJ-2 section. (C) Alternating beds of grey siliceous claystone and grey or dark grey chert in the AJ-3-1 section. (D) Dark grey bedded chert in the AJ-3-2 section. Note the slip plane in (C) and (D). The stratigraphic way up is to the top in all photos. The black ruler in (A) to (C) is 1 m long. The black board in (D) is 20 cm × 30 cm.

samples (more than 2000 specimens in total). Conodonts in siliceous claystone were preserved as moulds, while those in chert were dark grey skeletons or white or orange casts. Although most of the specimens were broken and unidentifiable, 194 specimens were identified at the species level (Table 1; Plates 1–7). Conodont animals are taxonomically classified based on their apparatuses that comprise an assemblage of conodont elements (Clark *et al.*, 1981; Orchard, 2005; Sweet, 1988), but some morphologically distinguishable elements are yet to be assigned to any apparatus. Such elements are classified as form groups and are indicated in this paper with quotation marks.

Conodonts from the siliceous claystone that alternates

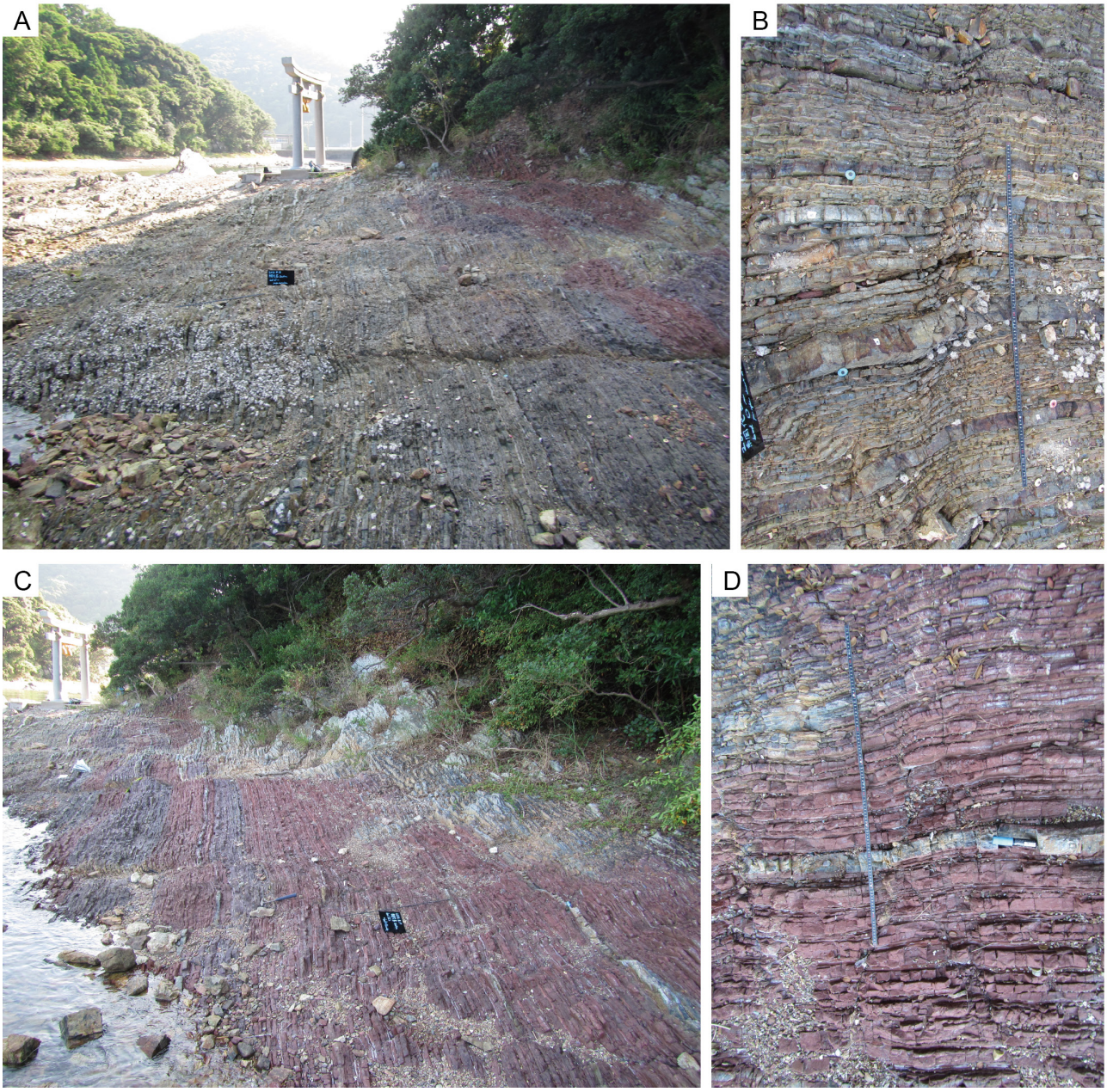

Fig. 8 Outcrop photographs of the AJR section. (A) The upward lithofacies change from greenish grey bedded chert to purple and red bedded chert. (B) Greenish grey bedded chert. (C) Purple and red bedded chert. (D) Red bedded chert. Note that the colour is altered to greenish grey in some parts. The stratigraphic way up is to the right in (A) and (C), and to the top in (B) and (D). The black ruler and board in the photos as scale are the same as that in Fig. 7.

(p.53) Fig. 9
Lithostratigraphy, conodont biostratigraphy, radiolarian biostratigraphy and magnetostratigraphy of the Ajiro Island section. The range chart for conodonts excludes some specimens that were not identified at the species level. See Table 1 for full list and numbers of identified conodonts. Radiolarian biostratigraphy is after Onoue *et al.* (2011) and Uno *et al.* (2012). Magnetic polarity zones are after Uno *et al.* (2012). *brevissimus-collinsoni* Zone: *Nv. brevissimus-I. collinsoni* Zone; *timorensis* Z.: *Ch. timorensis* Zone; *excelsa* Z.: *Pg. excelsa* Zone. The species names denoted in quotation marks are form species defined based on discrete conodont elements.

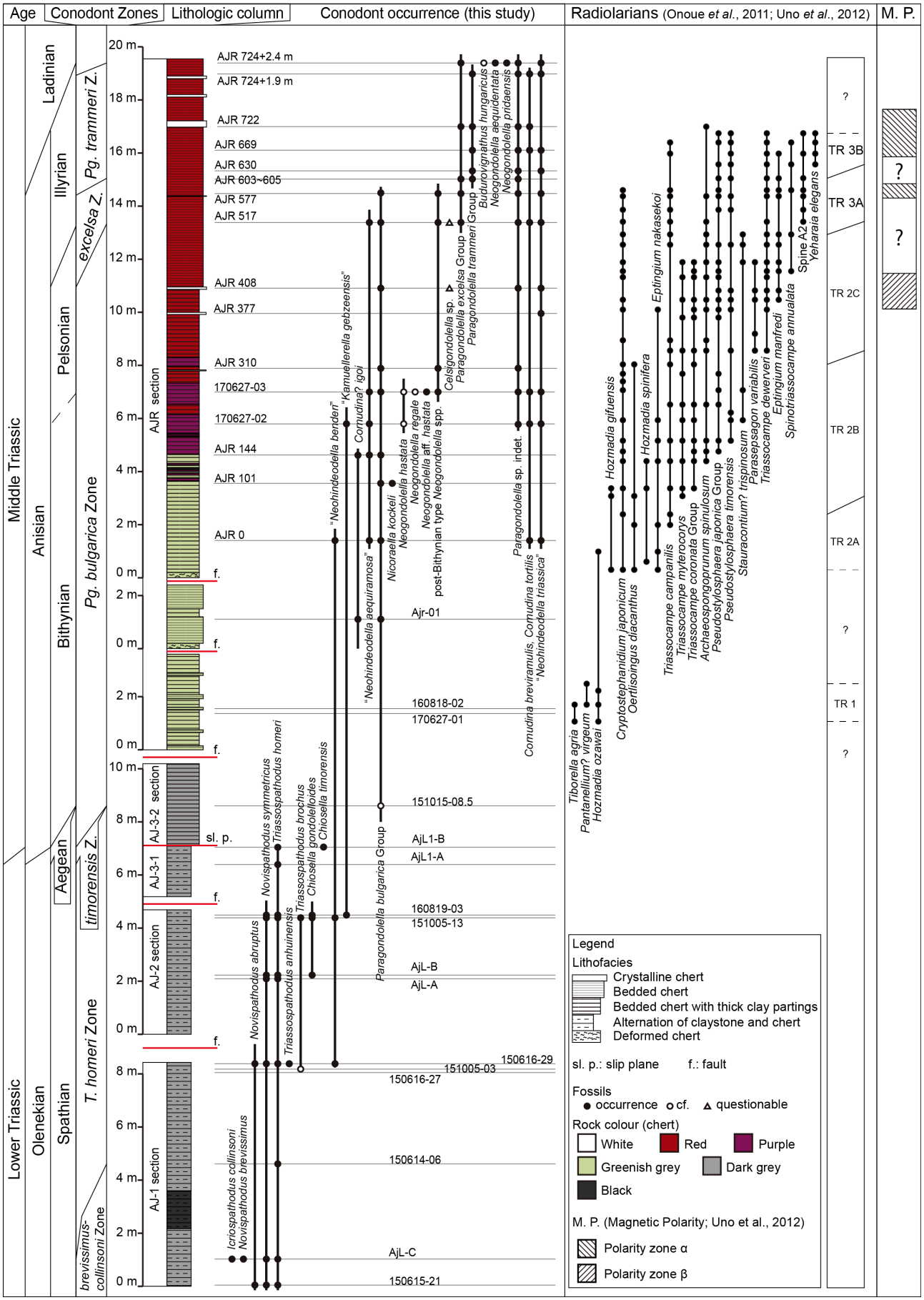
Age
Conodont Zones
Lithologic column
Conodont occurrence (this study)
Radiolarians (Onoue et al., 2011; Uno et al., 2012)
M. P.
Middle Triassic
Lower Triassic
Anisian
Olenekian
Ladinian
Illyrian
Pelsonian
Bithynian
Aegean
Spathian
Pg. trammeri Z.
excelsa Z.
Pg. bulgarica Zone
timorensis Z.
T. homeri Zone
brevissimus-collinsoni Zone
AJR section
AJ-3-2 section
AJ-3-1
AJ-2 section
AJ-1 section
AJR 724+2.4 m
AJR 724+1.9 m
AJR 722
AJR 669
AJR 630
AJR 603~605
AJR 577
AJR 517
AJR 408
AJR 377
AJR 310
170627-03
170627-02
AJR 144
AJR 101
AJR 0
Ajr-01
160818-02
170627-01
151015-08.5
AjL1-B
AjL1-A
160819-03
151005-13
AjL-B
AjL-A
150616-29
151005-03
150616-27
150614-06
AjL-C
150615-21
"Neohindeodella benderi"
"Kamuellerella gebzeensis"
Comudina? igoi
"Neohindeodella aequiramosa"
Nicoraella kockeli
Neogondolella hastata
Neogondolella regale
Neogondolella aff. hastata
post-Bithynian type Neogondolella spp.
Celsigondolella sp.
Paragondolella excelsa Group
Paragondolella trammeri Group
Budurovignathus hungaricus
Neogondolella aequidentata
Neogondolella pridaensis
Paragondolella sp. indet.
Comudina breviramulis, Comudina tortilis
"Neohindeodella triassica"
Paragondolella bulgarica Group
Novispathodus symmetricus
Triassospathodus homeri
Triassospathodus brochus
Chiosella gondolelloides
Chiosella timorensis
Novispathodus abruptus
Triassospathodus anhuinensis
Icriospathodus collinsoni
Novispathodus brevissimus
Tiborella agria
Pantanellium? virgeum
Hozmadia ozawai
Cryptostephanidium japonicum
Oertlisoingus diacanthus
Hozmadia gifuensis
Hozmadia spinifera
Triassocampe campanilis
Triassocampe myterocorys
Triassocampe coronata Group
Archaeospongoprunum spinulosum
Pseudostylosphaera japonica Group
Pseudostylosphaera timorensis
Stauracontium? trispinosum
Parasepsagon variabilis
Triassocampe deweverii
Eptingium manfredi
Spinotriassocampe annualata
Spine A2
Yeharaia elegans
Eptingium nakasekoi
TR 3B
TR 3A
TR 2C
TR 2B
TR 2A
TR 1
Legend
Lithofacies
Crystalline chert
Bedded chert
Bedded chert with thick clay partings
Alternation of claystone and chert
Deformed chert
sl. p.: slip plane
f.: fault
Fossils
occurrence
cf.
questionable
Rock colour (chert)
White
Red
Purple
Greenish grey
Dark grey
Black
M. P. (Magnetic Polarity; Uno et al., 2012)
Polarity zone α
Polarity zone β

Table 1. Occurrence list of conodonts from the Ajiro Island section. Underlined numbers indicate the number of conferred specimens. Bracketed numbers indicate the number of questionable specimens. The species names denoted in quotation marks are form species defined based on discrete conodont elements.

	Icriospathodus collinsoni (Solien)	*Novispathodus brevissimus* (Orchard)	*Novispathodus* sp.	*Nv. abruptus* (Orchard)	*Nv. symmetricus* (Orchard)	*Triassospathodus homeri* (Bender)	*T. anhuinensis* (Ding)	*T. brochus* (Orchard)	*Triassospathodus* sp.	*Triassospathodus* or *Novispathodus* sp.	*Chiosella gondolelloides* (Orchard)	*Chiosella* sp.	*Chiosella timorensis* (Nogami)	"*Neohindeodella benderi* (Kozur & Mostler)"	"*Kamuellerella gebzeensis* Gedik"	*Cornudina? igoi* Koike	"*Nh. aequiramosa* Kozur & Mostler"	*Paragondolella bulgarica* Group	*Nicoraella kockeli* (Tatge)	*Nicoraella* sp.	*Neogondolella* sp.	*Ng. hastata* Golding & Orchard	*Neogondolella regale* Mosher	*Neogondolella* spp. or *Paragondolella* sp.	*Ng.* aff. *hastata* Golding & Orchard	post-Bithynian type *Neogondolella* sp.	*Celsigondolella* sp.	*Pg. excelsa* Group	*Pg. trammeri* Group	*Budurovignathus hungaricus* (Kozur & Vegh)	*Ng. aequidentata* Kozur et al.	*Ng. pridaensis* (Nicora)	*Cornudina breviramulis* (Tatge)	*Co. tortilis* (Kozur & Mostler)	*Paragondolella* sp.	*Cornudina* sp.	"*Nh. triassica* (Müller)"	"*Neohindeodella* sp."
AJR724+2.4m																											1		2	1	1			3 (13)	(1)	3	
AJR724+1.9m																		1										2			1	3	7 (8)		3	5
AJR722																											1 1	1				1	6 (2)			1
AJR669																												1				1	1		1	
AJR630																												3					3 (2)	(1)	1	
AJR603-605																											2	1					3 (2)			
AJR577																	3 2									1	3						1 (2)		2	
AJR517																1	5									1	(1)	1				2	6 (1)		3	1
AJR408																	3										(3)						3		3	
AJR377																																			2	
AJR310																	3									1							1			

170627-03																	1				6	2	2	4	2	5	2	5	3		
170627-02															2		3			2		2					1	1 (1)	1	1	
AJR144																1	1	7			1							(1)		2	
AJR101																		2 1	1												
AJR 0														2	1	1	3	3									1			1	2
Ajr-01																		1													
160818-02	no identifiable elements																														
170627-01	no identifiable elements																														
151015-08.5																		1													
AjL1-B						2							1																		2
AjL1-A						1			1			1																			
160819-03			1		8 1	5				2	1				1																3
151005-13			1		9	12		2 1	2		3	1		1																	5
AjL-B			1		2	5					1																				2
AjL-A					1 1	2																									
150616-29			1	1	1 1	2	1		(1)					1																	
151005-03								1																							
150615-27	no identifiable elements																														
150614-06			1 (1)			1 1									1																
AjL-C	1	1	1		2	1																									5
150615-21			2	1	3	1																									

with chert in the AJ-1, AJ-2 and AJ3-1 sections include many adult specimens, but conodonts from the bedded chert in the AJR section are mostly juvenile forms. Especially, species of *Paragondolella*, which occurred abundantly from the AJR section, are almost entirely represented by juvenile stages with incomplete platform development.

Species belonging to the genus *Paragondolella* are difficult to distinguish in juvenile forms. Identification of our specimens is further hindered by the fact that they are partly immersed in the host rock. Hence, in the case of specimens of *Paragondolella*, we referred to a group of species that share some important morphological characters (see the palaeontological notes in Chapter 9 for details). Specifically, three "Groups" are used in this paper: the *Paragondolella bulgarica* Group (*Pg. bulgarica*, *Paragondolella bifurcata* and *Paragondolella hanbulogi*), the *Paragondolella excelsa* Group (*Pg. excelsa*, *Paragondolella fueloepi* and *Paragondolella liebermani*), and the *Paragondolella trammeri* Group (*Pg. trammeri* and *Paragondolella alpina*). Note that these "Groups" do not necessarily represent taxonomic lineages.

Based on the occurrence of conodonts, six conodont biozones were recognised in the Ajiro Island section: the *Novispathodus brevissimus-Icriospathodus collinsoni* Zone, the *Triassospathodus homeri* Zone, the *Chiosella timorensis* Zone, the *Pg. bulgarica* Zone, the *Pg. excelsa* Zone and the *Pg. trammeri* Zone in ascending order (Fig. 9).

The *Nv. brevissimus-I. collinsoni* Zone is characterised by the occurrence of *Nv. brevissimus* and *I. collinsoni.* Its base is not defined in the Ajiro Island section and its top is defined by the last occurrence (LO) of the two species. This zone is recognised in the lowermost part of the AJ-1 section (Fig. 9). Other associated species are *Novispathodus abruptus*, *Novispathodus symmetricus* and *T. homeri*.

The *T. homeri* Zone is characterised by the occurrence of *Nv. abruptus*, *Nv. symmetricus* and *T. homeri*. Its base is defined by the LO of *Nv. brevissimus* and *I. collinsoni* and its top is defined by the first occurrence (FO) of *Ch. timorensis*. This zone is recognised in the main part of the AJ-1 section and the lower part of the AJ-2 section (Fig. 9). Other associated species are *Chiosella gondolelloides*, *Triassospathodus anhuinensis* and "*Neohindeodella benderi*".

The *Ch. timorensis* Zone is characterised by the occurrence of *Ch. timorensis*. Its base is defined by the FO of the nominal species and its top is defined by the FO of the *Pg. bulgarica* Group. This zone is recognised in the AJ-3-1 section (Fig. 9). *T. homeri* also occurred from this zone.

The *Pg. bulgarica* Zone is characterised by the occurrence of the *Pg. bulgarica* Group. Its base is defined by the FO of the *Pg. bulgarica* Group and its top is defined by the FO of the *Pg. excelsa* Group. This zone is recognised in the AJ-3-2 section and the lower to middle part of the AJR section (Fig. 9). "*Nh. benderi*", *Cornudina*? *igoi* and "*Kamuellerella gebzeensis*" occurred from the lower part of this zone. The middle part of this zone yielded *Neogondolella* cf. *hastata*, in addition to *Ng*. aff. *hastata* and *Neogondolella* cf. *regale*, as well as species of *Neogondolella* with a large cusp that is fused to the posterior platform brim (post-Bithynian type *Neogondolella*; detailed explanation in Section 5.3.). Other associated species are *Cornudina breviramulis*, "*Neohindeodella aequiramosa*" and "*Neohindeodella triassica*".

The *Pg. excelsa* Zone is characterised by the occurrence of the *Pg. excelsa* Group. Its base is defined by the FO of the *Pg. excelsa* Group and its top is defined by the FO of the *Pg. trammeri* Group. This zone is recognised in the upper part of the AJR section (Fig. 9). Other associated conodonts are the *Pg. bulgarica* Group, *Co. breviramulis*, "*Nh. aequiramosa*" and "*Nh. triassica*".

The *Pg. trammeri* Zone is characterised by the occurrence of the *Pg. trammeri* Group. Its base is defined by the FO of the *Pg. trammeri* Group and its top is defined by the FO of *Budurovignathus* cf. *hungaricus*. This zone is recognised in the uppermost part of the AJR section (Fig. 9). Other associated conodonts are the *Pg. excelsa* Group, *Co. breviramulis*, *Cornudina tortilis* and "*Nh. triassica*". At the top of this zone, *Neogondolella aequidentata* and *Neogondolella pridaensis* co-occurred with *B.* cf. *hungaricus*.

4. 2 Kurusu section

4. 2. 1 Field mapping

The Kurusu section is exposed on the east bank of the Kiso River in Kurusu, Inuyama City, Aichi Prefecture, Chubu District (Fig. 3). Strata in this outcrop are deformed by many faults and folds (Fig. 10). The outcrop is divided into two parts that have different lithology by a fault ("dividing fault" in Fig. 10). The eastern part includes the area mapped by Yao and Kuwahara (1997), and the section observed in this part of the outcrop is named the Kr-2-YK section (Fig. 10). The western part was studied by Ikeda *et al.* (2010), and the section observed here is named the Kr-2-I section.

The outcrop of the Kr-2-YK section has a complicated geological structure (Fig. 10). The orientation of the bedding plane is variable due to folding. Tracing of characteristic black claystone and black chert beds revealed that the lower part of this section is repeated by folds. In some parts, the bedding of the strata was difficult to identify due to strong deformation. The Kr-2-YK section was observed in parts of the outcrop where deformation was minimal, which include the area studied by Yao and Kuwahara (1997). The Kr-2-YK section is composed mainly of grey bedded chert with intercalations of grey siliceous claystone (Fig. 11A). Black claystone and black chert beds also occur in several horizons. The transition between grey chert layers and grey siliceous claystone layers is gradual. Therefore, the contrast

between the chert layers and the siliceous claystone layers is not strongly expressed in the configuration of the outcrop surface. This may have led to the description of the strata as "siliceous claystone" by Yao and Kuwahara (1997). However, the rocks have moderate vitreous luster and are not fissile, which indicate that its lithology is better described as chert. This is further supported by the presence of numerous radiolarian tests and quartz matrix confirmed in thin sections (Fig. 11D). Dolomite occurs as beds or planar nodules in two horizons. The lithology of the Kurusu section deserves further detailed observation, because it likely represents a transitional lithofacies between the Lower Triassic siliceous claystone ("Toishi"; Imoto, 1984) and Middle Triassic bedded chert. However, it is beyond the scope of this paper, and we will tentatively refer to the chert beds that grade into siliceous claystone as "muddy" chert.

The section studied by Yao and Kuwahara (1997), which corresponds directly to the upper 7 m of the Kr-2-YK section, was regarded as continuous in the previous studies. However, a fault was identified in the middle part of this interval (Fig. 11C). This fault is accompanied by a highly deformed sheared zone on both sides of the fault plane. Therefore, the displacement and consequent stratigraphic gap of this fault could be considerable.

The Kr-2-I section is composed mainly of "muddy" chert with intercalations of black claystone (Figs. 10, 11B). Intense folding such as that observed in the outcrop of the Kr-2-YK section is not observed in this part of the outcrop. However, the strata have experienced significant deformation, represented by the distortion of the bedding by numerous cm-scale faults and slip planes (Fig. 11B). The Kr-2-I section corresponds almost exactly to the section reported by Ikeda *et al.* (2010), but was not observed in exactly the same part of the outcrop, because some parts that they observed had become covered by thick gravel. Ikeda *et al.* (2010) assumed that the stratigraphic way up in this section is to the northeast. However, the general younging of the strata is to the southwest in this part of the Inuyama area (see Section 2.2.), which is consistent with outcrop-scale biostratigraphy in the Kurusu section (Yao and Kuwahara, 1997). Therefore, it would be more orthodox to assume that the stratigraphic way up is to the southwest, which will be adopted in this study. Nonetheless, it should be noted that the way up in the Kr-2-I section remains indeterminate, even considering our biostratigraphic data presented in Subsection 4.2.2.

4. 2. 2 Conodont biostratigraphy

Conodonts were found from all of the investigated samples (more than 200 specimens in total). Conodonts occurred as dark grey skeletons. Although most conodonts were broken, 28 specimens were identified at the species level (Table 2; Plates 8–10). Since conodont occurrence from the Kurusu section is sporadic, independent zonation for this section will not be defined. Instead, we will refer to the conodont biozones recognised in the Ajiro Island section (Fig. 12).

The Kr-2-YK section yielded *Ch. timorensis* and "*Nh. aequiramosa*". These conodonts indicate that the Kr-2-YK section is mostly correlative to the *Ch. timorensis* Zone.

The Kr-2-I section yielded *Nv. symmetricus*, *T. homeri*, *Ch. gondolelloides* and "*Nh. benderi*". These conodonts indicate that the Kr-2-I section is referable to the *T. homeri* Zone. *Co. breviramulis*, *Co.*? *igoi*, *Neostrachanognathus tahoensis* and "*K. gebzeensis*" also occurred from this section. Since the Kr-2-YK section is referable to the *Ch. timorensis* Zone, the Kr-2-I section is stratigraphically below the Kr-2-YK section. Ikeda *et al.* (2010) and Ikeda and Tada (2014) argued that the Kr-2-I section and Section M of Sugiyama (1997) in the Inuyama area can be partly correlated by key beds to produce a continuous lithostratigraphy, based on the assumption that the Kr-2-I section is equivalent to the Kr-2-YK section. However, since the Kr-2-I section does not overlap with the Kr-2-YK section, their correlation is not valid. Consequently, the lowermost part of the composite section of the Inuyama bedded chert by Ikeda *et al.* (2010) and Ikeda and Tada (2014) that concerns the Kr-2-I section is not continuous.

5. Age assignment of the conodont biozones

5. 1 The Lower-Middle Triassic (Olenekian-Anisian) boundary (OAB)

The global boundary stratotype section and point (GSSP) for the Olenekian-Anisian boundary (OAB) is yet to be ratified. The Desli Caira section in north Dobrogea, Romania has been proposed as a candidate (Gradinaru *et al.*, 2007), while the Guandao section in Guizhou Province, South China is a potential reference section (Ogg, 2012). The OAB is classically defined by the ammonoid *Japonites welteri* (Balini *et al.*, 2010; Bucher, 1989). This has been applied to the Desli Caira section (Gradinaru *et al.*, 2007), but the Guandao section lacks a significant ammonoid fauna (Ogg, 2012). On the other hand, Orchard *et al.* (2007a, b) and Orchard (2010) proposed that the first appearance datum (FAD) of *Chiosella timorensis*, that occurs readily from both Desli Caira and Guandao, can be used as a marker for the OAB. Subsequently, Goudemand *et al.* (2012) concluded that the FAD of *Ch. timorensis* is very close to, but is slightly below the ammonoid-defined OAB and is within the uppermost Spathian. Based on high-resolution investigation of conodont biostratigraphy in the Desli Caira section and the Guandao section, Goudemand *et al.* (2012) placed the OAB above the FAD of *Ch. timorensis* and below the last appearance datum (LAD) of *Novispathodus symmetricus* and *Triassospathodus homeri*, so that the ammonoid based age assignment (Bucher, 1989) is followed. Our definition of the OAB will follow that by Goudemand *et al.* (2012).

In the Ajiro Island section, the first occurrence (FO) of *Ch. timorensis* and the last occurrence (LO) of *T. homeri* are both at the level of Sample AjL1-B, which is the base of the *Ch. timorensis* Zone (Fig. 9). Therefore, the OAB

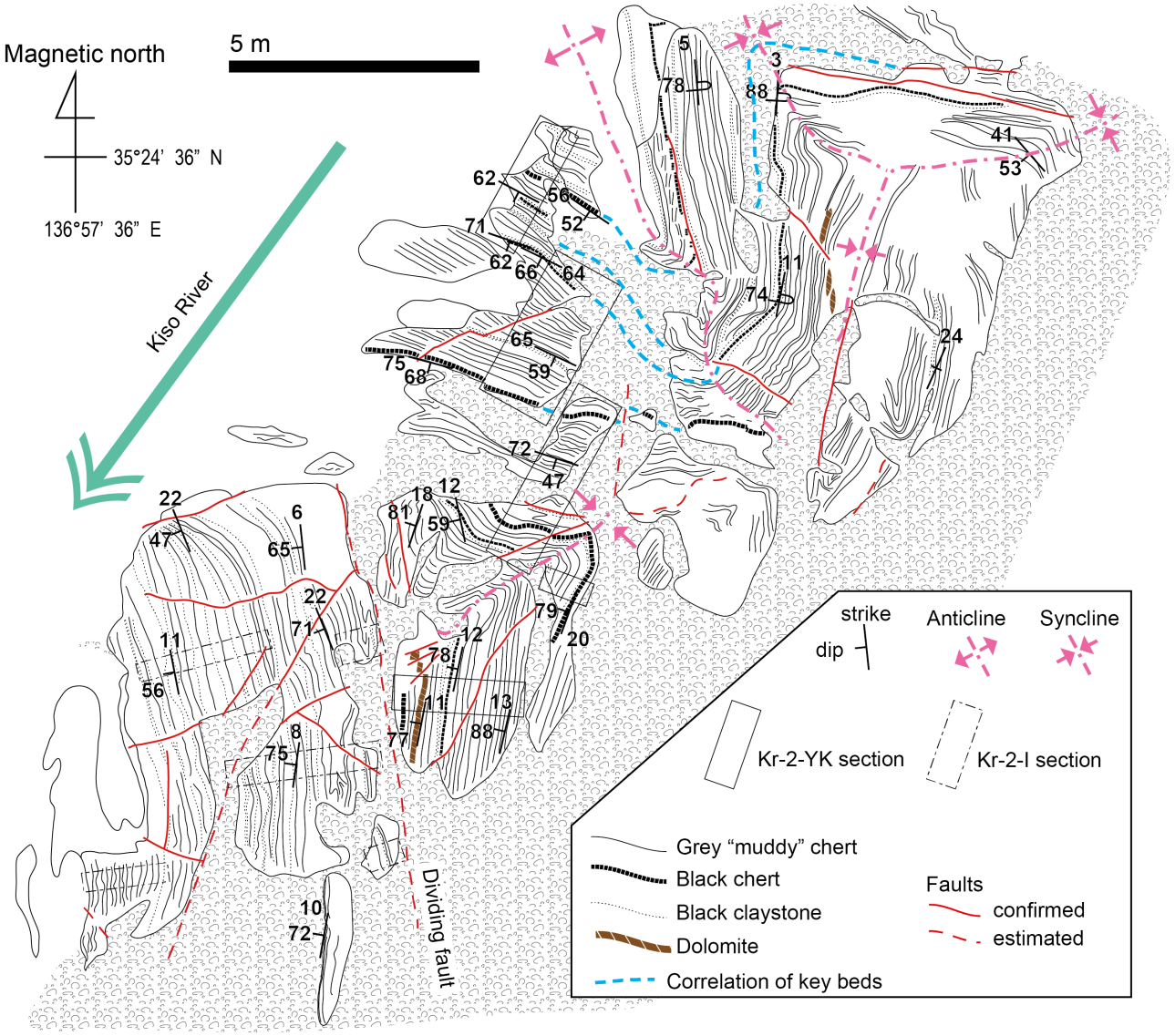

Fig. 10 Geological map of the outcrop of the Kurusu section. Note that the Kr-2 section of Yao and Kuwahara (1997) and Ikeda *et al.* (2010) (Kr-2-YK and Kr-2-I sections, respectively) correspond to different parts of the outcrop.

is placed between the level of Sample AjL1-B and the level of Sample AjL1-A. The placement of the OAB at the base of the *Ch. timorensis* Zone indicates that the underlying *Novispathodus brevissimus-Icriospathodus collinsoni* Zone and the *T. homeri* Zone are of Olenekian age. The occurrence of *Nv. brevissimus* and *I. collinsoni* is confined to the basal part of the Spathian (Chen *et al.*, 2015; Koike, 1981, 2004; Orchard, 1995, 2007; Zhao *et al.*, 2007). Therefore, the *Nv. brevissimus-I. collinsoni* Zone is correlated to the lower Spathian, and the succeeding *T. homeri* Zone to the upper Spathian.

In the Kurusu section, *Nv. symmetricus* and *T. homeri* did not co-occur with *Ch. timorensis*. Therefore, the interval referred to the *Ch. timorensis* Zone in this section is likely to be of Anisian age. Thus, the OAB is in the lower 1 m or below the base of the Kr-2-YK section (Fig. 12).

The thickness of the *Ch. timorensis* Zone is different between the Ajiro Island and Kurusu sections. An explanation can be given by the slip plane between the AJ-3-1 section and the AJ-3-2 section at Ajiro Island. That is, lowermost Anisian strata are missing at the slip plane above the *Ch. timorensis* Zone in the Ajiro Island section. If this is the case, the *Ch. timorensis* Zone in the Kurusu section mostly corresponds in age to an interval that is missing at the slip plane in the Ajiro Island section.

5. 2 The Anisian-Ladinian boundary (ALB)

The Anisian-Ladinian boundary (ALB) was ratified at the base of the *Eoprotrachyceras curionii* ammonoid zone in the Bagolino section in Brescia, Northern Italy (Brack, 2010; Brack *et al.*, 2005). This horizon is above the FO of species belonging to the *Paragondolella trammeri* Group

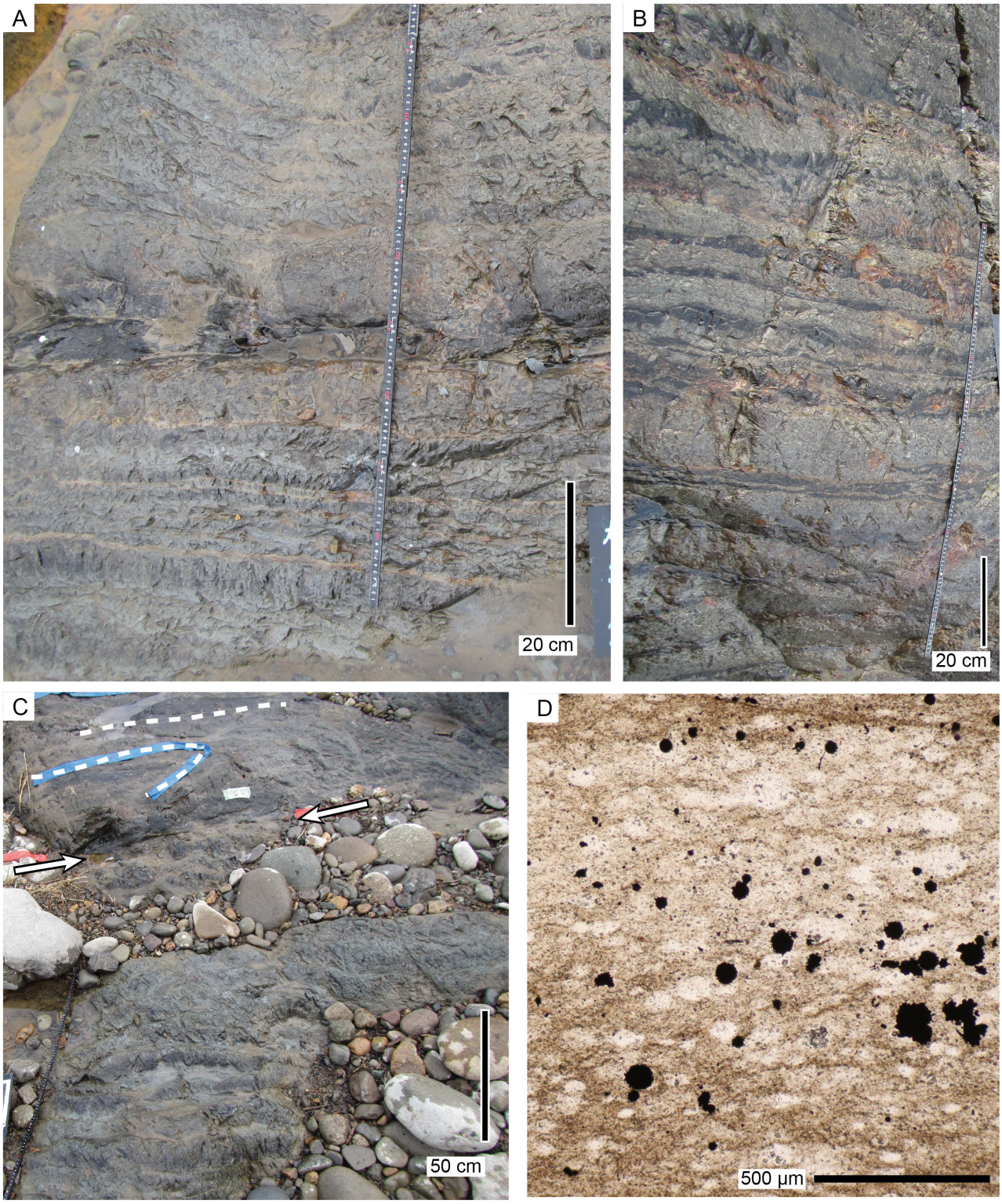

Fig. 11 (A–C) Outcrop photographs of the Kurusu section. (A) The Kr-2-YK section. (B) The Kr-2-I section. (C) The fault in the Kr-2-YK section. The fault runs between the arrows. Broken lines represent bedding planes. (D) Photo-micrograph of muddy chert from the Kr-2-YK section viewed in plane-polarised light.

Table 2 Occurrence list of conodonts from the Kurusu section. Underlined numbers indicate the number of conferred specimens. The species names denoted in quotation marks are form species defined based on discrete conodont elements.

	Cornudina breviramulis (Tatge)	*Cornudina? igoi* Koike	*Neostrachanognathus tahoensis* Koike	*Novispathodus symmetricus* (Orchard)	*Novispathodus* sp.	*Triassospathodus homeri* (Bender)	*Chiosella gondolelloides* (Orchard)	"*Kamuellerella gebzeensis* Gedik"	"*Neohindeodella benderi* (Kozur & Mostler)"	"*Nh. aequiramosa* Kozur & Mostler"	*Ch. timorensis* (Nogami)	*Chiosella* sp.	"*Neohindeodella* sp."
Kr2-YK section													
Kr1-02											2	1	
Kr1-03										1	1		
Kr1-04											3 1	3	1
Kr1-05	no identifiable elements												
Kr-2-I section													
Kr2-03					3	1	1	1	1			1	
Kr2-01	2	1	1	3	2	1	1		3 1				

and below the FO of *Budurovignathus hungaricus* (Brack *et al.*, 2005). The same is true for the ALB (the base of the *curionii* amonnoid zone) in the Balaton Highland, Hungary (Kovács, 1994). Therefore, the ALB can be placed within the *Pg. trammeri* Zone in the Ajiro Island section (Fig. 9). In the GSSP, the FO of the conodont *Budurovignathus praehungaricus* is very close to the ALB (Brack *et al.*, 2005), and provides a good correlation marker for the boundary (Chen *et al.*, 2016b; Ogg, 2012; Orchard, 2010). However, this species has not been found from the Ajiro Island section. Another potentially useful marker species is *Neogondolella aequidentata*, which has a short range straddling the ALB (Chen *et al.*, 2016b; Muttoni *et al.*, 2004; Orchard, 2010). In the Ajiro Island section, *Ng. aequidentata* occurred from the top of the *Pg. trammeri* Zone, suggesting that the ALB is near this horizon in the upper part of the zone.

5. 3 The Anisian substages

The Anisian Stage is divided into four substages: Aegean, Bithynian, Pelsonian and Illyrian in ascending order. The Aegean is characterised by *Ch. timorensis* all over the world (Chen *et al.*, 2016b; Lehrmann *et al.*, 2015; Nicora, 1977). In Europe and North America, the Bithynian is characterised by *Paragondolella bulgarica* (Nicora, 1977), and the Pelsonian is characterised by *Nicoraella kockeli* (Nicora, 1976; Pisa *et al.*, 1980). On the other hand, *Ni. kockeli* occurs from below the FO of *Pg. bulgarica* in South China (Lehrmann *et al.*, 2015). Hence, the stratigraphic order of the FOs of these species requires further investigation, and the recognition of the Pelsonian based on the occurrence of *Ni. kockeli* may not be valid on the global scale. In any case, the occurrence of *Ni. kockeli* from our studied sections is too sporadic to determine substage boundaries. Therefore, we refrain from conclusively determining the Bithynian-Pelsonian boundary. Based on the fact that species of the *Paragondolella excelsa* Group characterises the Illyrian (Kozur, 1980), the *Pg. bulgarica* Zone is correlated to the Bithynian to Pelsonian interval, and the *Pg. excelsa*

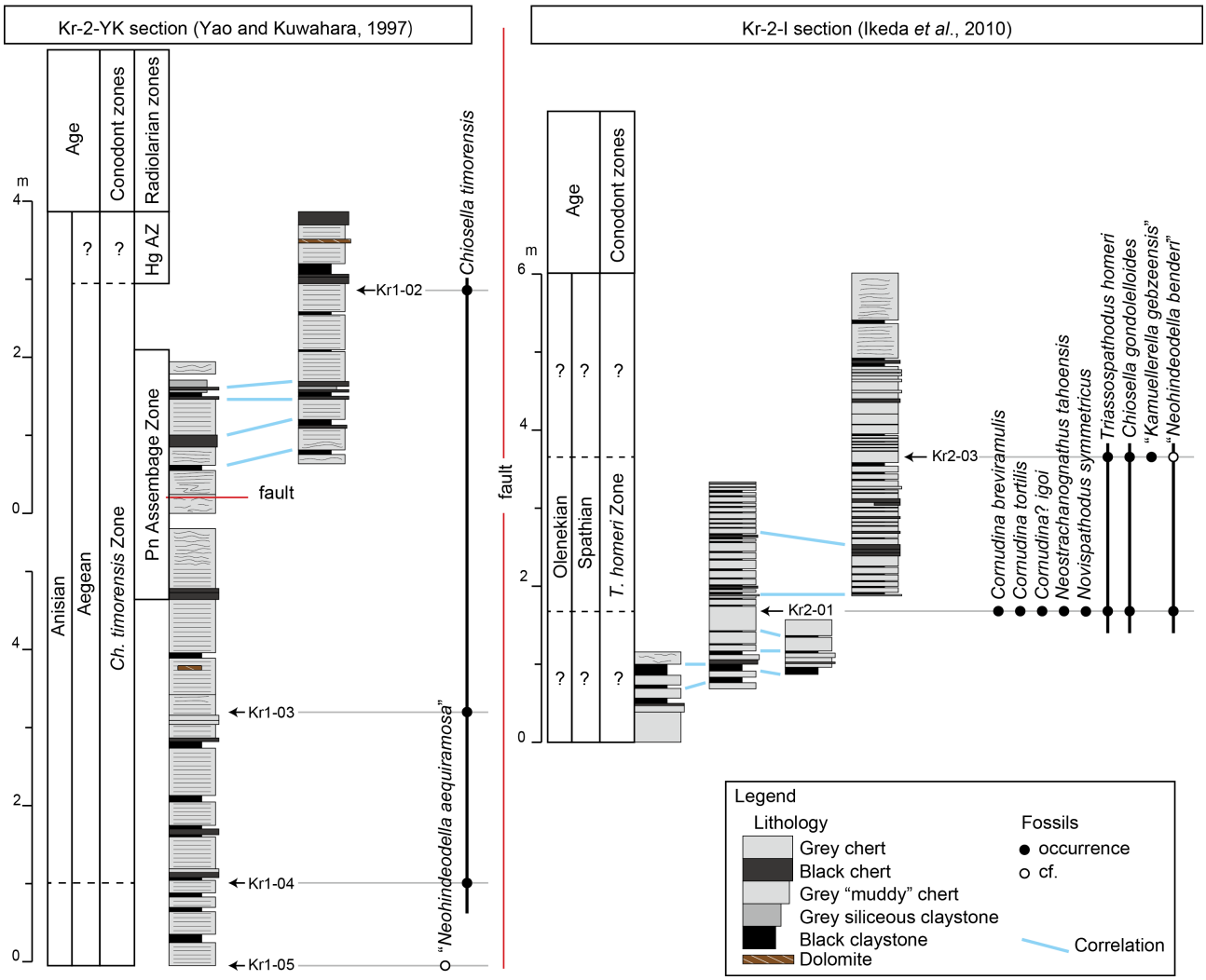

Fig. 12 Lithostratigraphy and conodont occurrence of the Kurusu section. The radiolarian biozones for the Kr-2-YK section are after Yao and Kuwahara (1997). Pn Assemblage Zone: *Parentactinia nakatsugawaensis* Assemblage Zone. Hg AZ: *Hozmadia gifuensis* Assemblage Zone. The species names denoted in quotation marks are form species defined based on discrete conodont elements.

Zone to the lower Illyrian (the Illyrian likely extends to the lower part of the *Pg. trammeri* Zone; see section 5.2) (Fig. 9).

It is notable that a type of *Neogondolella* characteristic to the Pelsonian and younger age occurs from the upper part of the *Pg. bulgarica* Zone. These are species of *Neogondolella* that possess a large cusp that is fused to the posterior platform margin and occupies the posterior end of the element. Such forms can be referred to species such as *Neogondolella cornuta*, *Neogondolella constricta* and *Neogondolella shoshonensis*. In fact, some of our specimens have characteristics that may be referable to *Ng. shoshonensis* (Plate 3, Figs. 5, 6). The species of *Neogondolella* mentioned above are known only from the Pelsonian and younger strata (Chen *et al.*, 2016b). Therefore, we refer to them as post-Bithynian type *Neogondolella*. In the Ajiro Island section, the FO horizon of the post-Bithynian type *Neogondolella* is sample 170627-03 and the Bithynian-Pelsonian boundary may be placed at this horizon (Fig. 9).

6. Age calibration of the radiolarian biozones

According to the radiolarian zonation proposed by Sugiyama (1997), the OAB was regarded to be correlative to the TR 1-TR 2A radiolarian biozone boundary, and the ALB to the TR 3A-TR 3B radiolarian biozone boundary. Our conodont-based age control proved that the age assignment is erroneous for the TR 1-TR 2A boundary, and probably also for the TR 3A-TR 3B boundary (Fig. 13). In the following text, the age calibration of the radiolarian biozones TR 1 to TR 3B (Sugiyama, 1997) is discussed in ascending order.

In the Ajiro Island section, the TR 1 Zone was

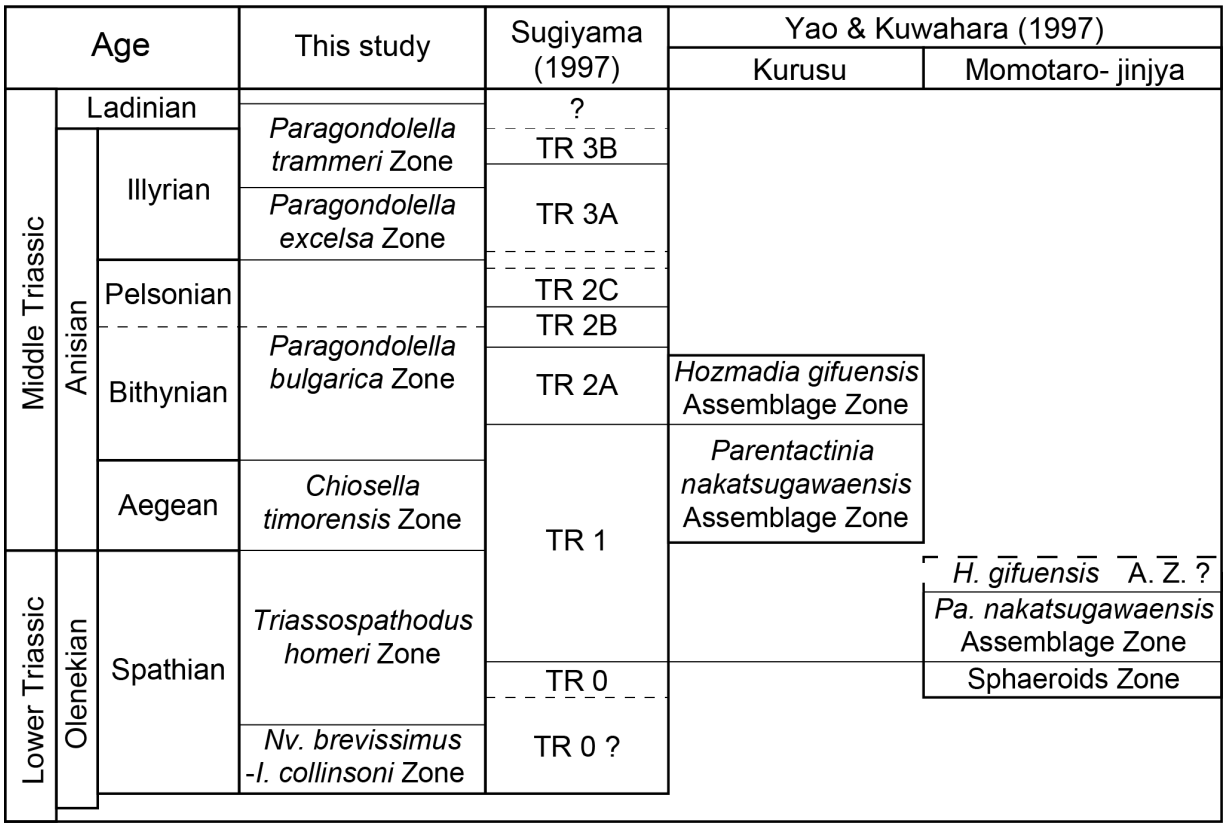

Fig. 13 Age calibration of the Anisian radiolarian biozones. Dashed lines represent uncertain boundaries. The *Nv. brevissimus-I. collinsoni* Zone was not recognized in the sections of Sugiyama (1997), but is inferred to be encompassed in the TR 0 Zone, because conodonts from the Momotaro-jinja section indicate that the TR 0 Zone extends to the Smithian (Yamakita *et al.*, 2010).

recognised in the *Paragondolella bulgarica* Zone, well above the OAB (Onoue *et al.*, 2011; Uno *et al.*, 2012) (Fig. 9). In the Kurusu section, the TR 1-TR 2A boundary is approximated by the boundary between the *Parentactinia nakatsugawaensis* Asemblage Zone and the *Hozmadia gifuensis* Assemblage Zone (Yao and Kuwahara, 1997), which is well above the base of the *Chiosella timorensis* Zone (Fig. 12). Thus, the TR 1 Zone includes part of the *Pg. bulgarica* Zone, which is of Bithynian to Pelsonian age. This age assignment is consistent with the finding of a radiolarian assemblage indicating the TR 1 Zone from the Bithynian to Pelsonian interval in the pelagic deep-sea Ogama section in Kuzuu, Tochigi Prefecture, Japan (Muto *et al.*, 2018). On the other hand, pelagic deep-sea siliceous claystone correlative with the TR 1 Zone and the underlying TR 0 Zone in the Momotaro-jinja section in the Inuyama area (Sugiyama, 1997; Yao and Kuwahara, 1997) yielded Spathian conodonts *Novispathodus symmetricus* and "*Neohindeodella benderi*" (Takahashi *et al.*, 2009). Based on data of the Ajiro Island section, the Kurusu section and the Momotaro-jinja section, the TR 1 Zone is correlated to the upper Spathian to the lower part of the Bithynian to Pelsonian interval, and the OAB is within this zone (Fig. 13).

The entire part of the TR 2A and TR 2B Zones and most of the TR 2C Zone is encompassed in the *Pg. bulgarica* Zone, and is correlated to the Bithynian to Pelsonian interval (Figs. 9, 13). This age assignment is consistent with the occurrence of *Pg. bulgarica* from the TR 2B and TR 2C Zones reported from bedded chert sections in the Inuyama area (Mizutani and Koike, 1982; Sugiyama, 1997). If the placement of the Bithynian-Pelsonian boundary at the FO of post-Bithynian type conodonts in the Ajiro Island section is correct, this boundary is within the TR 2B Zone (Figs. 9, 13). The TR 3A Zone is mostly correlated to the Illyrian *Paragondolella excelsa* Zone, but its base may be within the uppermost part of the *Pg. bulgarica* Zone, and its top is in the basal part of the *Paragondolella trammeri* Zone (Figs. 9, 13). It is possible that the upper part of the TR 3A Zone extends into the Ladinian (Fig. 13), but this is unlikely given that the ALB is probably in the upper part of the *Pg. trammeri* Zone (detailed in Section 5.4.).

The top of the TR 3B Zone was not recognised in the Ajiro Island section (Onoue *et al.*, 2011; Uno *et al.*, 2012). We assume that only the lower part of the TR 3B Zone of Sugiyama (1997) is present in the Ajiro Island section, because it lacks radiolarians such as *Triassocampe*

postdewerveri that appear in the upper part of the TR 3B Zone (Onoue *et al.*, 2011; Uno *et al.*, 2012). The lower part of the TR 3B Zone is within the *Pg. trammeri* Zone, and therefore falls within the upper Illyrian to the lower Fassanian (lower substage of the Ladinian). Since the ALB is probably in the upper part of the *Pg. trammeri* Zone, the lower part of the TR 3B Zone is likely to be correlative to the upper Illyrian (uppermost Anisian). Unfortunately, radiolarian biostratigraphy has not been investigated for the upper part of the *Pg. trammeri* Zone. Therefore, we cannot determine whether the TR 3B Zone extends above the top of the *Pg. trammeri* Zone. Further study is needed in order to clarify the age of the top of the TR 3B Zone.

7. Correlation with rock magnetic records

The Ajiro Island section has been studied for rock magnetic records by Uno *et al.* (2012), who recognised two magnetic polarity zones in the red bedded chert. A reference record of Middle Triassic magnetic reversals was compiled by Hounslow and Muttoni (2010) based mainly on sedimentary records of the Tethys, many of which have been studied also for conodont biostratigraphy. We attempted to correlate the rock magnetic records of the Ajiro Island section to the reference record by Hounslow and Muttoni (2010) based on the framework of conodont biostratigraphy (Fig. 14). However, a single solution was not obtained and there are two possible options, as detailed below.

In Option 1 (Fig. 14A), polarity zone β in the Ajiro Island section is correlated to the reversed polarity in magnetozone MT4 to MT5. The two stratigraphically isolated intervals of polarity zone α are either correlated to the two separate normal polarities in magnetozones MT6 and MT7, or together correlated to the normal polarity in magnetozone MT7. In this case, the ALB in the Ajiro Island section is above polarity zone α and below the FO of *Budurovignathus* cf. *hungaricus*, within the upper 1.5 m of the *Pg. trammeri* Zone. This option agrees with Uno *et al.* (2012) in that polarity zone α is correlated to a normal polarity and polarity zone β to a reversed polarity, suggesting deposition in the southern hemisphere.

In Option 2 (Fig. 14B), polarity zone β in the Ajiro Island section is correlated to the normal polarity in magnetozone MT6, whereas zone α of the Ajiro Island section is correlated to the reversed polarity in magnetozones MT6 to MT8. In this case, the ALB is placed in the lower part of the *Paragondolella trammeri* Zone, ~1 m above its base. This option assumes that polarity zones α and β are correlated to reversed and normal polarities, respectively, contradictory to Uno *et al.* (2012). Hence, this option suggests the deposition of the bedded chert of the Ajiro Island section took place in the northern hemisphere.

The ambiguity in the correlation of mangnetic polarities results mainly from two reasons. Firstly, the gaps in the polarity zones in the Ajiro Island section due to the difficulty in recovering primary magnetic records from deep-sea chert (Uno *et al.*, 2012) allow a considerable amount of speculation in the correlation. Another reason is the lack of both biostratigraphic and magnetostratigraphic data within the MT6 magnetozone of the reference magnetostratigraphy from the Tethys sections (Hounslow and Muttoni, 2010). Thus, further studies in both the Panthalassic deep-sea sections in Japan and the reference Tethyan sections are required to establish a conclusive correlation of integrated Anisian bio-magnetostratigraphy between the two regions.

8. Conclusions

We investigated conodont biostratigraphy in the Ajiro Island section in Oita Prefecture and the Kurusu section in Aichi Prefecture. Six conodont biozones were recognised: the lower Spathian *Novispathodus brevissimus-Icriospathodus collinsoni* Zone, the upper Spathian *Triassospathodus homeri* Zone, the Aegean *Chiosella timorensis* Zone, the Bithynian to Pelsonian *Paragondolella bulgarica* Zone, the lower Illyrian *Paragondolella excelsa* Zone, and the upper Illyrian to basal Fassanian *Paragondolella trammeri* Zone, in ascending order. The age of the radiolarian biozones previously recognised in the studied sections were assigned based on conodont biostratigraphy. The TR 1 Zone was assigned to the upper Spathian to Bithynian (or Pelsonian) and thus the Olenekian-Anisian boundary is within this zone. The TR 2A Zone, the TR 2B Zone and most of the TR 2C Zone are correlated to the Bithynian to Pelsonian interval. The uppermost part of the TR 2C Zone and the lower part of the TR 3A Zone are definitely correlated to the Illyrian. The upper part of the TR 3A Zone and the lower part of the TR 3B Zone fall within the upper Illyrian to the basal Fassanian, while the possibility that both intervals are correlative to the upper Illyrian is more likely. The Anisian-Ladinian boundary is within the TR 3B Zone or above it, and further study is needed to clarify its position relative to the radiolarian biozones. Our conodont data are helpful in correlating the magnetic polarity zones detected from the Ajiro Island section to the reference magnetostratigraphy of the Triassic obtained in the Tethys realm. Further studies will establish an integrated bio-magnetostratigraphic correlation between the pelagic Panthalassic deep-sea sections and the Tethyan sections.

9. Palaeontological notes

(Form species defined by discrete elements rather than multi-element apparatuses are shown in quotation marks.)

Budurovignathus* cf. *hungaricus (Kozur & Vegh)
(Plate 1, Figs. 1, 2.)

Epigondolella hungarica Kozur & Vegh in Kozur & Mock, 1972. p. 8–9, Plate 2, Figs. 3–7.

Remarks: This species is distinguished by a short free blade, a sinuous but unornamented platform and a posterior process. The platform margins are unornamented unlike

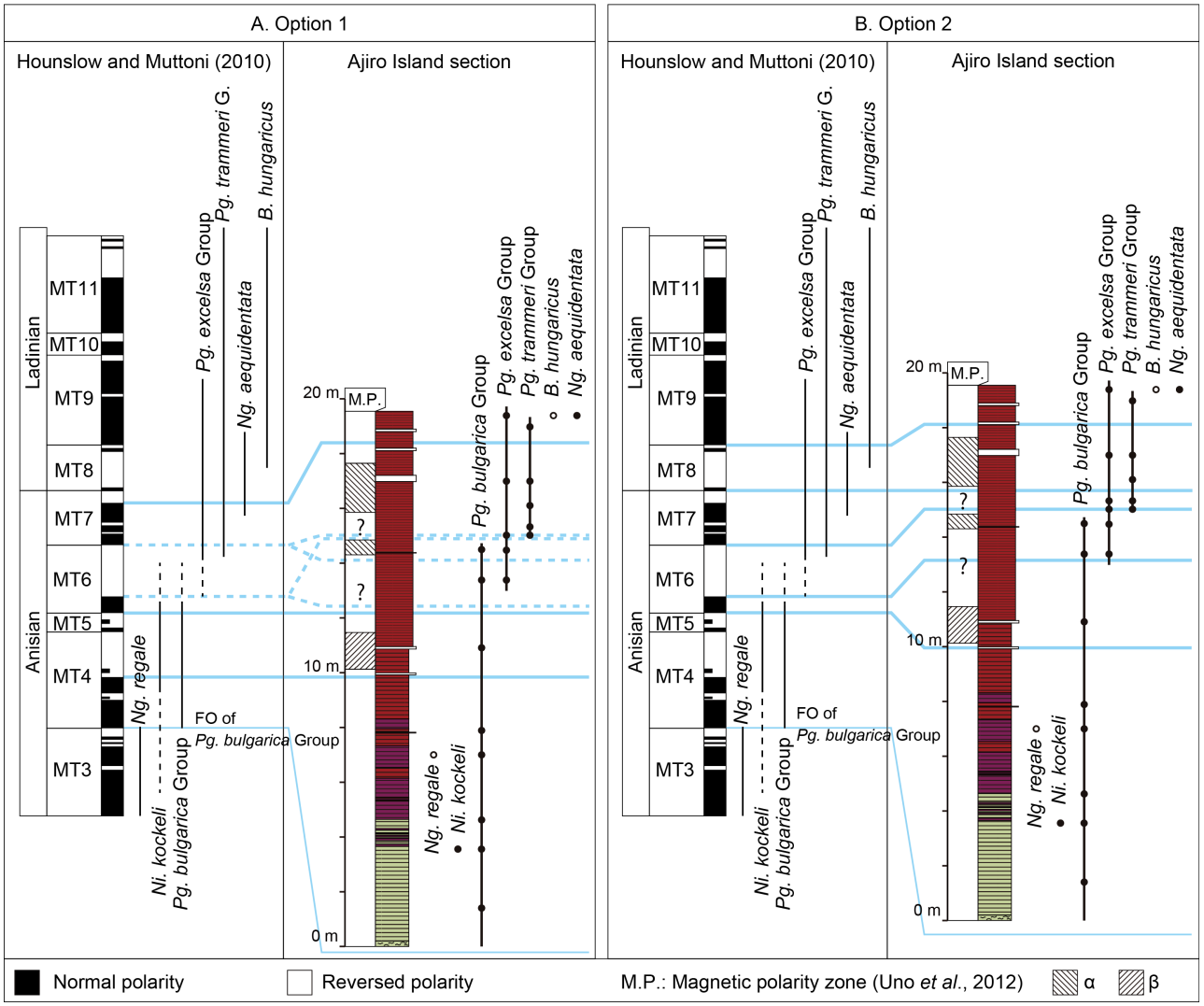

Fig. 14 Correlation of magnetic polarity zones in the Ajiro Island section (Uno *et al.*, 2012) to the reference magnetostratigraphy by Hounslow and Muttoni (2010). The range of *Ni. kockeli*, *Pg. bulgarica* Group and *Pg. excelsa* is not well understood in magnetozone MT6, but they are known to overlap to some extent (Kovács, 2011; Kozur, 1980). See Fig. 9 for legends of lithofacies and fossil occurrence.

younger species of *Budurovignathus*.

The specimen illustrated in Plate 1, Fig. 1 has a short free blade and a sinuous but unornamented platform. The posterior denticles are broken, and therefore the presence of a posterior process is not confidently confirmed. The specimen illustrated in Plate 1, Fig. 2 has a sinuous platform and a posterior process extending behind the basal pit, which are characteristics of *Budurovignathus*. The posterior platform margin is not pointed, which is a characteristic only seen in *B. hungaricus*. The anterior part is broken, and therefore the presence of a free blade cannot be confirmed.

Chiosella gondolelloides (Bender)
(Plate 1, Figs. 3, 4, Plate 9, Figs. 1, 2.)
Spathognathodus gondolleloides Bender, 1970. p. 529–530, Plate 10, Figs. 17, 19, 20.
Neospathodus gondolleloides (Bender). Orchard, 1995. p. 115, Figs. 2.4, 2.5.

Remarks: The specimens are pectiniform elements characterised by a faint mid-lateral rib. *Chiosella timorensis* is similar to *Ch. gondolelloides*, but the former has a more developed mid-lateral rib that rises sharply from the blade, a higher length: height ratio (greater than 2.5:1) and a smaller basal cavity. *Ch. gondolelloides* is similar to *Triassospathodus homeri*, *Triassospathodus brochus* and *Novispathodus symmetricus* in lateral profile, but the former can be distinguished from the latter three species by the presence of a mid-lateral rib. *Ch. gondolelloides* differs from *T. brochus* also in having more fused denticles.

Chiosella timorensis (Nogami)

(Plate 1, Fig. 5, Plate 8, Figs. 1–6.)

Gondolella timorensis Nogami, 1968. p. 127–128, Plate 10, Figs. 17–21.

Neogondolella timorensis (Nogami). Koike, 1981. Plate 2, Fig 7.

Chiosella timorensis (Nogami). Goudemand *et al.*, 2012. Figs. 2.1–14, 3.1–8.

Remarks: The specimens are pectiniform elements characterised by a prominent mid-lateral rib, small basal cavity and increasingly inclined denticles at the posterior end. The specimen illustrated in Plate 1, Figure 5 is a juvenile form, which is shorter and has a less prominent mid-lateral rib compared with adult forms. The basal cavity, which is terminally located, is relatively small. The specimen is similar to juvenile forms of *Ch. gondolelloides*, *T. homeri*, *T. brochus* and *Nv. symmetricus*, but can be distinguished from the latter four species by the narrower basal cavity.

Cornudina breviramulis (Tatge)

(Plate 1, Figs. 6–8, Plate 9, Figs. 3, 4.)

Ozarcodina breviramulis Tatge, 1956. p. 139, Plate 5, Figs. 12.

Cornudina breviramulis (Tatge). Koike, 1996. p. 118–119, Figs. 3.1–3.21.

Cornudina breviramulis (Tatge). Koike, 2016. p. 168–170, Figs. 4.1–4.3.

Remarks: The specimens are angulate pectiniform elements with a thick long cusp and short anterior and posterior processes. The anterior process bears up to four small discrete denticles that increase in size and inclination to the posterior. The posterior process bears up to three denticles that are smaller than those of the anterior process.

Cornudina tortilis Kozur & Mostler (Plate 2, Figs. 2, 3.)

Cornudina tortilis Kozur & Mostler, 1970. p. 432–433, Plate 1, Figs. 10, 16, 20, 24.

Cornudina tortilis Kozur & Mostler. Koike, 1981. Plate 1, Fig. 34.

Remarks: The specimens are characterised by a short anterior process and a very long and curved cusp. The posterior process bears small denticles of equal size. *Cornudina tortilis* is considered to be the P2 element of *Co. breviramulis* (Koike, 1996, 2016).

Cornudina*? *igoi Koike

(Plate 1, Fig. 9, Plate 2, Fig. 1, Plate 9, Fig. 5.)

Cornudina igoi Koike, 1996. p. 119–120, Figs. 4.1–4.20.

Remarks: The specimens identified as this species is distinguished by a long cusp and a very short anterior process that bears only two denticles. Although this species may not belong to the genus *Cornudina*, which typically has a posterior process, it is tentatively included in this genus following the original description.

Icriospathodus collinsoni (Solien) (Plate 2, Fig. 5.)

Neospathodus collinsoni Solien, 1979. p. 302–303, Plate 3, Figs. 10, 12–20.

Neospathodus? *collinsoni* Solien. Koike, 1981. Plate 1, Figs. 42–44.

Remarks: *Icriospathodus collinsoni* (Solien) is a species characterised by a biserial row of denticles that form ridges extending laterally across the element, that commonly possess short lateral processes. Although the biserial nature of the denticles cannot be observed in lateral view, the ridge-like form of the denticles and the lateral process can be observed in the specimen illustrated in Plate 2, Fig. 5. This specimen also shows affinity to the holotype in that the element is relatively low and decreases height gradually to the anterior. The specimen illustrated in Plate 2, Fig. 6 also shows affinity to the holotype in lateral view, but the biserial nature and ridge-like form of the denticles cannot be confirmed.

"*Kamuellerella gebzeensis* Gedik" (form species)

(Plate 2, Fig. 4, Plate 9, Fig. 6.)

Kamuellerella gebzeensis Gedik, 1975. p. 124–125, Plate 8, Figs. 1, 2, 4.

Remarks: The specimens are bipennate ramiform elements characterised by an anterior process that is bent downwards and bears relatively high denticles, and a posterior process that bears numerous thin erect denticles.

Neogondolella aequidentata Kozur *et al.*

(Plate 2, Fig. 7.)

Neogondolella aequidentata Kozur *et al.*, 1994a. p. 278–279, Plate 2, Figs. 5–9.

Remarks: This species is characterised by a curved element with a platform that runs its entire length and a high carina of uniform height. The lateral platform margins are sub-parallel. *Neogondolella regale* also has a carina of uniform height, but it is not arched and it has more fused denticles.

Neogondolella* cf. *hastata Golding & Orchard

(Plate 2, Figs. 8–11.)

Neogondolella hastata Golding & Orchard, 2016. p. 1205–1206, Fig. 9.

Remarks: The specimens are characterised by a platform that extends from the anterior end to the anterior side of the base of the large terminal cusp and a uniform carina of discrete denticles. The platform is widest around mid-length. It does not surround the cusp, and terminates before the cusp in juvenile forms. The cusp is conspicuously higher and thicker than the other denticles.

Neogondolella* aff. *hastata Golding & Orchard

(Plate 3, Figs. 1, 2.)

Remarks: The specimens are similar to *Neogondolella hastata* in having a platform that is widest around mid-length and terminates at the anterior base of the conspicuously large cusp, and a relatively low carina of uniform height. However, their carina is composed of fused denticles as opposed to discrete denticles in *Ng.*

hastata. This species differs from *Ng. regale* in having a thick and high cusp.

Neogondolella pridaensis (Nicora, Kozur & Mietto) (Plate 3, Fig. 3.)

Neogondolella pridaensis Nicora *et al.*, 1981. p. 762–763, Plate 89, Figs. 1–9.

Remarks: The specimen is characterised by a reduced platform and a large terminal cusp. The platform terminates in a rib surrounding the posterior side of the cusp. The denticles are of even height and are fused. Species of *Paragondolella* differ from *Neogondolella pridaensis* in having a well-developed platform, which is particularly evident near the posterior end.

Neogondolella* cf. *regale Mosher (Plate 3, Fig. 4.)

Neogondolella regale Mosher, 1970. p. 741–742, Plate 110, Figs. 1, 2, 4, 5.

Neogondolella regale Mosher. Nicora, 1977. Plate 5, Figs 1–7.

Remarks: This species is distinguished by an almost straight element with a well-developed platform that runs almost its entire length, and a high carina of uniform height composed of moderately fused denticles. The platform has mostly uniform width throughout its length, and does not surround the terminal denticle. The specimens from the Ajiro Island sections show these characteristics, although they are partly not visible.

Neogondolella shoshonensis Nicora

Neogondolella shoshonensis Nicora, 1976. p. 640–642, Plate 83, Figs. 1–15, Plate 84, Fig. 17.

Remarks: This species is distinguished by a well-developed platform, a low carina that becomes extremely low around mid-length and an enormous, posteriorly reclined cusp with a large basal area that dominates the posterior end. Some of the specimens identified as "post-Bithynian type *Neogondolella*" (Plate 3, Figs. 5, 6) display the latter two features, but the platform is not well preserved. Therefore, the specific identification of these specimens is pending. Other specimens identified as "post-Bithynian type *Neogondolella*" (Plate 3, Figs. 7–9) are similar to *Ng. shoshonensis*, but some important characters are different or unconfirmed. The specimens illustrated in Plate 3, Fig. 7 and Fig. 8 have a large cusp and a very low carina, but the cusp does not recline posteriorly. The specimen illustrated in Plate 3, Fig. 9 has a very low anterior carina and an enormous cusp that reclines posteriorly, but the middle part of the carina is not visible.

"***Neohindeodella aequiramosa*** Kozur & Mostler" (form species) (Plate 3, Figs. 10, 11.)

"***Neohindeodella* cf. *aequiramosa*** Kozur & Mostler" (Plate 8, Fig. 8.)

Neohindeodella aequiramosa Kozur & Mostler, 1970. p. 445–446, Plate 2, Figs. 1, 2, 4, 5, 7, 8.

Neohindeodella aequiramosa Kozur & Mostler. Koike, 1982. Plate 8, Figs. 35–37.

Remarks: The specimens are bipennate ramiform elements characterised by an anterior process that bears relatively large, anteriorly reclined denticles. The basal margin is deflected downwards below the cusp and forms a convex down outline below the anterior process. The specimen illustrated in Plate 8, Fig. 8 is identical to "*Neohindeodella aequiramosa*" in the configuration of the basal margin and the denticulation of the anterior process, but its cusp and much of the posterior process is broken.

"***Neohindeodella benderi*** (Kozur & Mostler)" (form species) (Plate 3, Figs. 12, 13, Pl. 10, Figs. 1, 2.)

Hindeodella benderi Kozur & Mostler, 1970 p. 440–441, Plate 2, Figs. 10, 11, 13.

Neohindeodella benderi (Kozur & Mostler). Koike, 1981. Plate 1, Fig. 14.

Remarks: The specimens are bipennate ramiform elements marked by a short anterior process that is conspicuously downturned and bears an enormous denticle at the anterior end. Apart from this large denticle, there are no denticles or only one or two minute denticles on the anterior process.

This form species is identical to the S elements of the apparatus of *Neostrachanognathus* sp. A in Agematsu *et al.* (2008), which is referred to as *Neostrachanognathus tahoensis* in this paper.

"***Neohindeodella triassica*** (Müller)" (form species) (Plate 4, Fig. 1–3.)

Hindeodella triassica Müller, 1956. p. 826, Plate 96, Figs. 4, 5.

Neohindeodella triassica (Müller). Koike, 1981. Plate 1, Fig. 25.

Neohindeodella triassica (Müller). Koike, 1982. Plate 8, Figs. 21–30.

Remarks: The specimens are bipennate ramiform elements distinguished by a large cusp and denticles that are upright at the anterior and become reclined in the posterior part. The basal margin is convex under the cusp, and is relatively straight to the posterior. There is a short anterior process with relatively large denticles near the anterior end. "*Nh. aequiramosa*" differs from this species in the bending of the element below the cusp and the configuration of the basal margin, which is convex downwards below the anterior process and not below the cusp.

This form species is considered to be the S3/4 elements of *Cornudina breviramulis* (Koike, 2016), and also shows affinity to the S3 element of the apparatus of *Triassospathodus* reconstructed by Orchard (2005).

Neostrachanognathus tahoensis Koike.

(Plate 10, Fig. 3.)

Neostrachanognathus tahoensis Koike, 1998. p. 127–128, Figs. 9.10, 9.14, 9.16–23.

Neostrachanognathus sp. A. Agematsu *et al.*, 2008. Fig. 8.

Remarks: This specimen is a coniform element with a posteriorly elongated basal area. Agematsu *et al.* (2008)

redefined the original definition of *Neostrachanognathus tahoensis* by Koike (1998), and argued that the P1 element of this species is a coniform element without a posterior elongation of the basal area. However, the holotype of *Nc. tahoensis* has a posterior elongation of the basal area. Agematsu *et al.* (2008) also described another species of *Neostrachanognathus* (*Neostrachanognathus* sp. A), which has a coniform P1 element with a posterior elongation of the basal area, and is assigned here to *Nc. tahoensis*. The S element of *Nc. tahoensis* in Agematsu *et al.* (2008) (their *Neostrachanognathus* sp. A) is identical to "*Nh. benderi*".

Nicoraella kockeli (Tatge) (Plate 4, Fig. 4.)
Ozarkodina kockeli Tatge, 1956. p. 137, Plate 5, Figs. 13, 14.
Neospathodus kockeli (Tatge). Koike, 1982. Plate 6, Figs. 2–11.
Remarks: The specimens are pectiniform elements characterised by an angular profile of the upper margin due to the denticles decreasing in height in both anterior and posterior directions from the conspicuously wide cusp. The cusp is located posterior to the mid-length of the elements. The decrease in height of the denticles is rapid to the posterior side of the cusp. The basal cavity is not expanded laterally, and is positioned slightly anterior from the posterior end. This species is distinguished from *Novispathodus abruptus* by the forward-shifted position and unflared configuration of the basal cavity, and from *T. homeri* by the small basal cavity.

Novispathodus abruptus (Orchard) (Plate 4. Fig. 5.)
Neospathodus abruptus Orchard, 1995. p. 118–119, Figs. 3.16–3.19, 3.23–3.26.
Remarks: The specimens are pectiniform elements characterised by denticles that decrease height rapidly at the posterior end, resulting in the arcuate outline of the upper margin. This species is distinguished from *T. homeri* by the lack of a distinct posterior process.

Novispathodus brevissimus (Orchard) (Plate 4, Fig. 6.)
Neospathodus triangularis (Bender). Koike, 1981. Pl. 1, Fig. 6.
Neospathodus brevissimus Orchard, 1995. p. 119, Figs. 3.14–3.15, 3.20–3.22.
Remarks: The specimen is characterised by a blade composed of thin fused denticles and a basal cavity that expands widely in lateral directions and truncates abruptly at the posterior end. The height of the blade is equal for almost its entire length, giving the element a quadrate outline in lateral view.

Novispathodus symmetricus (Orchard)
(Plate 4, Figs. 7–10, Plate 10, Figs. 4, 5.)
Neospathodus symmetricus Orchard, 1995. p. 120–121, Figs. 2.6, 2.10–2.13, 2.18.
Remarks: The specimens are pectiniform elements characterised by sub-equal denticles that are slightly to moderately inclined to the posterior. This species is distinguished from *T. homeri* by the lack of a posterior process and abrupt truncation of the basal cavity, and from *T. brochus* by the more fused denticles and the lack of radiating denticles at the posterior end. Orchard (2007) assigned *Nv. symmetricus* to the genus *Triassospathodus*, which was distinguished from *Novispathodus* based on differences in their multielement apparatus (Orchard, 2005), but the apparatus of this particular species is yet to be reconstructed. As far as the P1 element is concerned, *Nv. symmetricus* is closer to *Nv. abruptus* than to *T. homeri* in that it lacks a well-developed posterior process. Hence, we include *Nv. symmetricus* in *Novispathodus*.

Novispathodus triangularis (Bender)
Spathognathodus triangularis Bender, 1970. p. 530, Plate 5, Fig. 22.
Neospathodus triangularis (Bender). Orchard, 1995. p. 116, 118, Figs. 3.1–3.4.
Remarks: *Novispathodus triangularisi* (Bender) was redefined by Orchard (1995) as a species with a conspicuous fold on the upper surface of the basal cup, that extends vertically to a sub-terminal cusp. The specimen illustrated in Plate 4, Figure 11 has a vertical groove above the basal cup, which may be the "fold" described by Orchard (1995). The specimen also has a length-height ratio similar to the specimens illustrated by Orchard (1995). However, the poor preservation of the specimen makes it difficult to make a conclusion.

Paragondolella bulgarica Group (Plate 5, Fig. 2–8.)
Paragondolella* cf. *bulgarica Group (Plate 5, Fig. 1.)
Paragondolella bulgarica Budurov & Stefanov, 1975. p. 794, Plate 1, Figs. 1–23.
Neogondolella bulgarica (Budurov & Stefanov). Nicora, 1977. Plate 5, Figs. 8–14.
Neogondolella bulgarica (Budurov & Stefanov). Koike, 1981. Plate 2, Figs. 1–3.
Neogondolella bulgarica (Budurov & Stefanov). Koike, 1982. Plate 4, Figs. 1–19, 22–24.
Paragondolella bifurcata Budurov & Stefanov. Chen *et al.*, 2016a. p. 728, Fig. 2.
Neogondolella unilobata Gedik, 1975. p. 133–134, Plate 1, Figs. 9–25.
Neogondolella hanbulogi Sudar & Budurov, 1979. p. 50–51, Plate 1, Figs. 9, 10, Plate 2, Figs. 1–9, Plate 3, Figs. 1–12.
Remarks: This group is distinguished by an arched element and a high-carina of moderately fused denticles that ends with a strong terminal cusp. A small denticle is often present behind the cusp. The last denticle is sometimes fused to the posterior brim of the platform. In juvenile specimens, the platform is not developed (Plate 5, Fig. 6) or confined to the posterior part (Plate 5, Figs. 4, 5). In later stages, the platform runs almost its entire length. These characteristics match with those of *Paragondolella*

bulgarica.

In juvenile stages, *Pg. bulgarica* is very similar to *Paragondolella bifurcata*, which is considered as a descendant of the former species (Chen *et al.*, 2016a). Since our specimens are almost entirely juveniles, it is impossible to separate them into the two species. We also follow Nicora (1977) and Chen *et al.*, (2016a) in treating *Paragondolella unilobata* as a junior synonym of *Pg. bulgarica*. Therefore, we will include *Pg. bifurcata* and *Pg. unilobata* in the *Pg. bulgarica* Group. In addition, Kovács and Rálisch-Felgenhauer (2005) reported transitional morphotypes between both these two species and *Paragondolella hanbulogi*. Hence, *Pg. hanbulogi* is also included in the *Pg. bulgarica* Group.

Paragondolella excelsa Group (Plate 5, Figs. 9–14.)

Paragondolella excelsa Mosher, 1968a. p. 938–939, Plate 118, Figs. 1–8.

Paragondolella excelsa Mosher. Mosher, 1968b. Plate 120, Figs. 1–7.

Gondolella liebermani Kovács & Krystyn in Kovács, 1994. p. 492–493, Plate 6, Figs. 1–3.

Gondolella fueloepi Kovács, 1994. p. 493.

Gondolella fueloepi fueloepi Kovács, 1994. Plate 7, Figs. 2, 3, Pl. 8, Fig. 4.

Gondolella fueloepi pseudobifurcata Kovács, 1994. Plate 8, Figs. 1, 3.

Remarks: The specimens are segminiplanate elements with a high blade and a thick platform developed in the posterior part of the element that surrounds the terminal cusp. The cusp is thick, reclined posteriorly and its tip is lower than the anterior denticles. These characteristics match with juvenile forms of *Paragondolella excelsa*. In adult forms, this species is characterised by a carina that is high at the anterior and decreases height posteriorly ending in a node-like cusp, and a massive platform that surrounds the terminal denticle. The low, thick cusp and well-developed platform in our specimens are regarded as a precursor of these adult characters. *Paragondolella liebermani* and *Paragondolella fueloepi* also has a carina that decreases to a low, node-like cusp and a thick platform that surrounds the posterior end. Hence, we treat *Pg. excelsa*, *Pg. liebermani* and *Pg. fueloepi* as the *Pg. excelsa* Group, although juvenile characters of the latter two species have not been thoroughly investigated.

In juvenile stages, the *Pg. excelsa* Group somewhat resembles the *Pg. bulgarica* Group, but the former has a thicker platform and a lower and more reclined cusp.

Paragondolella trammeri Group (Plate 6, Figs. 1–7.)

Gondolella haslachensis trammeri Kozur and Mock, 1972. p. 13, Plate 1, Figs. 3–7.

Paragondolella trammeri (Kozur) Kozur *et al.*, 1994b. p. 176–178, Plate 2, Figs. 19, 23, 24. Plate 3, Figs. 10, 13, 16.

Gondolella alpina Kozur & Mostler, 1982. p. 292–293, Plate 1, Fig. 1, Plate 2, Figs. 4, 5.

Gondolella alpina alpina Kozur & Mostler. Kovács, 1994. p. 488–489, Plate 4, Figs. 2, 4, Plate 5, Figs. 1–3.

Remarks: The specimens are segminiplanate elements characterised by a large posteriorly reclined cusp and a platform that merges at the posterior end into a pointed denticle behind the cusp. The platform is thicker in larger specimens (Plate 6, Fig. 6) reflecting ontogenic growth. These characters match with those of *Paragondolella trammeri*. *Paragondolella alpina* is similar to *Pg. trammeri*, but can be distinguished from the latter in adult specimens by the presence of a free blade. Immature specimens of *Pg. alpina* have not been well studied. We withhold from conclusively differentiating the two species in our specimens, and refer to them as the *Pg. trammeri* Group.

In earliest growth stages, the *Pg. trammeri* Group somewhat resembles late juvenile stages of the *Pg. bulgarica* Group in having a pointed posterior platform end behind the cusp. However, the former differs from the latter in the lower and more discrete denticles, and the higher cusp. In later juvenile stages, the *Pg. trammeri* Group differs from the *Pg. bulgarica* Group in having a thicker platform. *Pg. trammeri* Group is distinguished from the *Pg. excelsa* Group in having a small terminal denticle fused to the posterior brim of the platform.

Triassospathodus anhuinensis (Ding) (Plate 6, Fig. 8.)

Neospathodus anhuinensis Ding, 1983. p. 44, Plate 5, Figs. 9, 10.

Remarks: The specimen is characterised by a blade composed of small and fused denticles and a well-developed posterior process that occupies around one third of the element. It differs from *T. homeri* in having a much longer posterior process and smaller denticles.

Triassospathodus brochus (Orchard) (Plate 7, Fig. 1.)

Triassospathodus* cf. *brochus (Orchard) (Plate 7, Fig. 2.)

Neospathodus brochus Orchard, 1995. p. 119, Figs. 3.27, 3.28, 3.35, 3.36.

Remarks: This species is distinguished by a pectiniform element that possesses relatively discrete denticles that become increasingly reclined near the posterior end, so that the terminal denticle is orientated at a low angle to the basal margin. This species is distinguished from *T. homeri* by the more discrete denticles and radiating denticles at the posterior end.

The specimen illustrated in Plate 7, Fig. 2 is partly broken at the anterior side, but the observed features are identical to those of *T. brochus*.

Triassospathodus homeri (Bender)
(Plate 7, Figs. 3–6, Pl. 10, Figs. 6, 7.)

Spathognathodus homeri Bender, 1970. p. 528–529, Plate 5, Figs. 16, 18.

Neospathodus homeri (Bender). Orchard, 1995. p. 115–116, Figs. 2.1–2.3, 2.7–2.9, 2.14–2.17, 2.20–2.21.

Remarks: The specimens are pectiniform elements marked by a short posterior process that bears up to five denticles. The posterior process is commonly downturned and bears denticles that are sometimes smaller than the anterior process. This species is distinguished from *Nv. abruptus* and *Nv. symmetricus* by the presence of the distinct posterior process.

Acknowledgements

We are grateful for an anonymous reviewer who provided many fruitful comments. Sincere gratitude is expressed to H. Shirozu, H. Matsumoto, K. Yoshizawa and residents of the Enoura district in Tsukumi City for their kind support during fieldwork. This study was partly supported by Grant-in-aid for JSPS Research Fellow Number 16J04796 (to S. Muto) and 16J09728 (to K. Soda).

References

Agematsu, S., Orchard, M. J. and Sashida, K. (2008) Reconstruction of an apparatus of Neostrachanognathus tahoensis from Oritate, Japan and species of Neostrachanognathus from Oman. *Palaeontology*, **51**, 1201–1211.

Ando, A., Kodama, K. and Kojima, S. (2001) Low-latitude and Southern Hemisphere origin of Anisian (Triassic) bedded chert in the Inuyama area, Mino terrane, central Japan. *Jour. Geophys. Res. Solid Earth*, **106**, 1973–1986.

Balini, M., Lucas, S. G., Jenks, J. F. and Spielmann, J. A. (2010) Triassic ammonoid biostratigraphy: an overview. *Geolo. Soc. London, Spec. Publ*., **334**, 221–262.

Bender, H. (1970) Zur Gliederung der Mediterranen Trias II. Die Conodontenchronologie der Mediterranen Trias. *Annales Géologiques des Pays Hélleniques, Serie 1*, **19**, 465–540.

Brack, P. (2010) The "golden spike" for the Ladinian is set! *Albertiana*, **38**, 8–10.

Brack, P., Rieber, H., Nicora, A. and Mundil, R. (2005) The global boundary stratotype section and point (GSSP) of the Ladinian Stage (Middle Triassic) at Bagolino (Southern Alps, Northern Italy) and its implications for the Triassic time scale. *Episodes*, **28**, 233–244.

Bucher, H. (1989) Lower Anisian ammonoids from the northern Humboldt Range (northwestern Nevada, USA) and their bearing upon the Lower-Middle Triassic boundary. *Eclogae Geologicae Helvetiae*, **82**, 945–1002.

Budurov, K. and Stefanov, S. (1975) Neue Daten über die Conodontenchronologie der Balkaniden Mittleren Trias. *Doklady Bolgarskoi Akademii Nauk*, **28**, 791–794.

Chen, Y., Jiang, H., Lai, X., Yan, C., Richoz, S., Liu, X. and Wang, L. (2015) Early Triassic conodonts of Jiarong, Nanpanjiang Basin, southern Guizhou Province, South China. *Jour. Asian Earth Sci*., **105**, 104–121.

Chen, Y., Neubauer, T. A., Krystyn, L. and Richoz, S. (2016a) Allometry in Anisian (Middle Triassic) segminiplanate conodonts and its implications for conodont taxonomy. *Palaeontology*, **59**, 725–741.

Chen, Y., Krystyn, L., Orchard, M. J., Lai, X. L. and Richoz, S. (2016b) A review of the evolution, biostratigraphy, provincialism and diversity of Middle and early Late Triassic conodonts. *Papers in Palaeontology*, **2**, 235–263.

Clark, D. L., Sweet W. C., Bergström, S. M., Klapper, G., Austin, R. L., Rhodes, F. H. T., Müller, K. J., Ziegler, W., Lindström, M., Miller, J. F. and Harris, A. G. (1981) *Treatise on invertebrate paleontology. Part W Miscellanea, Supplement 2*, *Conodonta*. Geol. Soc. Amer. and Univ. Kansas, Boulder Colorado, and Lawrence, Kansas, 1–202.

Ding, M. (1983) Lower Triassic conodonts from the Mountain Majiashan in Anhui Province and their stratigraphic significance. *Earth Science-Journal of China University of Geosciences*, **2**, 37–48 (in Chinese).

Fujii, K. (1954) Stratigraphy and geological structure of the Usuki area, Oita Prefecture, Kyushu (1). *Jour. Geol. Soc. Japan*, **60**, 413–427 (in Japanese with English abstract).

Fujisaki, W., Sawaki, Y., Yamamoto, S., Sato, T., Nishizawa, M., Windley, B. F. and Maruyama, S. (2016) Tracking the redox history and nitrogen cycle in the pelagic Panthalassic deep ocean in the Middle Triassic to Early Jurassic: Insights from redox-sensitive elements and nitrogen isotopes. *Palaeogeogr., Palaeoclimatol., Palaeoecol*., **449**, 397–420.

Gedik, I. (1975) Die Conodonten der Trias auf der Kocaeli-Halbinsel (Türkei). *Palaeontographica, Abteiling A*, **150**, 99–160 (in German with English summary).

Golding, M. L. and Orchard, M. J. (2016) New species of the conodont Neogondolella from the Anisian (Middle Triassic) of northeastern British Columbia, Canada, and their importance for regional correlation. *Jour. Paleontol*., **90**, 1197–1211.

Goudemand, N., Orchard, M. J., Bucher, H. and Jenks, J. (2012) The elusive origin of *Chiosella timorensis* (Conodont Triassic). *Geobios*, **45**, 199–207.

Gradinaru, E., Orchard, M. J., Nicora, A., Gallet, Y., Besse, J., Krystyn, L., Sobolev, E. S., Atudorei, N.-V. and Ivanova, D. (2007) The global boundary stratotype section and point (GSSP) for the base of the Anisian stage: Deşli Caira Hill, North Dobrogea, Romania. *Albertiana*, **36**, 54–71.

Hayashi, S. (1968) Permian in the chert of the Adoyama Formation, Ashio Mountains, central Japan. *Earth Science (Chikyu Kagaku)*, **22**, 63–77 (in Japanese with English abstract and description).

Hoshizumi, H., Saito, M., Mizuno, K., Miyazaki, K., Toshimitsu, S., Matsumoto, A., Ohno, T. and Miyakawa, A. (2015). *Geological map of Japan*

1:200,000, Oita (2nd edition). Geol. Surv. Japan, AIST (in Japanese with English abstract).

Hounslow, M. W. and Muttoni, G. (2010) The geomagnetic polarity timescale for the Triassic: linkage to stage boundary definitions. *Geol. Soc. of London, Spec. Publ*., **334**, 61–102.

Ikeda, M. and Tada, R. (2014) A 70 million year astronomical time scale for the deep-sea bedded chert sequence (Inuyama, Japan): Implications for Triassic–Jurassic geochronology. *Earth Planet. Sci. Lett*., **399**, 30–43.

Ikeda, M,. Tada, R. and Sakuma, H. (2010) Astronomical cycle origin of bedded chert: A middle Triassic bedded chert sequence, Inuyama, Japan. *Earth Planet. Sci. Lett*., **297**, 369–378.

Imoto, N. (1984) Late Paleozoic and Mesozoic cherts in the Tamba Belt, Southwest Japan. *Bull. Kyoto Univ. Educ*., B 65, 15–71.

Isozaki, Y. and Matsuda, T. (1982) Middle and Late Triassic conodonts from bedded chert sequences in the Mino-Tamba Belt, Southwest Japan Part 1: Epigondolella. *Jour. Geosci. Osaka City Univ*., **25**, 103–136.

Isozaki, Y. and Matsuda, T. (1983) Middle and Late Triassic conodonts from bedded chert sequences in the Mino-Tamba Belt, Southwest Japan Part 2: Misikella and Parvigondolella. *Jour. Geosci. Osaka City Univ*., **26**, 65–86.

Isozaki, Y., Maruyama, S., Aoki, K., Nakama, T., Miyashita, A. and Otoh, S. (2010) Geotectonic Subdivision of the Japanese Islands Revisited: Categorization and definition of elements and boundaries of Pacific-type (Miyashiro-type) orogen. *Jour. Geogr. (Chigaku-Zasshi)*, **119**, 999–1053 (in Japanese with English abstract).

Kambe, N. and Teraoka, Y. (1968) *Geological map of Japan, Scale 1:50,000. Usuki sheet and its explanatory text.* Geol. Surv. Japan (in Japanese with English abstract).

Kimura, K. and Hori, R. (1993) Offscraping accretion of Jurassic chert-clastic complexes in the Mino-Tamba Belt, central Japan. *Jour. Structural Geol*., **15**, 145–161.

Koike, T. (1981) Biostratigraphy of Triassic conodonts in Japan. *Sci. Rep. Yokohama Nat. Univ*., *section 2*, **28**, 25–46.

Koike, T. (1982) Triassic conodont biostratigraphy in Kedah, west Malaysia. *Geol. Paleontol. Southeast Asia*, **23**, 9–51.

Koike, T. (1996) Skeletal apparatuses of Triassic conodonts of Cornudina. *Prof. Hisayoshi Igo commemorative volume on geology and paleontology of Japan and Southeast Asia*, 113–120.

Koike, T. (1998) Triassic coniform conodont genera Aduncodina and Neostrachanognathus. *Paleontol. Res.,* **2**, 120–129.

Koike, T. (2004) Early Triassic *Neospathodus* (Conodonta) apparatuses from the Taho Formation, southwest Japan. *Paleontol. Res*., **8**, 129–140.

Koike, T. (2016) Multielement conodont apparatuses of the Ellisonidae from Japan. *Paleontol. Res*., **20**, 161–175.

Kojima, S., Hayasaka, Y., Yoshikunihiroi, A., Sano, H., Sugamori, Y., Suzuki, N. and Takemura, S. (2016) 2b Pre-Cretaceous accretionary complexes. *In* Moreno, T., *et al.*, eds., *The Geology of Japan*, 61–100. The Geological Society of London, London.

Kovács, S. (1994) Conodonts of stratigraphical importance from the Anisian/Ladinian boundary interval of the Balaton Highland, Hungary. *Rivista Italiana di Paleontologia e Stratigrafia*, **99**, 473–514.

Kovács, S. (2011) Middle-Late conodont evolutionary events as recorded in the Triassic basinal deposits of Hungary. *Földtani Közlöny*, **141**, 141–166 (in Hungarian with English abstract).

Kovács, S. and Rálisch-Felgenhauer, E. (2005) Middle Anisian (Pelsonian) platform conodonts from the Triassic of the Mecsek Mts (South Hungary)-Their taxonomy and stratigraphic significance. *Acta Geologica Hungarica*, **48**, 69–105.

Kozur, H. (1980) Revision der Conodontenzonierung der Mittel- und Obertrias des tethyalen Faunenreichs. Geologisch-Paläontologische Mitteilungen Innsbruck, **10**, 79-112 (in German).

Kozur, H. and Mock, R. (1972) Neue Conodonten aus der Trias der Slowakei und ihre stratigraphische Bedeutung. *Geologisch Paläontologische Mitteilungen Innsbruck*, **2**, 1–20 (in German).

Kozur, H. and Mostler, H. (1970) Neue conodonten aus der Trias. *Berichte des Naturwissenschaftlich–medizinischen Vereins in Innsbruck*, **58**, 429–464 (in German with English abstract).

Kozur, H. and Mostler, H. (1982) Neue Conodontenarten aus dem Illyr und Fassan der Profile Fellbach und Karalm (Gailtaler Alpen, Kärnten, Österreich). *Geologisch Paläontologische Mitteilungen Innsbruck*, **11**, 291–298 (in German).

Kozur, H., Krainer, K. and Lutz, D. (1994a) Middle Triassic conodonts from the Gartnerkofel—Zielkofel area, Carnic Alps (Carinthia, Austria). *Jahrbuch der Geologischen Bundesanstalt*, **137**, 275-287.

Kozur, H., Krainer, K. and Mostler, H. (1994b) Middle Triassic conodonts from the southern Karawanken Mountains (Southern Alps) and their stratigraphic importance. *Geologisch Paläontologische Mitteilungen Innsbruck*, **19**, 165-200.

Lehrmann, D. J., Stepchinski, L., Altiner, D., Orchard, M. J., Montgomery, P., Enos, P., Ellwood, B. B., Bowring, S. A., Ramezani, J., Wang, H., Wei, J., Yu, M., Griffiths, J. D., Minzoni, M., Schaal, E. K., Li, X., Meyer, K. M. and Payne, J. L. (2015) An integrated biostratigraphy (conodonts and foraminifers) and chronostratigraphy (paleomagnetic reversals, magnetic susceptibility, elemental chemistry, carbon isotopes

and geochronology) for the Permian-Upper Triassic strata of Guandao section, Nanpanjiang Basin, south China. *Jour. Asian Earth Sci*., **108**, 117–135.

Matsuda, T. and Isozaki, Y. (1982) Radiolarians around the Triassic-Jurassic boundary from the bedded chert in the Kamiaso area, Southwest Japan. Appendix: "Anisian" radiolarians. *News Osaka Micropaleontol., Spec. Vol*., no. 5, 93–101 (in Japanese with English abstract).

Matsuda, T. and Isozaki, Y. (1991) Well-documented travel history of Mesozoic pelagic chert in Japan: from remote ocean to subduction zone. *Tectonics*, **10**, 475–499.

Matsuoka, A. (1986) Mesozoic strata of the Southern Chichibu Terrane in the Tsukumi area, Oita Prefecture. *News Osaka Micropaleontol., Spec. Vol*., no. 7, 219–223.

Matsuoka, A. and Yao, A. (1986) A newly proposed radiolarian zonation for the Jurassic of Japan. *Marine Micropaleontol*., **11**, 91–106.

Matsuoka, A. and Yao, A. (1990) Southern Chichibu Terrane. *In* Ichikawa, K. *et al.*, eds., *Pre-Cretaceous Terranes of Japan*. Tokai Univ. Press, Tokyo, Japan, 203–216.

Matsuoka, A., Yamakita, S., Sakakibara, M. and Hisada, K. (1998) Unit division of the Chichibu Composite Belt from a view point of accretionary tectonics and geology of western Shikoku, Japan. *Jour. Geol. Soc. Japan*, **104**, 634–653 (in Japanese with English abstract).

Mizutani, S. (1964) Superficial folding of the Paleozoic system of central Japan. *Jour. Earth Sci., Nagoya Univ.*, **12**, 17–83.

Mizutani, S. and Koike, T. (1982) Radiolarians in the Jurassic siliceous shale and in the Triassic bedded chert of Unuma, Kakamigahara City, Gifu Prefeture, central Japan. *News Osaka Micropalaeontol., Spec. Vol*., no. 5, 117–134 (in Japanese with English abstract).

Mosher, L. C. (1968a) Triassic conodonts from western North America and Europe and their correlation. *Jour. Paleontol*., **42**, 895–946.

Mosher, L. C. (1968b) Evolution of Triassic platform conodonts. *Jour. Paleontol*., **42**, 947–954.

Mosher, L. C. (1970) New conodont species as Triassic guide fossils. *Jour. Paleontol.*, **44**, 737–742.

Müller, K. J. (1956) Triassic conodonts from Nevada. *Jour. Paleontol*., **30**, 818–830.

Muto, S., Takahashi, S., Yamakita, S., Suzuki, N., Suzuki, N. and Aita, Y. (2018) High sediment input and possible oceanic anoxia in the pelagic Panthalassa during the latest Olenekian and early Anisian: Insights from a new deep-sea section in Ogama, Tochigi, Japan. *Palaeogeogr., Palaeoclimatol., Palaeoecol*., **490**, 687–707.

Muttoni, G., Nicora, A., Brack, P. and Kent, D. V. (2004) Integrated Anisian–Ladinian boundary chronology. *Palaeogeogr., Palaeoclimatol., Palaeoecol*., **208**, 85–102.

Nakada, R., Ogawa, K., Suzuki, N., Takahashi, S. and Takahashi, Y. (2014) Late Triassic compositional changes of aeolian dusts in the pelagic Panthalassa: response to the continental climatic change. *Palaeogeogr., Palaeoclimatol., Palaeoecol*., **393**, 61–75.

Nicora, A. (1976) Conodont-fauna, stratigraphic position and relations to the Tethyan successions of the Shoshonensis Zone (Pelsonian) of Nevada. *Rivista Italiana di Paleontologia e Stratigrafia*, **82**, 627–650.

Nicora, A. (1977) Lower Anisian platform-conodonts from the Tethys and Nevada: Taxonomic and stratigraphic revision. *Palaeontographia Abteilung A*, **157**, 88–107.

Nicora, A., Kozur, H. and Mietto, P. (1981) Gondolella pridaensis sp. n.: A new conodont species from the Middle Triassic. *Rivista Italiana di Paleontologia e Stratigrafia*, **86**, 761–768.

Nishi, T. (1994) Geology and tectonics of the Sambosan Terrane in eastern Kyushu, southwest Japan—stratigraphy, sedimentological features of the depositional setting of the Shakumasan Group. *Jour. Geol. Soc. Japan*, **100**, 199–215.

Nishikane, Y., Kaiho, K., Takahashi, S., Henderson, C. M., Suzuki, N. and Kanno, M. (2011) The Guadalupian-Lopingian boundary (Permian) in a pelagic sequence from Panthalassa recognized by integrated conodont and radiolarian biostratigraphy. *Marine Micropaleontol*., **78**, 84–95.

Nogami, Y. (1968) Trias-Conodonten von Timor, Malaysien und Japan (Palaeontological Study of Portuguese Timor, 5). *Mem. Fac. Sci. Kyoto Univ., Ser. Geol. Mineral*., **34**, 115–136 (in German with English abstract).

Oda, H. and Suzuki, H. (2000) Paleomagnetism of Triassic and Jurassic red bedded chert of the Inuyama area, central Japan. *Jour. Geophys. Res.: Solid Earth (1978–2012)*, **105**, 25743–25767.

O'Dogherty, L., Carter, E. S., Goričan, Š. and Dumitrica, P. (2010) Triassic radiolarian biostratigraphy. *Geol. Soc., London, Spec. Publ*., **334**, 163–200.

Ogg, J. G. (2012) The Triassic period. *In* Gradstein, F. M., *et al.*, eds., *A Geologic Time Scale*. Cambridge Univ. Press, Cambridge, UK, 681–730.

Onoue, T., Nakamura, T., Haranosono, T. and Yasuda, C. (2011) Composition and accretion rate of fossil micrometeorites recovered in Middle Triassic deep-sea deposits. *Geology*, **39**, 567–570.

Orchard, M. J. (1995) Taxonomy and correlation of Lower Triassic (Spathian) segminate conodonts from Oman and revision of some species of Neospathodus. *Jour. Paleontol*., **69**, 110–122.

Orchard, M. J. (2005) Multielement conodont apparatuses of Triassic Gondolelloidea. *Special Papers in Palaeontol*., **73**, 73–101.

Orchard, M. J. (2007) Conodont diversity and evolution through the latest Permian and Early Triassic upheavals. *Palaeogeogr., Palaeoclimatol.,*

Palaeoecol., **252**, 93–117.
Orchard, M. J. (2010) Triassic conodonts and their role in stage boundary definition. *Geol. Soc. London, Spec. Publ*., **334**, 139–161.
Orchard, M. J., Gradinaru, E. and Nicora, A. (2007a) A summary of the conodont succession around the Olenekian-Anisian boundary at Desli Caira, Dobrogea, Romania. *New Mexico Museum of Natural History and Science Bulletin*, **41**, 341–346.
Orchard, M. J., Lehrmann, D. J., Wei, J., Wang, H. and Taylor, H. J. (2007b) Conodonts from the Olenekian-Anisian boundary beds, Guandao, Guizhou Province, China. *New Mexico Museum of Natural History and Science Bulletin*, **41**, 347–354.
Pisa, G., Perri, C. and Veneri, P. (1980) Upper Anisian conodonts from Dont and M. Bivera Formations, Southern Alps (Italy). *Rivista Italiana di Paleontologia e Stratigrafia*, **85**, 807–828.
Sato, H., Onoue, T., Nozaki, T. and Suzuki, K. (2013) Osmium isotope evidence for a large Late Triassic impact event. *Nature Communications*, **4**, doi: 10.1038/ncomms3455.
Sato, H., Shirai, N., Ebihara, M., Onoue, T. and Kiyokawa, S. (2016) Sedimentary PGE signatures in the Late Triassic ejecta deposits from Japan: Implications for the identification of impactor. *Palaeogeogr., Palaeoclimatol., Palaeoecol*., **442**, 36–47.
Soda, K., Onoue, T. and Ikeda, M. (2015) Cyclostratigraphic examination of Middle Triassic (Anisian) bedded chert in the Chichibu Belt from Tsukumi area, eastern Kyushu, Japan. *Jour. Geol. Soc. Japan*, **121**, 147–152 (in Japanese with English abstract).
Solien, M. A. (1979) Conodont biostratigraphy of the Lower Triassic Thaynes FGormation, Utah. *Jour. Paleontol.*, **53**, 276–306.
Sudar, M. N. and Budurov, K. (1979) New conodonts from the Triassic in Yugoslavia and Bulgaria. *Geologica Balcanica*, **9**, 47–52.
Sugiyama, K. (1997) Triassic and Lower Jurassic radiolarian biostratigraphy in the siliceous claystone and bedded chert units of the southeastern Mino Terrane, Central Japan. *Bull. Mizunami Fossil Museum*, **24**, 79–193.
Sweet, W. C. (1988) *The Conodonta: morphology, taxonomy, paleoecology, and evolutionary history of a long-extinct animal phylum*. Oxford Monogr. Geol. Geophys, 10. Clarendon Press, Oxford.
Takahashi, O., Kawarazaki, T. and Ishii, A. (1998) Middle Triassic radiolarians from the Tsukumi area, eastern Kyushu, southwest Japan. *News Osaka Micropaleontol., Spec. Vol*., no. 11, 115–121.
Takahashi, S., Oba, M., Kaiho, K., Yamakita, S. and Sakata, S. (2009) Panthalassic oceanic anoxia at the end of the Early Triassic: A cause of delay in the recovery of life after the end-Permian mass extinction. *Palaeogeogr., Palaeoclimatol., Palaeoecol.*, **274**,185–195.
Takemura, A., Aita, Y., Sakai, T., Hori, S. R., Kodama, K., Yamakita, S., Kamata, Y., Suzuki, N., Spörli, K. B. and Campbell, H. J. (2001) Radiolarians from the Waipapa Terrane in North Island, New Zealand. *Topics on Palaeontology*, **2**, 17–24 (in Japanese).
Tanaka, K. (1980) Kanoashi Group, an olistostrome, in the Nichihara area, Shimane Prefecture. *Jour. Geol. Soc. Japan*, **86**, 613–628 (in Japanese with English abstract).
Tatge, U. (1956) Conodonten aus dem germanischen Muschelkalk. *Paläontologische Zeitschrift*, **30**, 108–147 (in German).
Uno, K., Onoue, T., Hamada, K. and Hamami, S. (2012) Palaeomagnetism of Middle Triassic red bedded cherts from southwest Japan: equatorial palaeolatitude of primary magnetization and widespread secondary magnetization. *Geophys. Jour. Internat.*, **189**, 1383–1398.
Wakita, K. (1988) Origin of chaotically mixed rock bodies in the Early Jurassic to Early Cretaceous sedimentary complex of the Mino terrane, central Japan. *Bull. Geol. Surv. Japan*, **39**, 675–757.
Wakita, K. and Metcalfe, I. (2005) Ocean plate stratigraphy in East and Southeast Asia. *Jour. Asian Earth Sci*., **24**, 679–702.
Yao, A. and Kuwahara, K. (1997) Radiolarian faunal change from Late Permian to Middle Triassic times. *News Osaka Micropalaeontol., Spec. Vol*., no. 10, 87–96 (in Japanese with English abstract).
Yao, A., Matsuda, T. and Isozaki, Y. (1980) Triassic and Jurassic radiolarians from the Inuyama area, central Japan. *Jour. Geosci. Osaka City Univ.*, **23**, 135–154.
Yamakita, S. and Otoh S. (2000) Tectonostratigraphic division of accretionary-sedimentary complex of the Tamba-Mino-Ashio Belt and comparison with the Northern and Southern Chichibu Belts. *Structural Geology*, **44**, 5–32 (in Japanese with English abstract).
Yamakita, S., Takahashi, S. and Kojima, S. (2010) Conodont-based age-determination of siliceous claystone in the lower part of the Momotaro-jinja section, Inuyama, central Japan. *Abstract, The 2010 Annual Meeting of the Palaeontological Society of Japan*, 47 (in Japanese).
Zhao, L., Orchard, M. J., Jinnan, T., Zhiming, S., Jinxun, Z., Suxin, Z. and Ailing, Y. (2007) Lower Triassic conodont sequence in Chaohu, Anhui Province, China and its global correlation. *Palaeogeogr., Palaeoclimatol., Palaeoecol*., **252**, 24–38.
Ziegler, A. M., Gibbs, M. T. and Hulver, M. L. (1998) A mini-atlas of oceanic water masses in the Permian Period. *Proc. Royal Society of Victoria*, **110**, 323–343.

Recieved December 19, 2017
Accepted January 18, 2019

コノドント生層序による中部三畳系アニシアン遠洋深海層状チャートにおける放散虫化石帯年代の再検討

武藤　俊・高橋　聡・山北　聡・曽田勝仁・尾上哲治

要　旨

超海洋パンサラッサの遠洋域深海で堆積した層状チャートは，放散虫化石層序により年代が決められてきた．一方で，三畳系の放散虫化石帯は国際基準の地質年代との厳密な対比には用いられない場合が多い．本研究は，放散虫化石帯が確立され，中部三畳系アニシアン階に対比されていた大分県津久見地域の網代島セクションと愛知県犬山地域の栗栖セクションの珪質粘土岩・層状チャートにおいてコノドント化石層序を検討した．結果，オレネキアン階の上部の*Novispathodus brevissimus-Icriospathodus collinsoni* 帯と*Triassospathodus homeri* 帯，アニシアン階の下部の*Chiosella timorensis* 帯，アニシアン階の中部の*Paragondolella bulgarica* 帯，アニシアン階の上部の*Paragondolella excelsa* 帯，アニシアン階の最上部からラディニアン階の最下部の*Paragondolella trammeri* 帯が認識された．上記のコノドント化石層序との比較により，Sugiyama (1997, *Bull. Mizunami Foss. Mus*., vol. 24, p. 79–193)による放散虫化石帯の年代を再検討した．従来オレネキアン階に対比されていたTR 1化石帯はオレネキアン階の上部からアニシアン階の中部に対比された．TR 2A化石帯，TR 2B化石帯，及びTR 2C化石帯の下部はアニシアン階の中部に対比され，TR 2C化石帯の上部とTR 3A化石帯の下部はアニシアン階の上部に対比された．TR 3A化石帯の上部とTR 3B化石帯の下部はアニシアン階の最上部に対比される可能性が高いが，ラディニアン階の最下部に対比される可能性も否めない．

難読･重要地名

Tsukumi：津久見，Youra：四浦，Sambosan：三宝山，Yukagi：床木，Tsui：津井，Shakumasan：尺間山，Enoura：江ノ浦，Ajiro：網代，Kurusu：栗栖，Inuyama：犬山，Kamiaso：上麻生

Plate 1 Stereo-photographs and sketches of conodonts from the Ajiro Island section. Figs. 3–5 are reversely arranged so that the moulds appear as casts. All other figures are normally arranged. Scale bars are 200 μm.

1, 2: *Budurovignathus* cf. *hungaricus* (Kozur & Vegh). Sample AJR 724+2.4m.
3, 4: *Chiosella gondolelloides* (Bender). 3. Sample AjL-B. 4. Sample 151005-13.
5: *Chiosella timorensis* (Nogami). Sample AjL-1-B.
6–8: *Cornudina breviramulis* (Tatge). 6. Sample 170627-02. 7. Sample 170627-03. 8. Sample AJR 724+1.9m.
9: *Cornudina*? *igoi* Koike. Sample AJR 0.

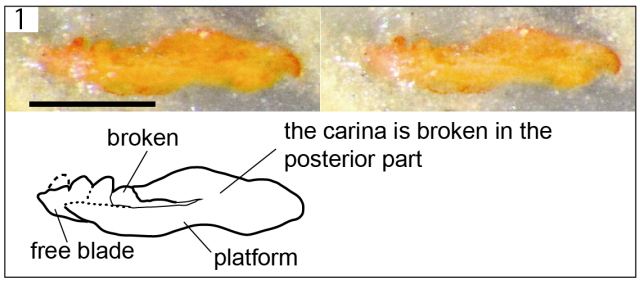
1
broken
the carina is broken in the posterior part
free blade
platform

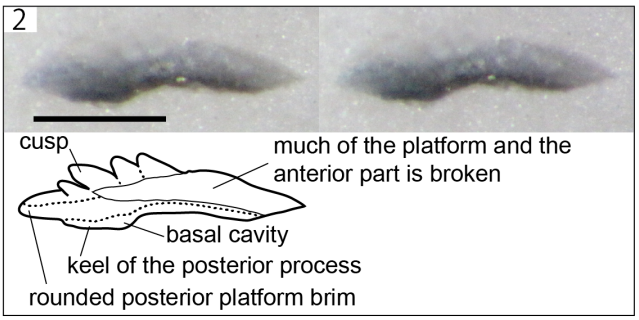
2
cusp
much of the platform and the anterior part is broken
basal cavity
keel of the posterior process
rounded posterior platform brim

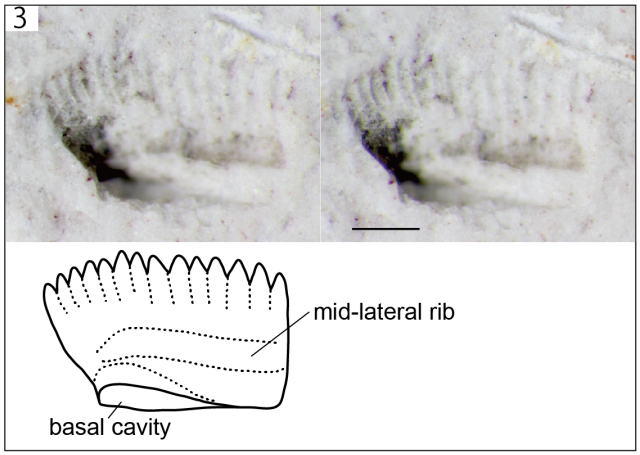
3
mid-lateral rib
basal cavity

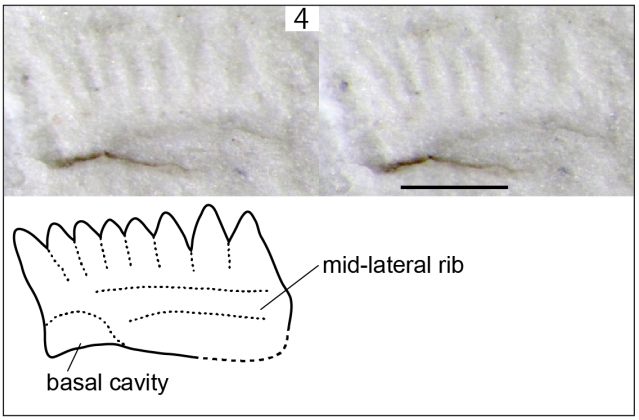
4
mid-lateral rib
basal cavity

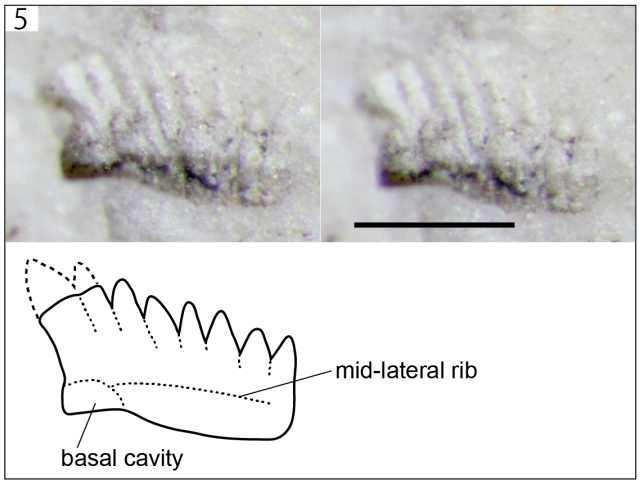
5
mid-lateral rib
basal cavity

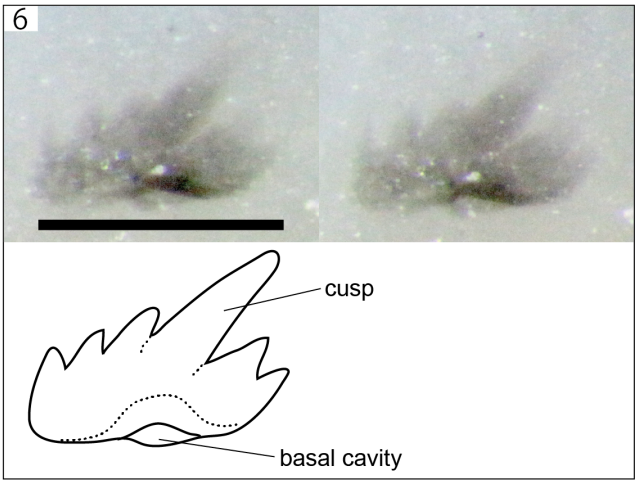
6
cusp
basal cavity

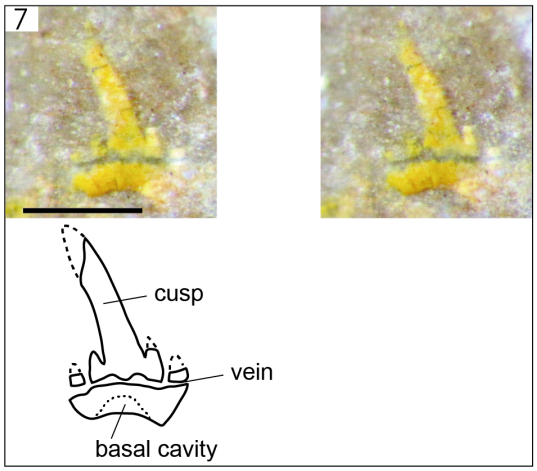
7
cusp
vein
basal cavity

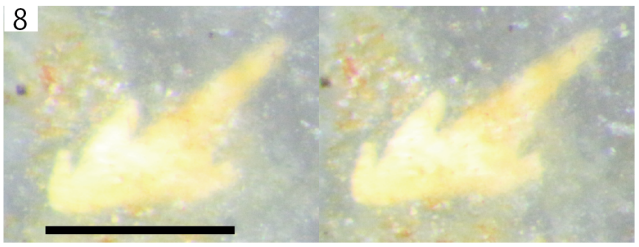
8

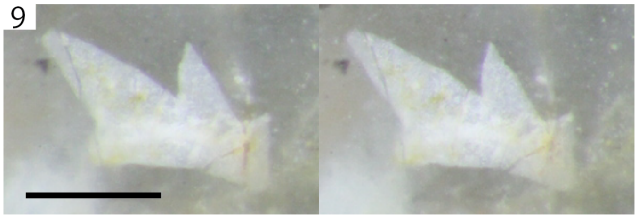
9

Plate 2 Stereo-photographs and sketches of conodonts from the Ajiro Island section. Fig. 5 is reversely arranged so that the mould appears as a cast. All other figures are normally arranged. Scale bars are 200 μm.

1: *Cornudina*? *igoi* Koike. Sample AJR 144.
2, 3: *Cornudina tortilis* Kozur & Mostler. 2. Sample AJR 722. 3. Sample AJR 724+1.9m.
4: "*Kamuellerella gebzeensis* Gedik". Sample 170627-02.
5: *Icriospathodus collinsoni* (Solien). Sample AjL-C.
6: *Icriospathodus* sp.? Sample AjL-C.
7: *Neogondolella aequidentata* Kozur. Sample AJR 724+2.4m.
8–11: *Neogondolella* cf. *hastata* Golding & Orchard. 8, 9. Sample 160627-02. 10, 11. Sample 160627-03.

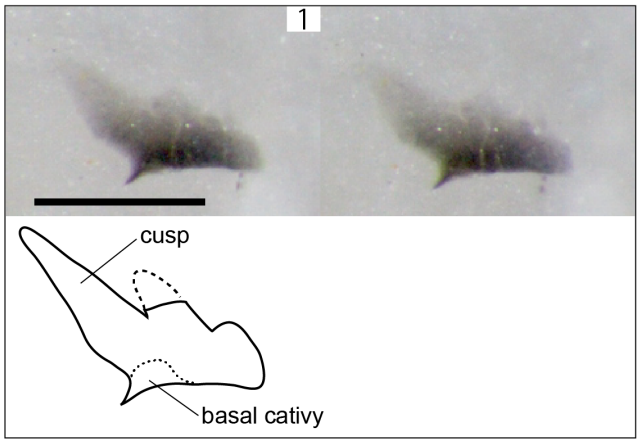
1
cusp
basal cativy

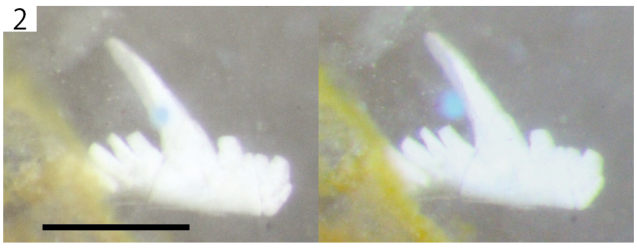
2

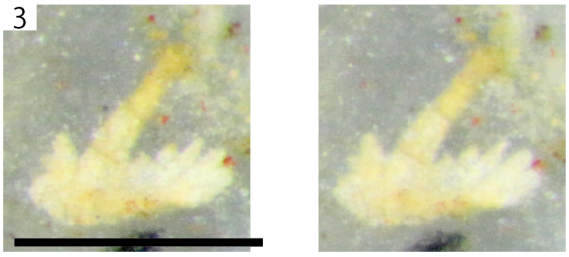
3

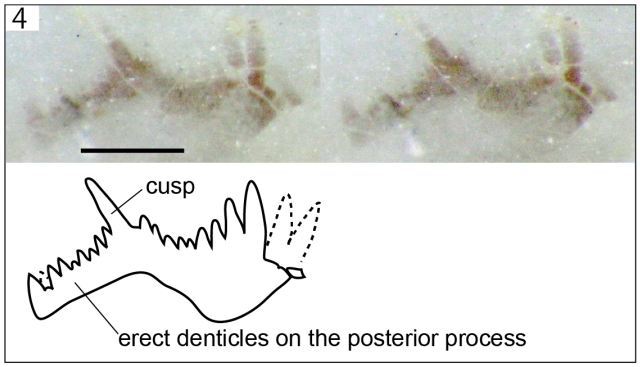
4
cusp
erect denticles on the posterior process

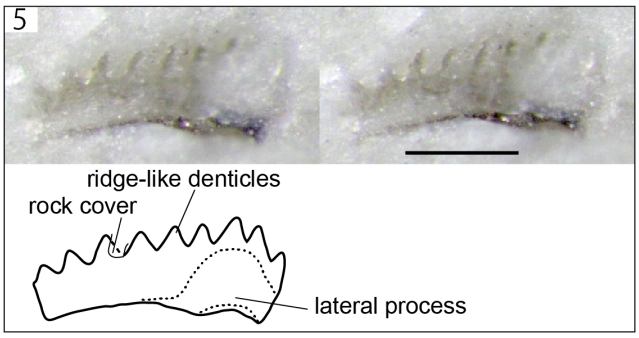
5
ridge-like denticles
rock cover
lateral process

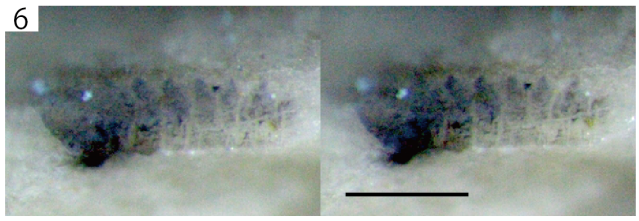
6

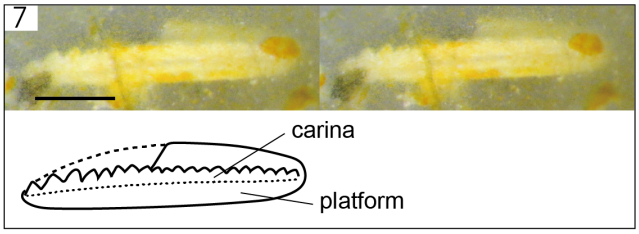
7
carina
platform

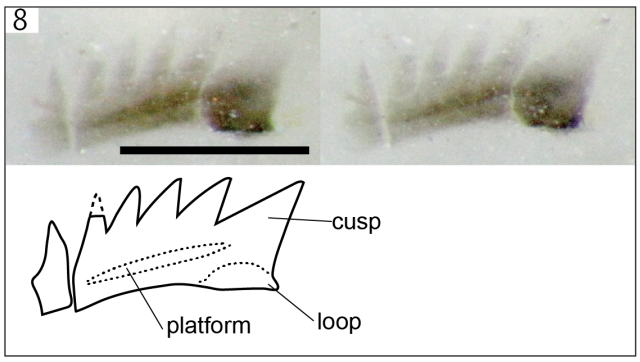
8
cusp
platform
loop

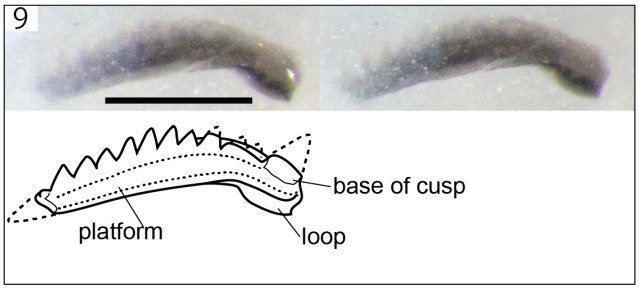
9
base of cusp
platform
loop

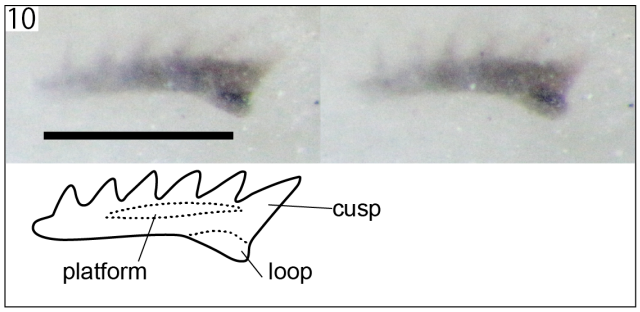
10
cusp
platform
loop

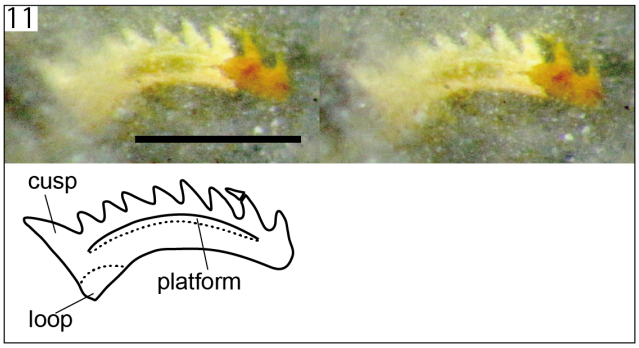
11
cusp
platform
loop

Plate 3 Stereo-photographs and sketches of conodonts from the Ajiro Island section. Fig. 12 is reversely arranged so that the mould appears as a cast. All other figures are normally arranged. Scale bars are 200 μm.

1, 2: *Neogondolella* aff. *hastata* (Golding & Orchard). Sample 170627-03.
3: *Neogondolella pridaensis* (Nicora, Kozur & Mietto). Sample AJR 724+2.4m.
4: *Neogondolella* cf. *regale* Mosher. Sample 170627-03.
5–9: post Bithynian type *Neogondolella*. 5, 7. Sample 170627-03. 6. Sample AJR 577. 8. Sample AJR 310. 9. Sample AJR 517.
10, 11: "*Neohindeodella aequiramosa* Kozur & Mostler". 10. Sample AJR 144. 11. Sample 170627-02.
12, 13: "*Neohindeodella benderi* (Kozur & Mostler)". 12. Sample 151005-13. 13. Sample AJR 0.

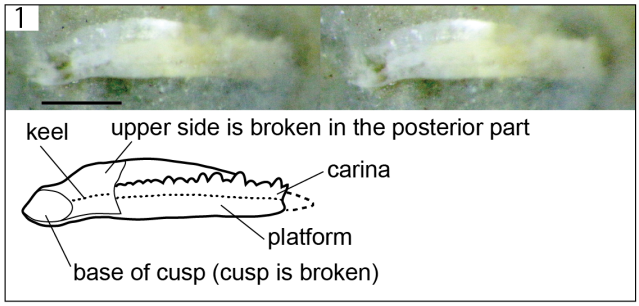
1
keel
upper side is broken in the posterior part
carina
platform
base of cusp (cusp is broken)

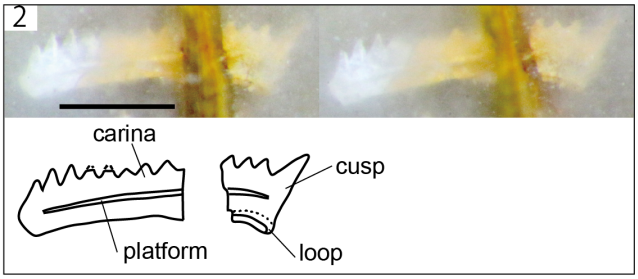
2
carina
cusp
platform
loop

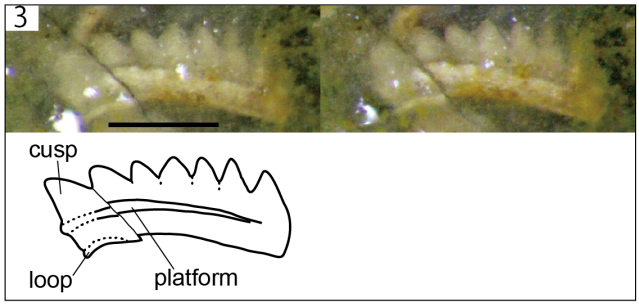
3
cusp
loop
platform

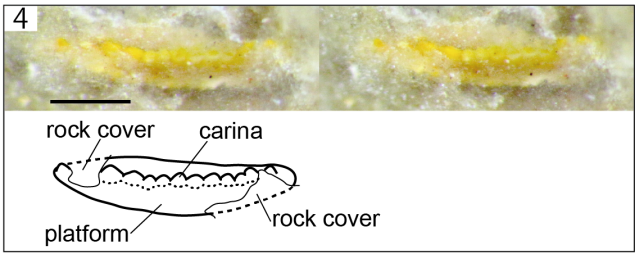
4
rock cover
carina
platform
rock cover

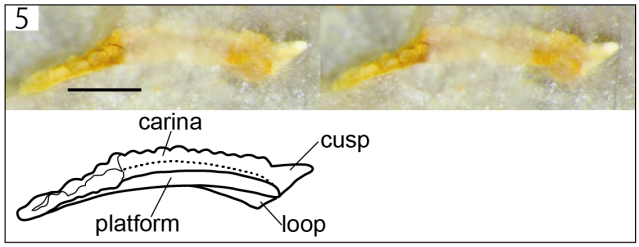
5
carina
cusp
platform
loop

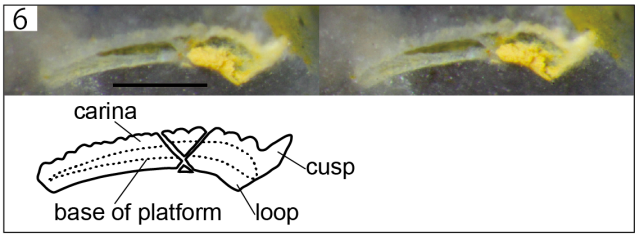
6
carina
cusp
base of platform
loop

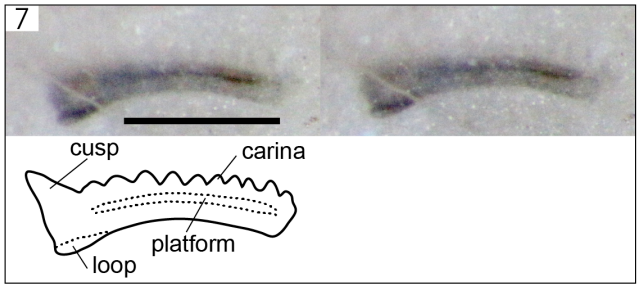
7
cusp
carina
platform
loop

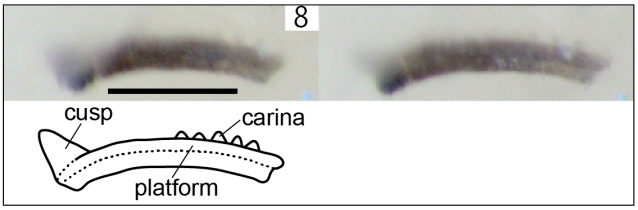
8
cusp
carina
platform

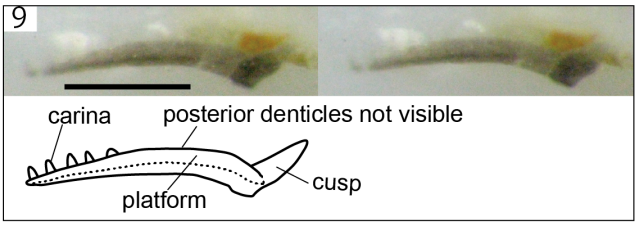
9
carina
posterior denticles not visible
cusp
platform

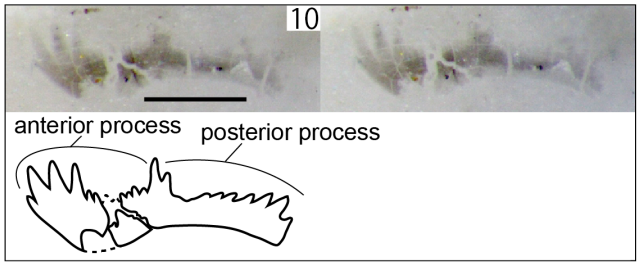
10
anterior process
posterior process

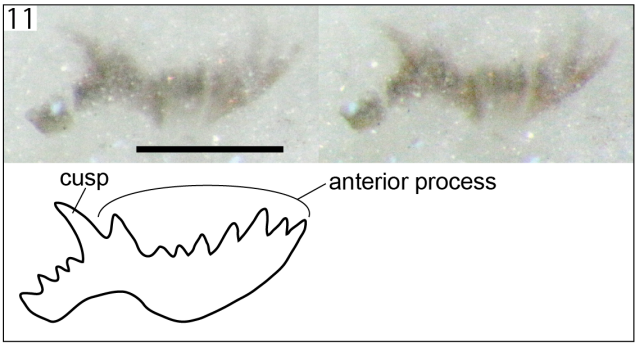
11
cusp
anterior process

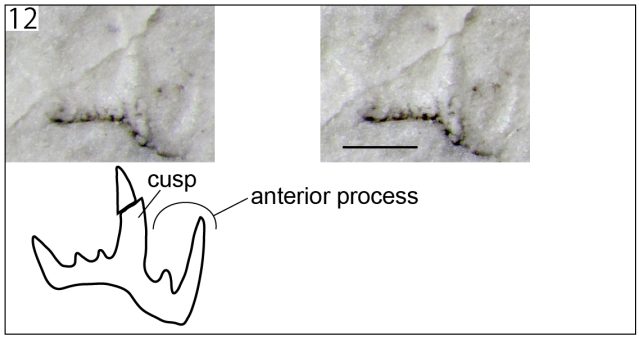
12
cusp
anterior process

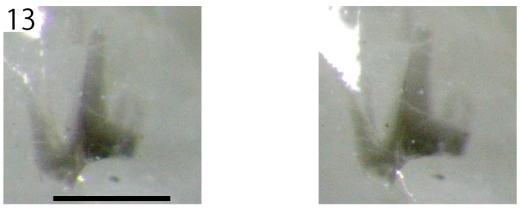
13

Plate 4 Stereo-photographs and sketches of conodonts from the Ajiro Island section. Figs. 5, 7–11 are reversely arranged so that the moulds appear as casts. All other figures are normally arranged. Scale bars are 200 μm.

1–3: "*Neohindeodella triassica* (Müller)". 1. Sample AJR 144. 2. Sample AJR 517. 3. Sample AJR 724+1.9m.
4: *Nicoraella kockeli* (Tatge). Sample AJR 101.
5: *Novispathodus abruptus* (Orchard). Sample 150615-21.
6: *Novispathodus brevissimus* (Orchard). Sample AjL-C.
7–10: *Novispathodus symmetricus* (Orchard). 7. Sample 150615-21. 8. Sample AjL-B. 9. Sample 151005-13. 10. Sample 160819-03.
11: *Novispathodus* sp. indet. Sample AjL-B.

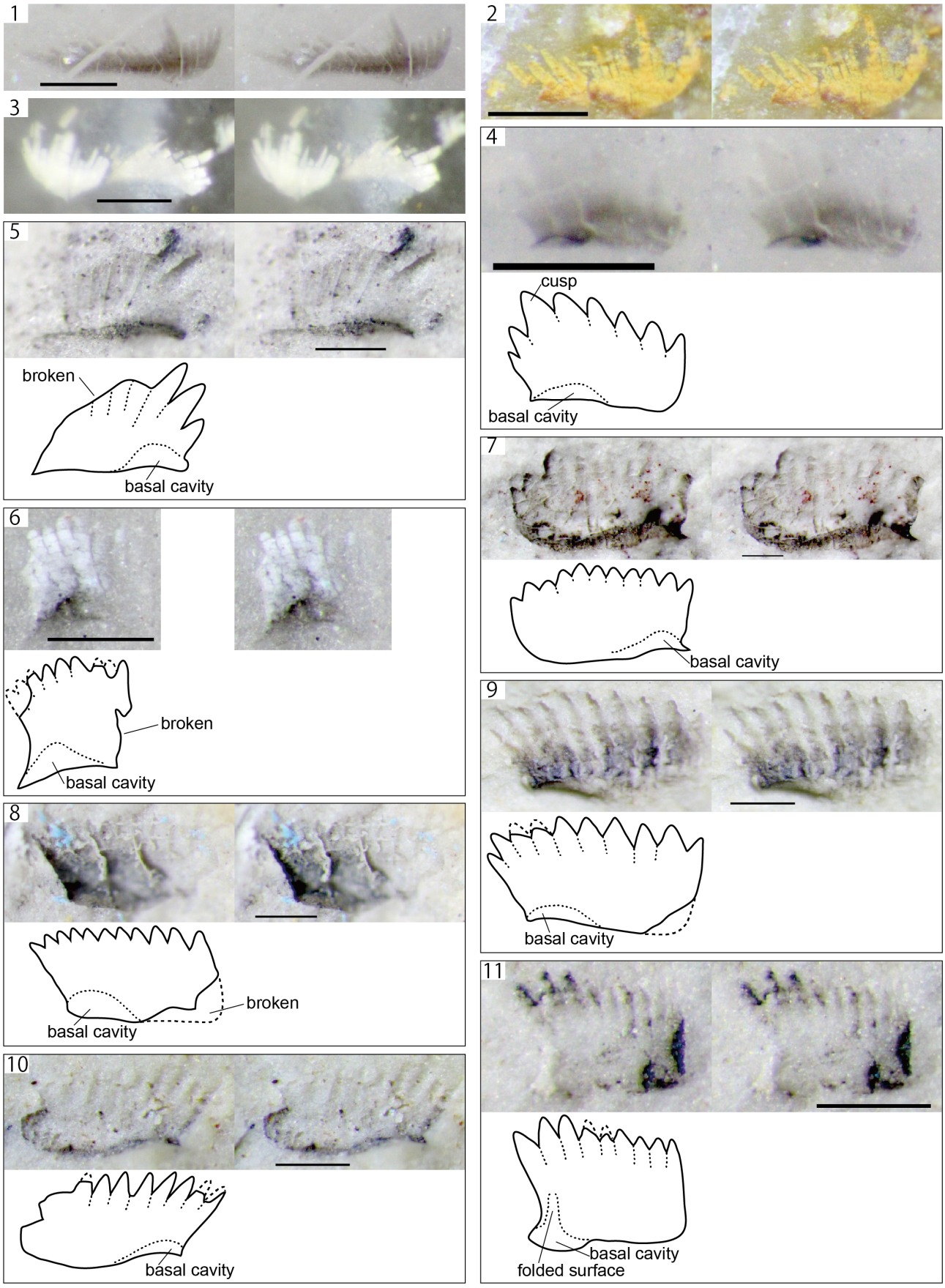
1
2
3
4
cusp
basal cavity
5
broken
basal cavity
6
broken
basal cavity
7
basal cavity
8
broken
basal cavity
9
basal cavity
10
basal cavity
11
basal cavity
folded surface

Plate 5 Stereo-photographs and sketches of conodonts from the Ajiro Island section. All figures are normally arranged. Scale bars are 200 μm.

1: *Paragondolella* sp. cf. *Paragondolella bulgarica* Group. Sample 151015-08.5.
2–8: *Paragondolella bulgarica* Group. 2. Sample AJR 0. 3, 4. Sample AJR 144. 5. Sample AJR 310. 6, 7. Sample AJR 517. 8. Sample AJR 577.
9–14: *Paragondolella excelsa* Group. 9. Sample AJR 517. 10–12. Sample AJR 577. 13. Sample AJR 722. 14. Sample AJR 724+2.4m.

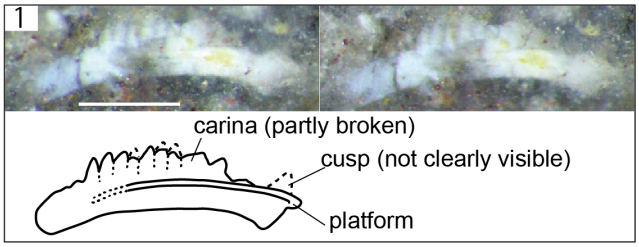
1
carina (partly broken)
cusp (not clearly visible)
platform

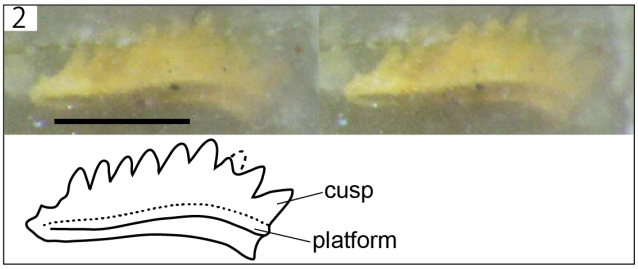
2
cusp
platform

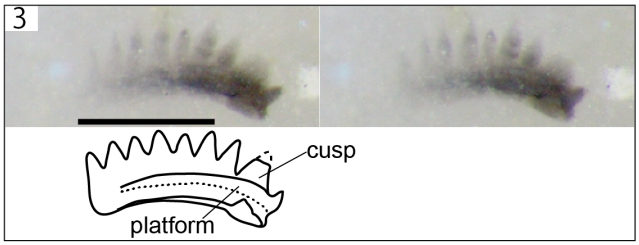
3
cusp
platform

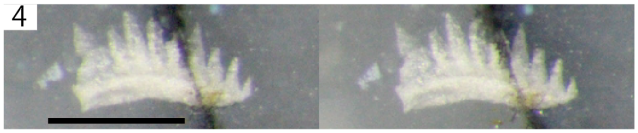
4

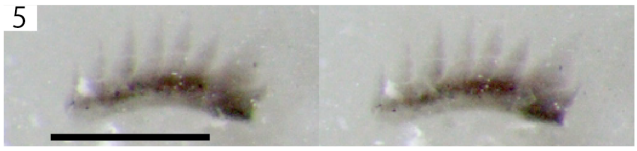
5

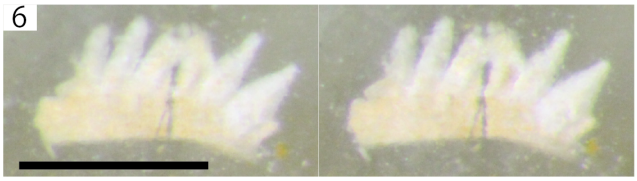
6

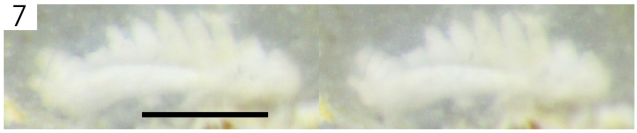
7

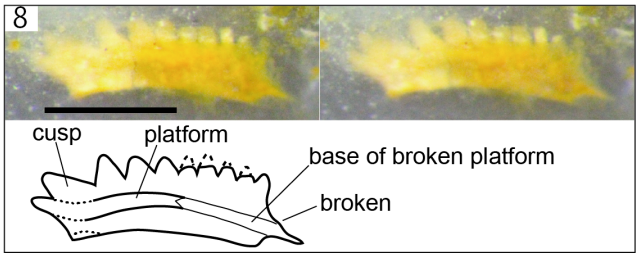
8
cusp
platform
base of broken platform
broken

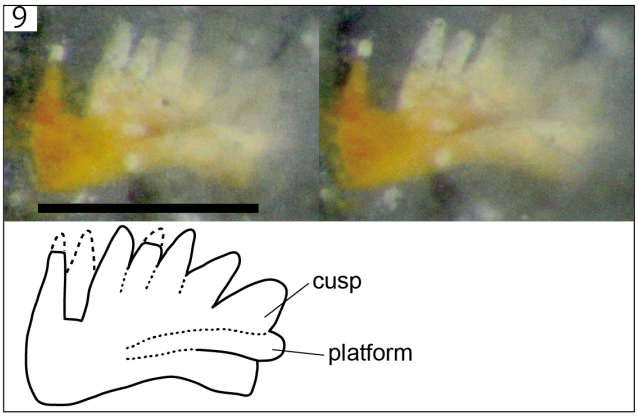
9
cusp
platform

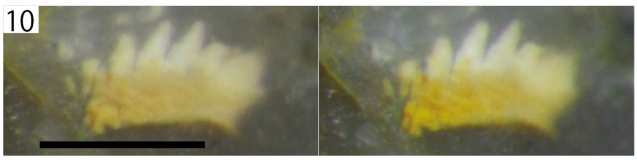
10

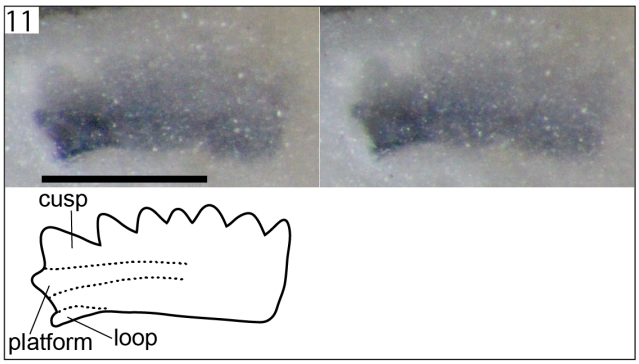
11
cusp
platform
loop

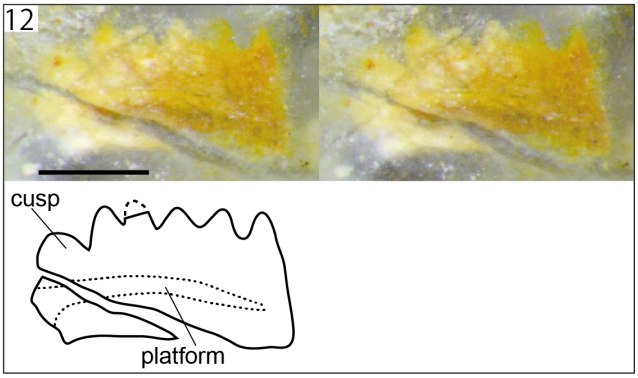
12
cusp
platform

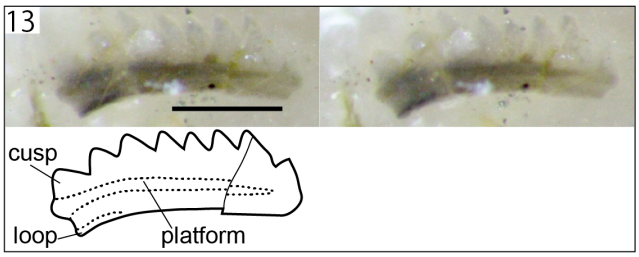
13
cusp
loop
platform

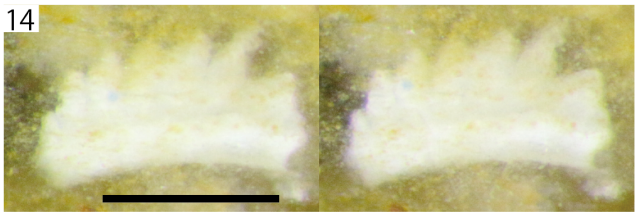
14

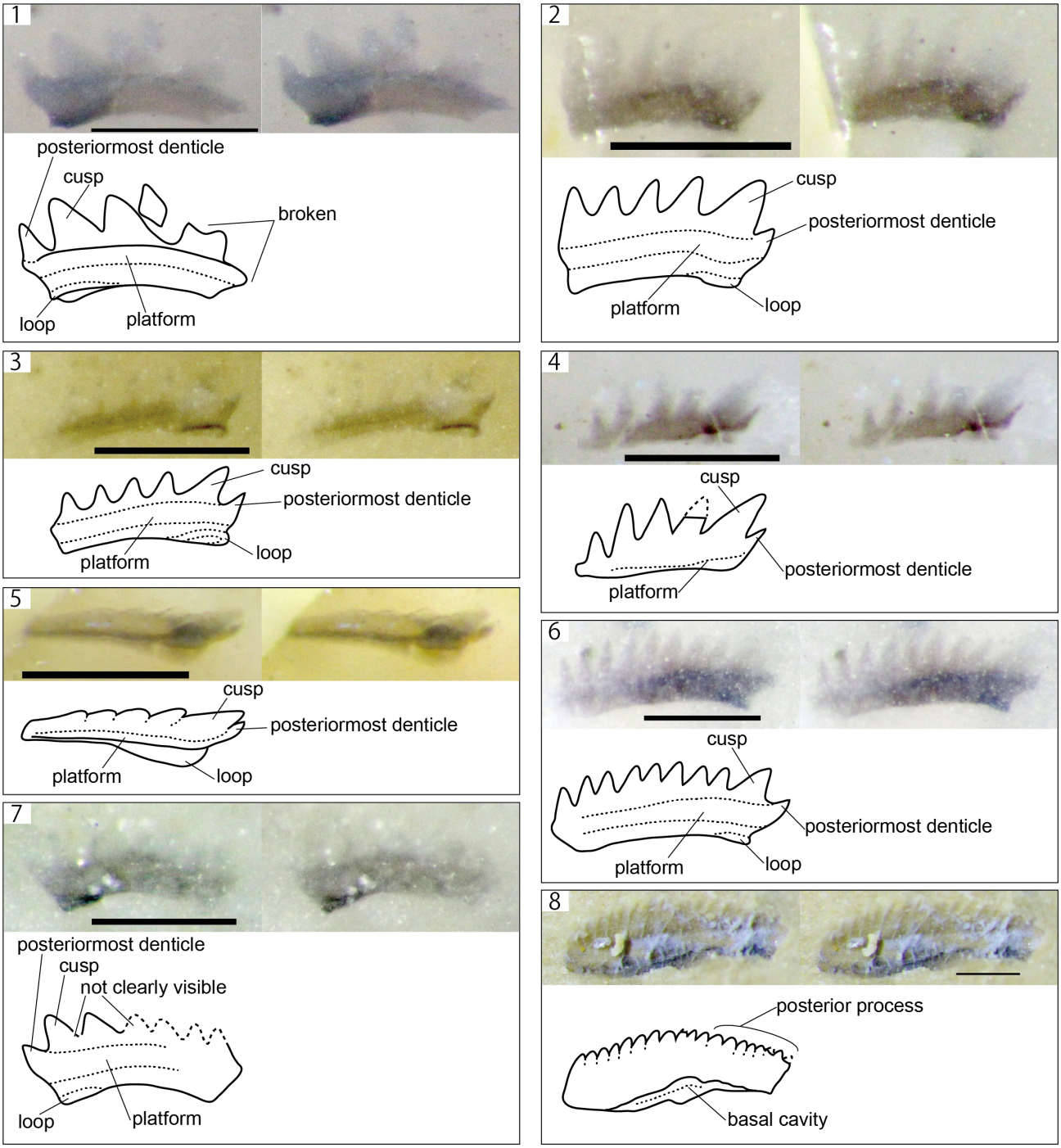

Plate 6 Stereo-photographs and sketches of conodonts from the Ajiro Island section. Fig. 8 is reversely arranged so that the mould appears as a cast. All other figures are normally arranged. Scale bars are 200 μm.

1–7: *Paragondolella trammeri* Group. 1. Sample AJR 603–605. 2–4. Sample AJR 630. 5. Sample AJR 722. 6, 7. Sample AJR 724+1.9m.
8: *Triassospathodus anhuinensis* (Ding). Sample 150616-29.

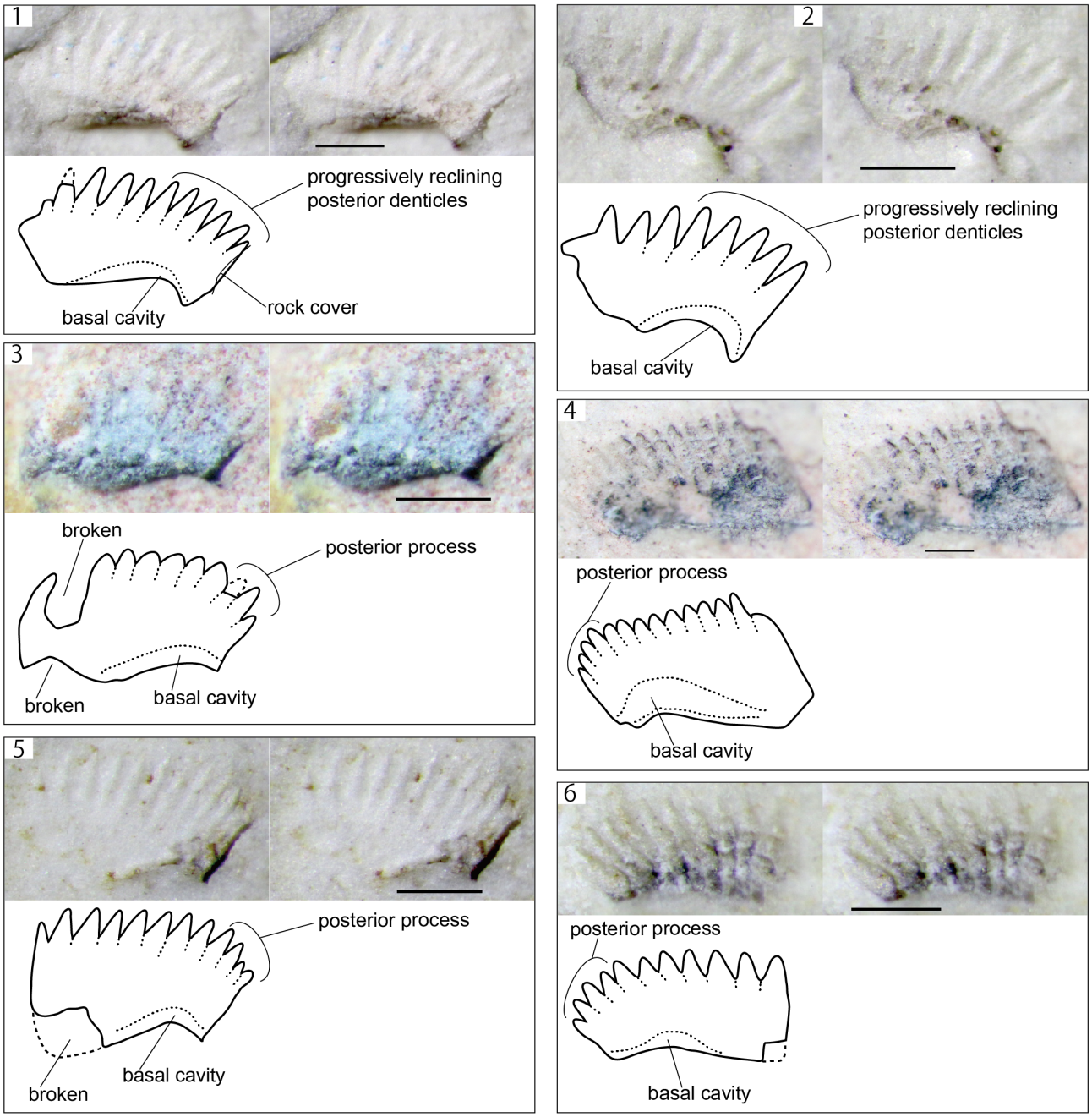

Plate 7 Stereo-photographs and sketches of conodonts from the Ajiro Island section. All figures are reversely arranged so that the moulds appear as casts. Scale bars are 200 μm.

1: *Triassospathodus brochus* (Orchard). Sample 151005-13.
2: *Triassospathodus* cf. *brochus* (Orchard). Sample 151005-13.
3–6: *Triassospathodus homeri* (Bender). 3. Sample 150615-21. 4. Sample AjL-B. 5. Sample 151005-13. 6. Sample AjL1-A.

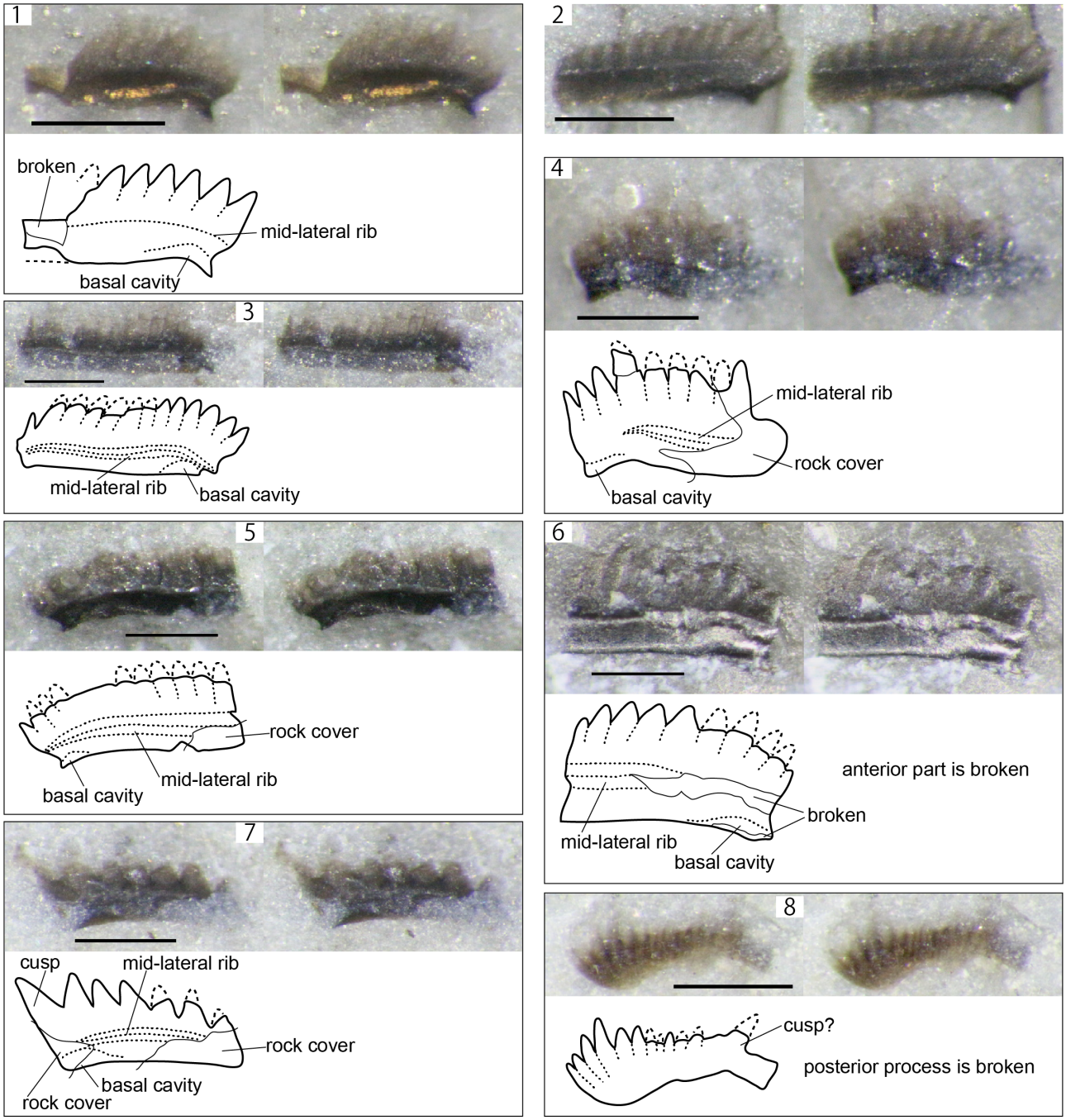

Plate 8 Stereo-photographs and sketches of conodonts from the Kr-2-YK section. All figures are normally arranged. Scale bars are 200 μm.

1–6: *Chiosella timorensis* (Nogami). 1–3. Sample Kr1-04. 4. Sample Kr1-03. 5, 6. Sample Kr1-02.
7: *Chiosella* sp. Sample Kr1-04.
8: "*Neohindeodella* cf. *aequiramosa* Kozur & Mostler". Sample Kr1-03.

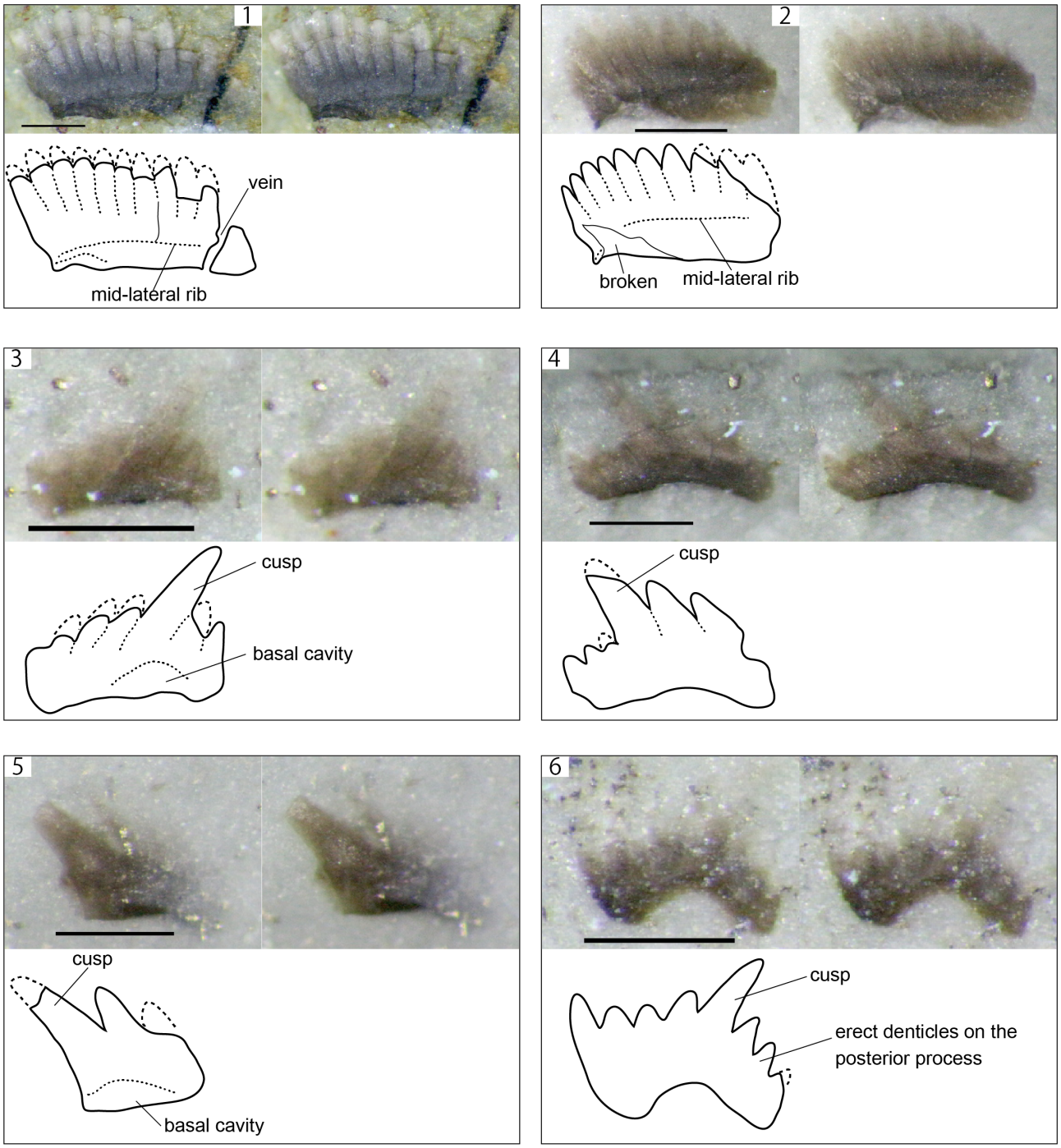

Plate 9 Stereo-photographs and sketches of conodonts from the Kr-2-I section. All figures are normally arranged. Scale bars are 200 μm.

1, 2: *Chiosella gondolelloides* (Bender). 1. Sample Kr2-01. 2. Sample Kr2-03.
3, 4: *Cornudina breviramulis* (Tatge). Sample Kr2-01.
5: *Cornudina*? *igoi* Koike. Sample Kr2-01.
6: "*Kamuellerella gebzeensis* Gedik". Sample Kr2-03.

Plate 10 Stereo-photographs and sketches of conodonts from the Kr-2-I section. All figures are normally arranged. Scale bars are 200 μm.

1, 2: "*Neohindeodella benderi* (Kozur & Mostler)". Sample Kr2-01.
3: *Neostrachanognathus tahoensis* Koike. Sample Kr2-01.
4, 5: *Novispathodus symmetricus* (Orchard). Sample Kr2-01.
6, 7: *Triassospathodus homeri* (Bender). 6. Sample Kr2-01. 7. Sample Kr2-03.

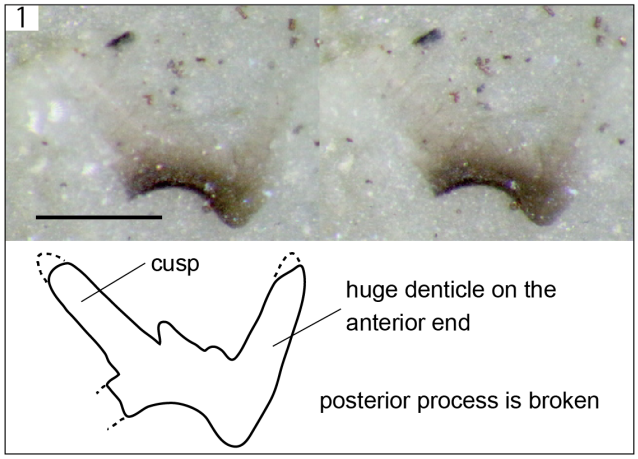
1
cusp
huge denticle on the anterior end
posterior process is broken

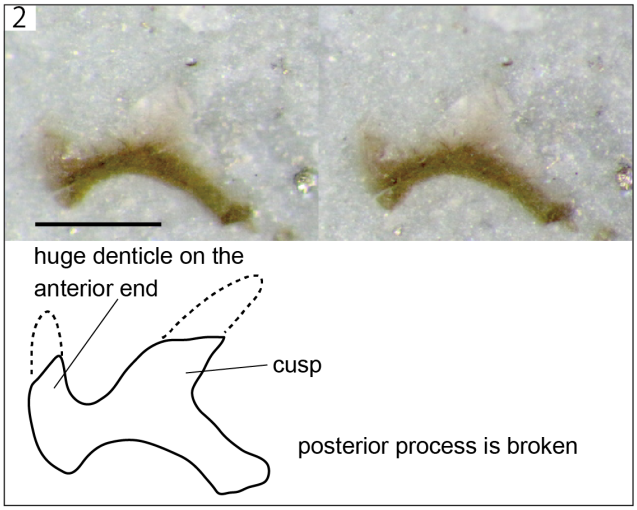
2
huge denticle on the anterior end
cusp
posterior process is broken

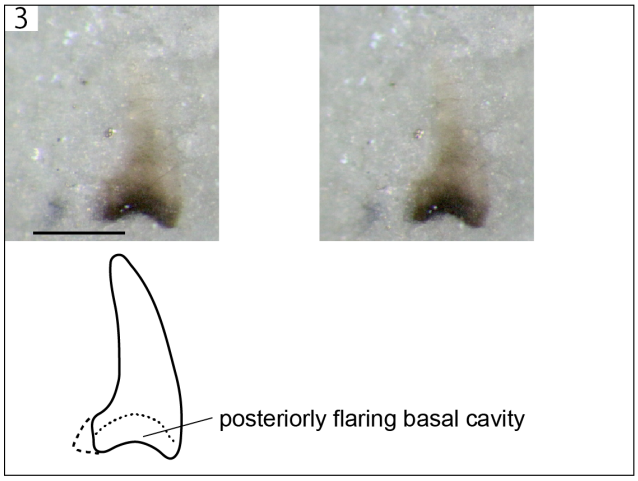
3
posteriorly flaring basal cavity

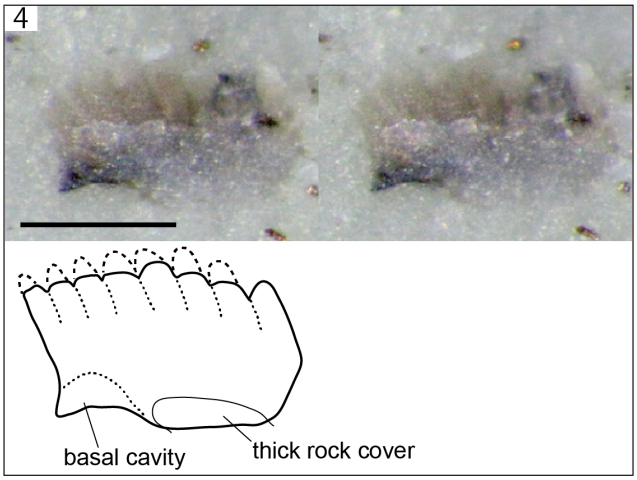
4
basal cavity
thick rock cover

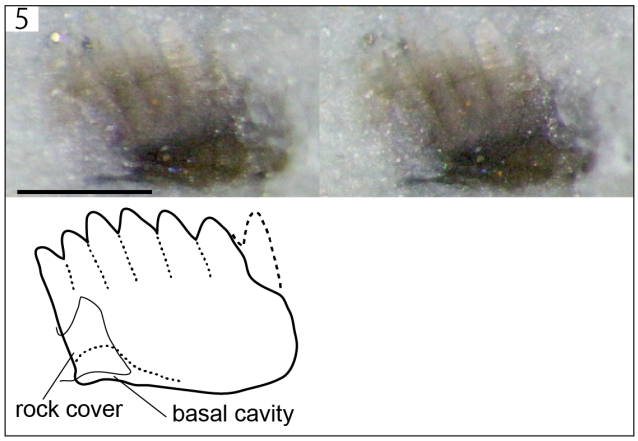
5
rock cover
basal cavity

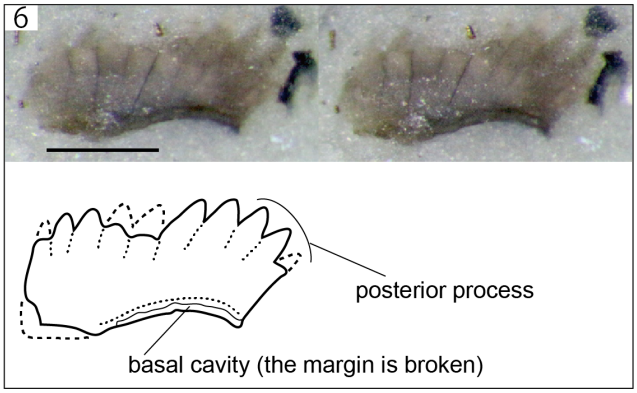
6
posterior process
basal cavity (the margin is broken)

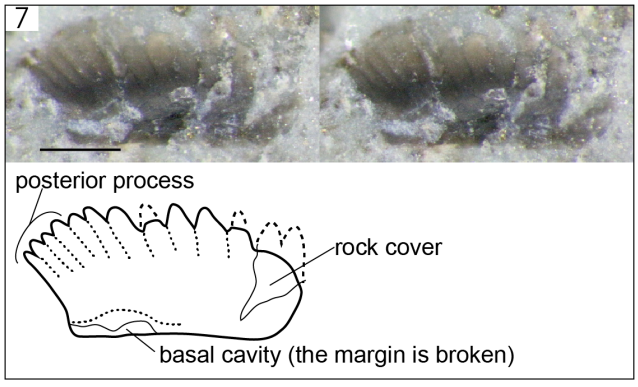
7
posterior process
rock cover
basal cavity (the margin is broken)